

KfK 3163  
April 1981

# Velocity and Temperature Profiles in Rough Annuli

L. Meyer  
Institut für Neutronenphysik und Reaktortechnik

Kernforschungszentrum Karlsruhe



KERNFORSCHUNGSZENTRUM KARLSRUHE

Institut für Neutronenphysik und Reaktortechnik

KfK 3163

Velocity and Temperature Profiles in Rough Annuli

L. Meyer

Kernforschungszentrum Karlsruhe GmbH, Karlsruhe

**Als Manuskript vervielfältigt  
Für diesen Bericht behalten wir uns alle Rechte vor**

**Kernforschungszentrum Karlsruhe GmbH  
ISSN 0303-4003**

## Abstract

Velocity and temperature profiles were measured in an annular flow cross section. Three different rough rods in two outer tubes each were investigated. The slopes of the nondimensional logarithmic velocity profile in both the inner 'rough' zone and the outer 'smooth' zone vary with the Reynolds number. The slopes of the nondimensional temperature profile deviate from a logarithmic line in a large portion of the flow cross section. The turbulent Prandtl number is smaller than one and varies with the distance from the wall.

## Geschwindigkeits- und Temperaturprofile in rauhen Ringspalten

### Zusammenfassung

In einem Ringspalt wurden Geschwindigkeits- und Temperaturprofile gemessen. Dabei wurden drei verschiedene raue Stäbe jeweils in zwei glatten Außenrohren untersucht. Die Steigung des logarithmischen Geschwindigkeitsprofils ändert sich sowohl in der 'glatten' Außen- als auch in der 'rauen' Innenzone mit der Reynoldszahl. Die Steigung des logarithmischen Temperaturprofils weicht im größten Teil des Strömungsquerschnittes von einer logarithmischen Geraden ab. Die turbulente Prandtlzahl ist kleiner als eins und ändert sich mit dem Wandabstand.

## 1. Introduction

From measurements in rectangular channels /1,2,3,5/, and other investigations /4,14/ it is known that the velocity profiles at artificial roughnesses do not obey the 'law of the rough wall'

$$u^+ = A_r \ln \frac{y}{h} + R \quad (1)$$

with a constant value for  $A_r$ . The present investigation was undertaken to find out, whether we get the same results in annular geometry and whether the nondimensional temperature profile can be described by

$$T^+ = A_r \ln \frac{y}{h} + G \quad (2)$$

In an annular geometry the heat transfer and pressure drop measurements at single rough rods are normally performed /6,7,8,9/. The experimental results are transformed to eliminate the effect of the smooth outer tube, by methods which are based on equations (1) and (2) /10,6,7/.

Since the largest deviations of the nondimensional velocity profile from the 'law of the wall' occurred at roughnesses which produced the highest friction factors, the present investigation was performed at such roughnesses, namely a roughness with two-dimensional ribs ( $p/h=9$ ) and one with three-dimensional ribs.

## 2. The experiment

The basic experimental apparatus was the same as it was used before /6,7/. It is run with air at pressures only little above atmospheric pressure. The heated rough rods are up to 2000 mm long. At the lower end of the test section a measuring device was inserted which could be rotated and carried three cross slides for a Pitot tube and two temperature probes. The circular Pitot tube had an outer diameter of 0.6 mm and a length of 10 mm. The temperature was measured by means of Chromel/Alumel thermocouples with a sheath-diameter of 0.36 mm. The details can be seen in figure 1. Since three different outer tubes were tested, the measuring device had to be adapted to the respective diameter. The geometrical parameters of the roughnesses and the annuli can be taken from table 1. The range of Reynolds numbers was limited at the upper bound by the Mach-number or the capacity of the compressor and at the lower bound by the difficulties to measure a stable velocity profile. The experimental parameters are listed together with the results in table 2 and 3.

The pressure drop and the wall temperatures along the test section were measured together with the velocity and temperature profiles. Since the three cross slides for the temperature probes and the Pitot tube were mounted  $120^{\circ}$  apart in circumferential direction the temperature and the velocity profiles were measured at different positions. Before each test series the velocity profiles at different circumferential positions were measured. It was not possible to get an axisymmetrical velocity distribution in any test section, fabrication tolerances were obviously too large. Therefore, the measurements were taken at a circumferential position where the velocity distribution was similar to the average one. Measurements were also taken at different positions. This explains partly the scatter of the results.

### 3. Evaluation

The bulk measurements of the pressure drop and heat transfer were evaluated as described before /6,8,10/. The transformation of the bulk data to the rough zone was performed with the methods based on equations (1) and (2) using a constant  $A_r=2.5$ . The hydraulic diameter was defined volumetrically for all calculations.

The shear stress at the smooth outer wall  $\tau_2$  was determined from the differential pressure between the Preston tube and the static pressure hole in the smooth wall. The density of the air was calculated with the temperature at this position.

The shear stress at the rough rod was determined from the total shear stress  $\tau_m$ , which is known from the axial pressure drop, and the shear stress at the smooth wall  $\tau_2$ :

$$\tau_1 = \frac{\beta^2 - \alpha^2}{\alpha (1 - \beta^2)} \tau_2 \quad (3)$$

with

$$\beta = \left[ 1 - \frac{\tau_2}{\tau_m} (1 - \alpha) \right]^{1/2} \quad (4)$$

The mean velocities  $u(r)$  were calculated with the differential pressure between Pitot tube and the wall tapping on the same plane. For non-isothermal conditions the density of the air was determined with the temperature at the respective radial position.

No corrections on the Pitot tube readings were applied. Neither were any corrections applied to the temperature readings.

Average velocities and temperatures for the smooth and rough zone and the whole flow cross section were determined by integrating numerically over the respective areas:



$$\bar{u} = \frac{2\pi \sum_i u(r_i) \rho(r_i) (r_i^2 - r_{i-1}^2)}{A \bar{\rho}} \quad (5)$$

$$\bar{T} = \frac{2\pi \sum_i T(r_i) u(r_i) \rho(r_i) c_p(r_i) (r_i^2 - r_{i-1}^2)}{A \bar{u} \bar{\rho} \bar{c}_p} \quad (6)$$

with A being the respective cross section of the zones or the total annulus and the bar denoting the average value in the respective area. The calculation was performed iteratively over  $\bar{T}$ .

The non-dimensional velocity  $u^+$  and temperature  $T^+$  was formed with the friction velocity  $u_\tau$ , which was determined at the average temperature of the smooth or rough zone, respectively.

$$u_{\tau 2} = (\tau_2 / \rho_s)^{1/2} \quad (7)$$

and 
$$u_{\tau 1} = (\tau_1 / \rho_r)^{1/2} \quad (8)$$

$$u^+ = u / u_{\tau 1} \quad (9)$$

$$T^+ = \frac{(T_{w1} - T)}{q} \rho_r c_{pr} u_{\tau 1} \quad (10)$$

From the velocity and temperature traverses the quantities eddy viscosity and eddy conductivity can be determined, if the shear stress distribution and heat flux distribution are known.

By a force balance and the condition  $\partial p / \partial r = 0$  the shear stress distribution in the inner rough zone is given by

$$\frac{\tau}{\tau_1} = \frac{\beta^2 - (r/r_2)^2}{\beta^2 - a^2} \frac{a}{(r/r_2)} \quad (11)$$

and for the outer smooth zone it is

$$\frac{\tau}{\tau_2} = \frac{(r/r_2)^2 - \beta^2}{1 - \beta^2} \frac{1}{r/r_2} \quad (12)$$

Neglecting the kinematic viscosity  $\nu$  the eddy viscosity is defined by

$$\tau = \rho \epsilon \frac{\partial u}{\partial r} \quad (13)$$

A non-dimensional eddy viscosity  $\epsilon^+$  can be derived from (11), (12) and (13):

$$\epsilon_r^+ = \frac{\epsilon_r}{u_{\tau 1} \hat{Y}_r} = \frac{\beta^2 - (r/r_2)^2}{\beta^2 - \alpha^2} \frac{\alpha}{(r/r_2)} \frac{\partial (\frac{y}{Y_r})}{\partial u^+} \quad (14)$$

and

$$\epsilon_s^+ = \frac{\epsilon_s}{u_{\tau 2} \hat{Y}_s} = \frac{(r/r_2)^2 - \beta^2}{1 - \beta^2} \frac{r_2}{r} \frac{\partial (\frac{y}{Y_s})}{\partial u^+} \quad (15)$$

For a fully developed flow the heat flux distribution in the annulus is similar to the shear stress distribution. With the condition  $\partial T / \partial x = \text{const.}$  and  $q_2 = 0$ , the heat flux distribution is given by

$$\frac{q}{q_1} = \frac{r_1}{r} \frac{1 - (r/r_2)^2}{1 - \alpha^2} \quad (16)$$

The eddy conductivity is defined by

$$q = \epsilon_H \rho c_p \frac{\partial T}{\partial r} \quad (17)$$

From (16) and (17) a non-dimensional eddy conductivity is derived

$$\epsilon_H^+ = \frac{\epsilon_H}{u_{\tau 1} \hat{Y}_r} = \frac{q_1}{u_{\tau 1} \bar{c}_p \bar{\rho}} \frac{\alpha [1 - (r/r_2)^2]}{(\beta - \alpha)(1 - \alpha^2)} \frac{1}{r} \frac{\partial r}{\partial T} \quad (18)$$

An alternative assumption about the heat flux distribution leads to

$$\frac{q}{q_1} = \frac{r_1}{r} \frac{m_B^{-m(r)}}{m_B} \quad (19)$$

and to

$$\epsilon_H^+ = \frac{\epsilon_H}{u_{\tau 1} \hat{y}_r} = \frac{q_1}{\bar{\rho} \bar{c}_p u_{\tau 1}} \frac{\alpha}{\beta - \alpha} \frac{m_B^{-m(r)}}{m_B} \frac{1}{r} \frac{\partial r}{\partial T} \quad (20)$$

For the final evaluation equation (20) was used although the differences of the results using equation (18) were small.

The values of the eddy viscosity and the eddy conductivity were calculated directly from the measured velocities and temperatures.

The velocity profile parameters  $A_s$ ,  $A_r$  and  $R$  were determined from integral quantities such as the bulk velocities. By the conditions that the integration of equations (1) and the corresponding equation for the smooth zone

$$u_s^+ = A_s \ln y_s^+ + B \quad (21)$$

over the respective zones must yield the bulk velocities, and that the zero shear stress plane is given by the intersection of the two velocity profiles originating at the respective walls, the profile parameters are determined:

$$A_s = \frac{(\bar{u}_s^+ - B)}{\ln \hat{y}_s^+} - \frac{1}{2} \frac{3+\beta}{1+\beta} \quad (22)$$

$$A_r = \frac{(A_s \ln \hat{y}_s^+ + B) \frac{u_{\tau 2}}{u_{\tau 1}} - \bar{u}_r^+}{\frac{1}{2} \frac{3+\beta/\alpha}{1+\beta/\alpha}} \quad (23)$$

$$R = (A_s \ln \hat{y}_s^+ + B) \frac{u_{\tau 2}}{u_{\tau 1}} - A_r \ln(\hat{y}_r/h) \quad (24)$$

The parameter  $B$  was set to  $B=5.5$

Similar to the evaluation of the slope of the velocity profile  $A_r$  from integral quantities, a slope of the temperature profile  $A_H$  can be determined.

There are two conditions which have to be met by an artificial temperature profile:

- (1) integration over the entire annular flow cross section must yield the gas bulk temperature  $T_B$ ,
- (2) integration over the inner 'rough' zone must yield the bulk temperature of that zone  $T_1$ .

The temperature  $T_1$  is determined by numerical integration of the measured temperature and velocity profiles according to equation (6).

Condition (1) can be written as

$$\frac{(T_W - T_B) \rho_B c_{pB} u_B}{q_1} \frac{u_{\tau 1}}{u_B} = A_H \ln \left( \frac{1-\alpha}{h/r_2} \right) - \frac{A_H}{2} \frac{3+1/\alpha}{1+1/\alpha} + G^* \quad (25)$$

and condition (2) is

$$\frac{(T_W - T_1) \rho_B c_{pB} u_{\tau 1}}{q_1} = A_H \ln \left( \frac{\beta-\alpha}{h/r_2} \right) - \frac{A_H}{2} \frac{3+\beta/\alpha}{1+\beta/\alpha} + G^* \quad (26)$$

Equation (25) and (26) combined give

$$A_H = \frac{(T_1 - T_B) \rho_B c_{pB} u_{\tau 1}}{q_1 \left[ \ln \left( \frac{1-\alpha}{h/r_2} \right) - \ln \left( \frac{\beta-\alpha}{h/r_2} \right) + \frac{1}{2} \left\{ \frac{3+\beta/\alpha}{1+\beta/\alpha} - \frac{3+1/\alpha}{1+1/\alpha} \right\} \right]} \quad (27)$$

#### 4. Results

##### Parameters evaluated from point data

From the large amount of data only a sample fraction is presented in diagrams. All results are tabulated in table 2 and 3.

Figures 3 and 4 show the velocity distribution in the two extreme flow channels with  $\alpha=0.262$  and  $\alpha=0.468$ , separate for isothermal flow and one respectively two temperature ratios  $T_W/T_B$ . The symbols are rotated by  $45^\circ$  for different runs, which means different Reynolds numbers, and the pertinent parameters can be found in table 2 and 3 by the corresponding test number.

Temperature profiles for two test sections are shown in figures 5 and 6.

Mean velocity profiles of the smooth zone are plotted in figure 7 in non-dimensional form, together with a straight line representing the 'law of the smooth wall' according to equation (19) with  $A_s=2.5$  and  $B=5.5$ . Most measured points are below this line but the slope is very close to 2.5. This was the case for all test sections.

Figures 8,9 and 10 show non-dimensional velocity profiles in the rough zone together with a best fit line representing the 'law of the rough wall'. The corresponding parameters  $A_r$  and  $R$  are listed in table 3 (ARP, RHP). The slope  $A_r$  is generally below 2.5. There is no effect of the Reynolds number in the fully rough regime, but at low Reynolds numbers, respectively  $h^+$ -values, the slope  $A_r$  increases. Unfortunately the fluctuations of the flow became too big at low mass flow rates which made further measurements impossible. A compilation of all slopes  $A_r$  is shown in figures 11 and 12. There is no definite effect of the relative roughness height, neither is the effect of the temperature clear cut, although for nonisothermal flow the slope  $A_r$  is higher in most cases. The slopes at the 3-dimensional roughness are at the lower bound of the range of scatter.

Samples of non-dimensional temperature profiles are shown in the figures 13,14 and 15. A straight line with the slope  $A_r$  of the corresponding velocity profile is drawn through one of the measured points. For most of the profiles there is a region close to the wall, where this line fits quite well.

For small radius ratios  $\alpha$ , such as in test section 23-70, the logarithmic 'law of the wall' describes the temperature distribution up to the smooth wall with sufficient accuracy, taking the same slope  $A_r$  as for the velocity profile. For bigger radius ratios (test section 23-50) the deviation of the temperature profile from a straight line far away from the rough rod increases. This deviation is very large for the other test sections with a  $r_1=16.3$ . Those temperature profiles look all similar to those shown in figure 15. Here an additional line with a slope of 2.5 is shown. This line and the straight line of the upper profile intersect at the same G-value at  $y/h=1$ . The line with the slope 2.5 comes very close to the measured temperature at the smooth wall. This might explain, why the G-value determined by the temperature of the smooth wall together with a slope  $A_r=2.5$ , namely

$$G^+ = \frac{(T_{W1} - T_{W2}) \bar{\rho} \bar{c}_p u_{\tau 1}}{q_1} - A_r \ln \left( \frac{1-\alpha}{h/r_2} \right), \quad (28)$$

as it was proposed in /6/, yields reasonable results.

The next seven figures show samples of the eddy diffusivities of momentum and heat in non-dimensional form. Figures 16 shows the eddy viscosity in the smooth zone together with a best fit line. There was no appreciable difference between the different test sections. The maximum value of  $\epsilon_s^+$  was between 0.10 and 0.11 at a  $y_s/\hat{y}_s$  between 0.5 and 0.6 for all test sections, with the exception of test section 12-71 (not shown) where the maximum was between 0.11 and 0.12.

The eddy viscosity in the rough zone is shown in the figures 17, 18 and 19. The general trend for the maximum is to be higher for higher relative roughness heights and to be higher for the 3-dimensional roughness. The difference between test section 23-70 and 22-70 (minimum and maximum  $h/\hat{y}_r$ ) is approximately 0.015 and between 22-70 and 12-70 (2-dimensional and 3-dimensional roughness) again approximately 0.015.

The eddy diffusivity of heat is shown in the figures 20, 21 and 22 for the same three test sections. Its distribution is more uniform than that of the eddy viscosity.

From these results a turbulent Prandtl number can be found which is defined by

$$\text{Pr}_t = \frac{\epsilon_M}{\epsilon_H} . \quad (29)$$

Its reciprocal value is shown in figure 23 together with some data from the literature for turbulent flow in smooth tubes. The disparity of  $\text{Pr}_t$  measurements or analytical functions in the literature is very large, so only the minimum and the maximum data are shown, besides one of the more recent measurements by Mc Eligot /11/. The results for test section 12 and 22 in both outer tubes fall together in a narrow band.

#### Parameters evaluated from integral data

The slopes of the smooth and of the rough profiles,  $A_S$  and  $A_R$ , determined by equations (22) and (23) are plotted in figure 24 and 25.

The value of  $A_S$  was reduced by the  $h/\hat{y}_S$ -effect as it was found for flow at high Reynolds numbers in a rectangular channel /1,3,5/.

$$A_{SO} = A_S - 0.4/\ln \left( 0.1 \frac{h}{\hat{y}_S} \right) \quad (30)$$

The value of  $A_{SO}$  decreases at lower Reynolds numbers in all test sections. The amount of the decrease is smaller in the test sections with small relative roughness height (23-72 and 23-50). A mean function

$$A_{SO} = 2.55 - 55/Re_S^{0.56} \quad (31)$$

is plotted in figure 24.

The parameter  $A_r$  of the rough profile is plotted versus  $h^+$  in figure 25 together with a function

$$A_r = 1.5 + 20/h^+ \leq 2.5 \quad (32)$$

which describes the general trend of the data, but does not fit for all measurements.

A systematic effect of the different roughnesses or the different relative roughness heights can not be detected. The effect of different relative roughness heights which was found at higher values of  $h/\hat{y}_r$  in a rectangular channel /1/ was given by

$$A_r = 2.5 + E/\ln \left( \frac{h}{\hat{y}_r} \right) . \quad (33)$$

The maximum difference for the present measurements between test section 23-72 and 22-71 would be  $\Delta A_r = 0.17$  (with  $E=2.09$  for  $p-b/h=8$ ), a value which is within the uncertainty of the experiment. However, the slopes  $A_r$  at high Reynolds numbers are generally lower by approximately 0.4 than the prediction by equation (33).



The slope  $A_H$  of the temperature profile evaluated by equation (27) is plotted versus  $h_W^+$  in figure 25c. For the rods 12 and 22 in both outer tubes there is a general trend of  $A_H$  to increase with decreasing  $h_W^+$ . The line  $A_H=1.4+3/\log(h_W^+)$  of test section 22/85 is shown as a reference in all plots. The slopes  $A_H$  for rod 23 are constant with approximately  $A_H=1.75$ .

### Transformation of bulk data

The following figures show the data evaluated from the pressure drop and wall temperature measurements along the test section.

The bulk friction factor, the transformed friction factor  $f_1$  and the temperature corrected friction factor  $f_{1R}$  are shown in figures 26-31. The transformation was performed with  $A_r=2.5$  and a variable  $A_s$  as developed in /6/. The temperature effect was reduced by

$$f_{1R} = f_1 \left( \frac{T_W}{T_r} \right)^{0.29} \quad (34)$$

taken from /8/.

The bulk Stanton number, the temperature reduced Stanton number and the transformed Stanton number are plotted in figures 32-37. The temperature reduction and transformation which was applied was proposed in /8/.

The roughness parameters R and G of the velocity profile and of the temperature profile, respectively were evaluated with a constant slope  $A_r=2.5$  and are shown in figures 38-43. The G-parameter was determined by the bulk temperature ( $G^*$ ) and by the outer wall temperature ( $G^+$ ) (see Eq. (A-4) and (A-7) in the appendix).

In order to see the effect of the different slopes  $A_s$  and  $A_r$ , as they resulted from the present measurements the calculations were repeated with

$$A_S = 2.55 + \frac{0.4}{\ln(0.1 h/(r_2(1-\beta)))} - \frac{55}{Re_2^{0.56}} \quad (35)$$

and

$$A_r = 2.5 + \frac{3.0}{\ln(h/(r_2(\beta-\alpha)))} + \frac{20}{h^+} \quad (36)$$

The parameter E from equation (33) was increased to E=3.0 to take account of the lower slopes in the present experiment compared to the experiments performed in the rectangular channel.

The results are listed in table 3 and the new  $G^+, G^*$  and R-values are plotted in the figures 44-49. A comparison of the transformed friction factors shows that they are generally smaller with the new  $A_S$ - and  $A_r$ -functions by 1-6%. The difference is small at high Reynolds numbers (1-2%) and for small radius ratios (23-72). Large differences occur at small Reynolds numbers due to the decreasing value of  $A_S$ . The magnitude of  $A_r$  does not change the friction factor  $f_1$  considerably in the region of  $h/\hat{y}_r < 0.04$ . This was found in the rectangular flow channel, too /1,3,5/. The R- and G-functions, however, are quite different. Due to the increasing  $A_r$  with decreasing  $h^+$  the R-functions are no longer increasing. For the test sections 23-35 and 23-37 the resulting R-functions are not constant, the applied  $A_S$ - and  $A_r$ -functions need to be improved.

In figure 50 it can be seen that the new functions  $A_S$  and  $A_r$  improve the correlation of the R-parameter at different relative roughness heights. Here the R-parameter is plotted, which resulted of pressure drop measurements at test rod No.12 in four outer tubes of 40,50,70, and 85 mm I.D. The improvement is obvious, the R-function is constant down to  $h^+ = 20$ .

## 5. Conclusions

Because it was not possible to obtain an axis-symmetric flow in any of the annular test sections the uncertainty of the results is rather large. The effects of different relative roughness heights, the curvature of the flow channel, the temperature ratios and different roughnesses, on the velocity and temperature distribution could not or only partially be detected. There are, however, some new facts which can be derived from the measurements with a high degree of certainty.

The influence of the roughness on the flow in the smooth zone of a partially rough flow channel was confirmed. The slope  $A_g$  of the non-dimensional velocity profile at the smooth wall is lower than 2.5 and decreases further with decreasing Reynolds number. The slope  $A_r$  of the rough profile is approximately 1.5 at high  $h^+$ -values, for the roughnesses tested, and increases with falling  $h^+$ -values up to  $A_r=2.5$ . The effect on the transformed friction factor  $f_1$  of the rough zone by the changed slope  $A_g$  is bigger than that of a different  $A_r$  ( $A_r=1.5$  versus  $A_r=2.5$ ). In the range  $h/\hat{y}_r \leq 0.04$  the friction factor  $f_1$  decreases on the average by 1-2% at high  $h^+$ -values and up to 6% at low  $h^+$ . The R-functions of different relative roughness heights can be correlated better than before.

The slopes of the rough velocity profile describe the non-dimensional temperature profile only in a limited range of distances from the rough wall. The deviation from a logarithmic straight line is large far from the wall, especially for high roughnesses. In this case a slope of  $A_r=2.5$  fits quite well for the temperature  $T_{W2}$  at the opposite smooth wall, but not for the temperature distribution in the rest of the flow cross section.

The eddy diffusivities of momentum and heat are somewhat higher than for smooth channel flow, but the difference is small. The turbulent Prandtl number is smaller than 1 with a maximum near 1 at  $y/\hat{y} = 0.5$ .

Acknowledgement

The author wishes to thank Mr. J. Marek for constructing the measuring device, Mr. P. Durand for the performance of the experiments and Mr. A. Roth for the preparation of the drawings.

References

- /1/ L. Meyer:  
Turbulent flow in a plane channel having one or two rough walls. Int. J. Heat Mass Transfer, 23 (5), 591-608 (1980) see also: Turbulente Strömung an Einzel- und Mehrfachrauigkeiten im Plattenkanal, KfK-Bericht Nr. 2764 (1979), Dr.-Ing. Thesis, Univ. Karlsruhe (1978)
- /2/ W. Baumann:  
Geschwindigkeitsverteilung bei turbulenter Strömung an rauhen Wänden, KfK-Bericht Nr. 2618 (1978) und Nr. 2680 (1978), Dr.-Ing. Thesis, Univ. Karlsruhe (1978)
- /3/ L. Meyer and L. Vogel:  
The velocity distribution and pressure loss at artificial roughnesses with sharp and rounded edges, Kernforschungszentrum Karlsruhe, KfK-Report 2885 (1979)
- /4/ F.P. Berger and A.W. Whitehead:  
Fluid flow and heat transfer in tubes with internal square rib roughening, J. Br. Nucl. Energy Soc. 16,2,153-160 (1977)
- /5/ L. Meyer:  
The velocity distribution and pressure loss at three-dimensional roughnesses, OECD-NEA Co-ordinating Group on GCFR-Development, 6th Heat Transfer Specialists Meeting 1980, Berkeley, U.K.
- /6/ M. Dalle Donne, L. Meyer:  
Turbulent convective heat transfer from rough surfaces with two-dimensional rectangular ribs, Int. J. Heat Mass Transfer 20,6,583-620 (1977)
- /7/ M. Dalle Donne and L. Meyer:  
Turbulent convective heat transfer from rough surfaces with two-dimensional ribs: transitional and laminar flow, Report KfK-2566, EUR-5751e (1978)

- /8/ L. Meyer and K. Rehme:  
Heat Transfer and pressure drop measurements with roughened single pins cooled by various gases, Report KfK-2980 (1980)
- /9/ M. Dalle Donne, M. Hudina, M. Huggenberger, L. Meyer, K. Rehme:  
EIR, KfK joint heat transfer experiment on a single rod, roughened with trapezoidal rounded ribs and cooled by various gases, KfK-Bericht Nr. 2674 (1978)
- /10/ K. Maubach:  
Rough annuli pressure drop. Interpretation of experiments and recalculation for square ribs, Int. J. Heat Mass Transfer 15, 2489-2498 (1972)
- /11/ D.M. Mc Eligot, P.E. Pickett and M.F. Taylor:  
Measurement of wall region turbulent Prandtl numbers in small tubes, Int. J. Heat Mass Transfer, 19, 799-803 (1976)
- /12/ A. Quarmby and R. Quirk:  
Measurements of the radial and tangential eddy diffusivities of heat and mass in turbulent flow in a plane tube, Int. J. Heat Mass Transfer 15, 2309-2327 (1972).
- /13/ R.G. Deissler:  
Analysis of fully developed turbulent heat transfer at low Reynolds numbers in smooth tubes with application to liquid metals. N.A.C.A. R&M E 52 F 05 (1952)
- /14/ A. Aytakin:  
Turbulent flow and heat transfer in channels with combined rough and smooth surfaces, Ph.D. Thesis, Univ. London (1978)
- /15/ R. Firth:  
A method of analysing heat transfer and pressure drop data from partially roughened annular channels, UKAEA, Windscale, ND-R-301 (W) (1979)

Nomenclature

A	area of flow cross-section ( $m^2$ )
$A_r, A_s$	slopes of the logarithmic velocity profiles
B	constant of the logarithmic velocity profile at smooth walls;
b	width of the roughness rib (m)
$c_p$	specific heat at constant pressure ( $Ws\ kg^{-1}\ K^{-1}$ )
$d_h$	hydraulic diameter (m)
e	length (z-direction) of a rib (m)
f	friction factor = $2\tau/\rho u^2$
$f_o$	friction factor of a smooth tube
G	parameter in the logarithmic temperature profile
g	gap (z-direction) between two ribs (m)
h	height of roughness ribs (m)
$h^+$	dimensionless height of roughness rib = $h u_\tau/\nu$
p	axial pitch of the repeated roughness rib (m)
p	pressure ( $Nm^{-2}$ )
Pr	Prandtl number
q	heat flux ( $Wm^{-2}$ )
R	parameter of the logarithmic velocity profile at rough walls
r	radius (m)
Re	Reynolds number = $\bar{u}d_h/\nu$ .
St	Stanton number (=Nu/RePr)

T	temperature (K)
$T^+$	dimensionless temperature $(=(T_W - T) \rho c_p u_\tau / q)$
u	mean velocity ( $\text{ms}^{-1}$ )
$u_\tau$	friction velocity $= (\tau/\rho)^{1/2}$ ( $\text{ms}^{-1}$ )
$u^+$	dimensionless velocity $= u/u_\tau$
$\bar{u}$	average velocity in a section ( $\text{ms}^{-1}$ )
y	radial distance (m)
$y^+$	dimensionless distance from the wall $= yu_\tau/\nu$
$\hat{y}$	radial distance between wall and the zero shear stress plane (m)
x	axial distance

Greek symbols

$\alpha$	$r_1/r_2$
$\beta$	$r_o/r_2$ (m)
$\epsilon_M$	eddy diffusivity for momentum ( $\text{m}^2 \text{s}^{-1}$ )
$\epsilon_H$	eddy diffusivity for heat ( $\text{m}^2 \text{s}^{-1}$ )
$\epsilon^+$	non-dimensional eddy diffusivity
$\nu$	kinematic viscosity ( $\text{m}^2 \text{s}^{-1}$ )
$\rho$	density ( $\text{kgm}^{-3}$ )
$\tau$	shear stress ( $\text{Nm}^{-2}$ )

Subscripts

max	maximum
r	pertaining to the rough zone
s	pertaining to the smooth zone



vol volumetric definition of origin of velocity profil  
B bulk  
W wall  
1 refers to the inner rough rod  
2 refers to the outer smooth tube  
o position of zero shear stress

Appendix

Nomenclature of the tables (where not self-explaining)

Reduced Stanton number:

$$STPR = \frac{St_B}{1 + 14 Re_B^{-0.35} \lg \left[ 4.35 \left( \frac{x}{D_h} \right)^{-0.6} \right]} \left( \frac{T_W}{T_B} \right)^{-ex} Pr^{0.6} \quad /8/ \quad (A-1)$$

The denominator in (A-1) is set to 1, if it becomes smaller than 1.

Ratio of transformed to bulk Stanton number:

$$ST1+ / = \left( \frac{St_1}{St_B} \right)^+ = \frac{\frac{1}{St_B} \sqrt{\frac{f_1}{2}}}{G^+ + 2.5 \ln \left( \frac{\beta - \alpha}{h/r_2} \right) - \frac{A_r}{2} \frac{(1+3\alpha/\beta)}{(1+\alpha/\beta)}} \quad /6/ \quad (A-2)$$

$$ST1* / = \left( \frac{St_1}{St_B} \right)^* = \frac{\frac{1}{St_B} \sqrt{\frac{f_1}{2}}}{G^* + 2.5 \ln \left( \frac{\beta - \alpha}{h/r_2} \right) - \frac{A_r}{2} \frac{(1+3\alpha/\beta)}{(1+\alpha/\beta)}} \quad /6/ \quad (A-3)$$

$$STT+ / = St_{1T} / St_B, \quad \text{transformed with } G(h^+) \quad /8/$$

$$STT* / = St_{1T} / St_B, \quad \text{transformed with } G(h^+)^* \quad /8/$$

$$St1F = St_{1F} / St_B \quad St_{1F} \text{ obtained with Firth transformation } /15/$$

$$G^+ = \frac{(T_W - T_{W2}) \rho_B c_{pB} u_1^*}{q_1} - A_r \ln \left( \frac{1-\alpha}{h/r_2} \right) \quad (A-4)$$

$$GPR1 = \frac{G^+}{Pr^{0.44} \left( \frac{T_W}{T_B} \right)^{0.5} \left( \frac{h}{0.01(r_2 - r_1)} \right)^{0.053}} \quad (A-5)$$

$$G = \frac{\frac{G(h^+)}{\text{Pr}^{0.44}} - g'}{(T_W/T_B)^{0.68}} \quad \text{with } g' = 10^{(1.4872 - 0.1212 h_w^+)} / 16/ \quad (\text{A-6})$$

$$G^* = \frac{1}{\text{St}_B} \sqrt{\frac{f_1}{2}} \frac{u_1}{u_B} - A_r \ln \left( \frac{1-\alpha}{h/r_2} \right) + \frac{A_r}{2} \frac{(1+3\alpha)}{(1+\alpha)} \quad (\text{A-7})$$

$$G_R^* = \frac{1}{\text{St}_{BR}} \sqrt{\frac{f_1}{2}} \sqrt{\left( \frac{T_W}{T_1} \right)^{0.29}} \frac{u_1}{u_B} - A_r \ln \left( \frac{1-\alpha}{h/r_2} \right) + \frac{A_r}{2} \frac{(1+3\alpha)}{(1+\alpha)} \quad (\text{A-8})$$

with  $\text{St}_{BR}$  according to Eq. (A-1)

$$G_T = \frac{\sqrt{\frac{f_1}{2}}}{\text{St}_{1T}} - A_r \ln \left( \frac{\beta-\alpha}{h/r_2} \right) + \frac{A_r}{2} \frac{(1+3\alpha/\beta)}{(1+\alpha/\beta)} \quad (\text{A-9})$$

$\text{St}_{1T}$  is the Stanton number transformed with the method proposed in /8/.

$$G_{TR} = \frac{\sqrt{\frac{f_{1R}}{2}}}{\text{St}_{1TR}} - A_r \ln \left( \frac{\beta-\alpha}{h/r_2} \right) + \frac{A_r}{2} \frac{(1+3\alpha/\beta)}{(1+\alpha/\beta)} \quad (\text{A-10})$$

with

$$\text{St}_{1TR} = \frac{\text{St}_{1T}}{1 + 14 \text{Re}_1^{-0.35} \left[ \lg 4.35 \left( \frac{x}{D_1} \right) \right]^{-0.6}} \left( \frac{T_W}{T_1} \right)^{-\text{ex}} \text{Pr}^{0.6} \quad (\text{A-11})$$

$$\text{and } f_{1R} = f_1 \left( \frac{T_W}{T_1} \right)^{0.29} \quad (\text{A-12})$$

$$G_{TF} = \frac{\sqrt{\frac{f_1}{2}}}{\text{St}_{1F}} - A_r \ln \left( \frac{\beta-\alpha}{h/r_2} \right) + \frac{A_r}{2} \frac{(1+3\alpha/\beta)}{(1+\alpha/\beta)} \quad (\text{A-13})$$

with /15/:

$$St_{1F} = St \left[ \frac{f_1 D_h}{D_1 F} \right]^{0.5} \left[ 1 + \frac{9}{(1+D_1/8r_1)} St_1 \frac{(1-\beta^2)}{(1-\alpha^2)} \sqrt{\frac{2}{f_1}} \right] \quad (A-14)$$

$G_{TFR}$  is calculated with  $St_{1F}$ .

$$H+W = h_W^+ = \frac{h u_1^+}{v_W} \quad (A-15)$$

$$H+RW = h_{WR}^+ = \frac{h u_{1R}^*}{v_W} = h_W^+ \sqrt{\left( \frac{T_W}{T_1} \right)^{0.29}} \quad (A-16)$$

$$RH+ = R(h^+) = \sqrt{\frac{2}{f_1}} - A_r \ln \left( \frac{\hat{y}}{h} \right) + \frac{A_r}{2} \frac{1+3\alpha/\beta}{1+\alpha/\beta} \quad (A-17)$$

$$RH+R = R(h^+)_R = \sqrt{\frac{2}{f_{1R}}} - A_r \ln \left( \frac{\hat{y}}{h} \right) + \frac{A_r}{2} \frac{1+3\alpha/\beta}{1+\alpha/\beta} \quad (A-18)$$

$$X = \ln \left( \frac{\hat{y}}{h} \right) - \frac{1}{2} \frac{3+\beta/\alpha}{1+\beta/\alpha}$$

$$Y_R = \sqrt{2/f_1}$$

$$Y_G = \sqrt{2/f_1/St_{1F}}$$

$$ASI = A_s \quad (\text{Eq. 22})$$

$$ARI = A_r \quad (\text{Eq. 23})$$

$$RHI = R \quad (\text{Eq. 24})$$

$$ARP = A_r$$

$$RHP = R$$

$$G(H+)$$

} from least square fit

Symbols in the plots

□ isothermal runs

○ thermal runs, increasing  $T_w/T_B$ -ratio

△ with arrow; the exact  $T_w/T_B$ -ratios

↓ can be taken from the tables,

Test section	$r_2$	$r_1$ vol	$\frac{r_1 \text{ vol}}{r_2}$	$h/(r_2-r_1)$	Roughness	p	h	b	e	g
23-72	35.0	9.18	0.262	0.0116	2-dimensional	2.7	0.3	0.3		
23-50	25.0	9.18	0.368	0.0190		2.7	0.3	0.3		
22-85	42.45	16.38	0.386	0.0268		6.3	0.7	0.7		
22-71	35.0	16.38	0.468	0.0376		6.3	0.7	0.7		
12-85	42.45	16.26	0.383	0.0229	3-dim.	1.6	0.6	0.3	0.3	0.29
12-71	35.0	16.26	0.465	0.0320		1.6	0.6	0.3	0.3	0.29

Table 1: Testparameter



VERS.NR.	RE*E4	RE1*E4	F	F1	STB	STPR	F1/F2	TW/TB	TW/T1	PR	H/Y	BETA	H+	H+W	H+R	H+RW	RH+	RH+R	AS	AR
23-50- 1	1.95	2.96	.01021	.01780	.00523	.00462	2.42	1.32	1.27	.705	.0342	.719	16.2	10.6	16.7	11.0	4.27	3.91	2.42	2.50
23-50- 2	2.83	4.74	.01053	.02047	.00545	.00482	2.99	1.32	1.28	.705	.0318	.746	25.2	16.4	26.1	17.0	3.36	3.01	2.42	2.50
23-50- 3	4.27	7.59	.01040	.02162	.00550	.00486	3.43	1.33	1.29	.705	.0304	.763	39.1	25.1	40.5	26.0	2.97	2.62	2.41	2.50
23-50- 4	5.79	10.44	.00992	.02092	.00544	.00483	3.55	1.34	1.30	.706	.0301	.767	52.1	33.0	54.1	34.2	3.09	2.72	2.41	2.50
23-50- 5	8.76	16.34	.00953	.02075	.00515	.00459	3.83	1.35	1.31	.706	.0294	.777	78.6	48.9	81.8	50.9	3.07	2.69	2.41	2.50
23-50- 6	12.25	23.50	.00929	.02080	.00500	.00447	4.10	1.36	1.32	.706	.0288	.785	110.1	67.7	114.7	70.5	3.00	2.61	2.40	2.50
23-50- 7	17.38	34.00	.00889	.02022	.00460	.00412	4.27	1.37	1.33	.707	.0285	.790	154.5	93.8	161.1	97.8	3.13	2.72	2.40	2.50
23-50- 8	3.95	5.79	.00936	.01776	.00470	.00480	2.87	1.85	1.70	.701	.0332	.731	30.3	12.3	32.7	13.3	4.21	3.42	2.41	2.50
23-50- 9	8.13	13.16	.00888	.01848	.00467	.00479	3.46	1.86	1.73	.702	.0311	.756	64.5	25.3	69.8	27.4	3.81	3.01	2.41	2.50
23-50-10	11.84	19.63	.00846	.01796	.00446	.00461	3.62	1.89	1.76	.702	.0306	.762	92.8	35.6	100.7	38.6	3.92	3.09	2.40	2.50
23-50-11	16.85	35.84	.00952	.02231	.0	.0	4.58	1.00	1.00	.710	.0275	.803	163.5	163.5	163.5	163.5	2.54	2.54	2.40	2.50
23-50-12	11.31	23.49	.00987	.02257	.0	.0	4.29	1.00	1.00	.711	.0280	.796	110.4	110.4	110.4	110.4	2.53	2.53	2.40	2.50
23-50-13	7.80	15.82	.01025	.02287	.0	.0	4.04	1.00	1.00	.710	.0285	.789	76.7	76.7	76.7	76.7	2.51	2.51	2.41	2.50
23-50-14	5.73	11.33	.01048	.02271	.0	.0	3.77	1.00	1.00	.710	.0291	.780	56.2	56.2	56.2	56.2	2.59	2.59	2.41	2.50
23-50-15	4.06	7.69	.01050	.02164	.0	.0	3.36	1.00	1.00	.709	.0301	.767	39.0	39.0	39.0	39.0	2.91	2.91	2.41	2.50
23-50-16	2.88	5.35	.01103	.02219	.0	.0	3.19	1.00	1.00	.708	.0306	.760	28.0	28.0	28.0	28.0	2.84	2.84	2.42	2.50
23-50-17	2.58	4.74	.01117	.02224	.0	.0	3.12	1.00	1.00	.709	.0308	.757	25.2	25.2	25.2	25.2	2.85	2.85	2.42	2.50
23-50-18	1.80	3.09	.01103	.02021	.0	.0	2.63	1.00	1.00	.708	.0325	.737	16.8	16.8	16.8	16.8	3.47	3.47	2.42	2.50
23-50-19	31.70	71.22	.00958	.02398	.0	.0	5.47	1.00	1.00	.706	.0265	.822	317.2	317.2	317.2	317.2	2.17	2.17	2.39	2.50
23-50-20	18.90	40.76	.00960	.02288	.0	.0	4.79	1.00	1.00	.707	.0272	.808	185.4	185.4	185.4	185.4	2.40	2.40	2.40	2.50
23-50-21	12.01	25.04	.00983	.02257	.0	.0	4.34	1.00	1.00	.707	.0279	.797	117.2	117.2	117.2	117.2	2.52	2.52	2.40	2.50
23-50-22	8.78	17.87	.01002	.02239	.0	.0	4.05	1.00	1.00	.710	.0285	.789	85.5	85.5	85.5	85.5	2.60	2.60	2.41	2.50
23-50-23	5.95	11.93	.01067	.02354	.0	.0	3.92	1.00	1.00	.710	.0288	.785	59.3	59.3	59.3	59.3	2.41	2.41	2.41	2.50
23-50-24	4.26	8.29	.01092	.02327	.0	.0	3.62	1.00	1.00	.709	.0294	.775	42.3	42.3	42.3	42.3	2.53	2.53	2.41	2.50
23-50-25	2.93	5.50	.01128	.02312	.0	.0	3.32	1.00	1.00	.709	.0303	.765	29.0	29.0	29.0	29.0	2.64	2.64	2.42	2.50
23-50-26	1.95	3.38	.01096	.02032	.0	.0	2.69	1.00	1.00	.708	.0323	.740	18.2	18.2	18.2	18.2	3.42	3.42	2.42	2.50
23-50-27	1.49	2.17	.00947	.01405	.0	.0	1.81	1.00	1.00	.708	.0373	.690	11.8	11.8	11.8	11.8	5.83	5.83	2.43	2.50

VERS.NR.	RE*E4	Q<KW/M2>	ST1+ /	ST1* /	STT+ /	STT* /	STIF /	H+	G+	GPRI	G	G*	G*R	GT	GTR	GTF	GTFR	X	YR	YG
23-50- 1	1.95	6.1	1.15	1.11	1.20	1.16	1.24	16.2	9.4	9.2	7.7	9.9	13.0	8.7	11.7	8.2	11.2	2.54	10.60	14.6
23-50- 2	2.83	9.2	1.14	1.11	1.18	1.15	1.21	25.2	9.8	9.6	9.2	10.2	13.4	9.1	12.3	8.7	11.8	2.62	9.89	15.3
23-50- 3	4.27	14.2	1.12	1.10	1.17	1.15	1.20	35.1	10.1	9.9	9.7	10.4	13.6	9.5	12.7	9.1	12.3	2.67	9.62	15.8
23-50- 4	5.79	19.4	1.13	1.10	1.17	1.15	1.19	52.1	10.0	9.7	9.6	10.3	13.5	9.3	12.5	9.0	12.1	2.68	9.78	15.7
23-50- 5	8.76	28.3	1.12	1.09	1.16	1.14	1.18	78.6	10.9	10.6	10.4	11.3	14.5	10.3	13.6	10.0	13.2	2.71	9.82	16.8
23-50- 6	12.25	39.2	1.11	1.09	1.15	1.13	1.17	110.1	11.5	11.1	10.9	11.9	15.2	10.8	14.2	10.6	13.9	2.73	9.81	17.5
23-50- 7	17.38	52.0	1.10	1.08	1.14	1.12	1.15	154.5	12.9	12.4	12.2	13.3	16.8	12.2	15.9	12.1	15.5	2.74	9.94	18.9
23-50- 8	3.95	31.5	1.13	1.09	1.17	1.14	1.23	30.3	11.4	9.5	8.1	11.9	13.0	10.7	12.8	9.8	10.9	2.57	10.61	16.2
23-50- 9	8.13	65.4	1.11	1.09	1.16	1.14	1.21	64.5	11.9	9.8	9.1	12.2	13.3	11.2	13.3	10.4	11.5	2.64	10.40	17.0
23-50-10	11.84	92.2	1.11	1.09	1.15	1.13	1.20	92.8	12.5	10.3	9.5	12.9	13.9	11.8	13.8	11.1	12.1	2.66	10.55	17.7
23-50-11	16.85	0.0	0.0	0.0	0.0	0.0	0.0	163.5	0.0	0.0	0.0	0.0	0.0	0.0	0.0	0.0	0.0	2.78	9.47	0.0
23-50-12	11.31	0.0	0.0	0.0	0.0	0.0	0.0	110.4	0.0	0.0	0.0	0.0	0.0	0.0	0.0	0.0	0.0	2.76	9.41	0.0
23-50-13	7.80	0.0	0.0	0.0	0.0	0.0	0.0	76.7	0.0	0.0	0.0	0.0	0.0	0.0	0.0	0.0	0.0	2.74	9.35	0.0
23-50-14	5.73	0.0	0.0	0.0	0.0	0.0	0.0	56.2	0.0	0.0	0.0	0.0	0.0	0.0	0.0	0.0	0.0	2.72	9.38	0.0
23-50-15	4.06	0.0	0.0	0.0	0.0	0.0	0.0	39.0	0.0	0.0	0.0	0.0	0.0	0.0	0.0	0.0	0.0	2.68	9.61	0.0
23-50-16	2.88	0.0	0.0	0.0	0.0	0.0	0.0	28.0	0.0	0.0	0.0	0.0	0.0	0.0	0.0	0.0	0.0	2.66	9.49	0.0
23-50-17	2.58	0.0	0.0	0.0	0.0	0.0	0.0	25.2	0.0	0.0	0.0	0.0	0.0	0.0	0.0	0.0	0.0	2.65	9.48	0.0
23-50-18	1.80	0.0	0.0	0.0	0.0	0.0	0.0	16.8	0.0	0.0	0.0	0.0	0.0	0.0	0.0	0.0	0.0	2.59	9.95	0.0
23-50-19	31.70	0.0	0.0	0.0	0.0	0.0	0.0	317.2	0.0	0.0	0.0	0.0	0.0	0.0	0.0	0.0	0.0	2.82	9.13	0.0
23-50-20	18.90	0.0	0.0	0.0	0.0	0.0	0.0	185.4	0.0	0.0	0.0	0.0	0.0	0.0	0.0	0.0	0.0	2.79	9.35	0.0
23-50-21	12.01	0.0	0.0	0.0	0.0	0.0	0.0	117.2	0.0	0.0	0.0	0.0	0.0	0.0	0.0	0.0	0.0	2.76	9.41	0.0
23-50-22	8.78	0.0	0.0	0.0	0.0	0.0	0.0	85.5	0.0	0.0	0.0	0.0	0.0	0.0	0.0	0.0	0.0	2.74	9.45	0.0
23-50-23	5.95	0.0	0.0	0.0	0.0	0.0	0.0	59.3	0.0	0.0	0.0	0.0	0.0	0.0	0.0	0.0	0.0	2.73	9.22	0.0
23-50-24	4.26	0.0	0.0	0.0	0.0	0.0	0.0	42.3	0.0	0.0	0.0	0.0	0.0	0.0	0.0	0.0	0.0	2.70	9.27	0.0
23-50-25	2.93	0.0	0.0	0.0	0.0	0.0	0.0	29.0	0.0	0.0	0.0	0.0	0.0	0.0	0.0	0.0	0.0	2.67	9.30	0.0
23-50-26	1.95	0.0	0.0	0.0	0.0	0.0	0.0	18.2	0.0	0.0	0.0	0.0	0.0	0.0	0.0	0.0	0.0	2.60	9.92	0.0
23-50-27	1.49	0.0	0.0	0.0	0.0	0.0	0.0	11.8	0.0	0.0	0.0	0.0	0.0	0.0	0.0	0.0	0.0	2.44	11.93	0.0

Table 2 cont.





VERS.NR.	RE*E4	RE1*E4	F	F1	STB	STPR	F1/F2	TW/TB	TW/T1	PR	H/Y	BETA	H+	H+W	H+R	H+RM	RH+	RH+R	AS	AR
22-71- 1	2.18	3.72	.01350	.02793	.00577	.00508	3.70	1.30	1.28	.703	.0568	.821	45.2	29.3	46.9	30.4	3.51	3.21	2.42	2.50
22-71- 2	3.18	5.65	.01370	.02857	.00562	.00496	4.10	1.31	1.29	.704	.0552	.832	66.9	42.8	69.4	44.5	3.34	3.03	2.42	2.50
22-71- 3	3.87	7.01	.01365	.02897	.00558	.00493	4.34	1.31	1.29	.704	.0542	.838	82.0	52.4	85.1	54.4	3.19	2.88	2.42	2.50
22-71- 4	5.32	9.84	.01335	.02885	.00517	.00459	4.61	1.33	1.31	.704	.0534	.844	112.5	70.5	117.0	73.3	3.16	2.84	2.41	2.50
22-71- 5	6.97	13.15	.01305	.02875	.00524	.00467	4.87	1.34	1.32	.704	.0526	.849	147.6	91.0	153.7	94.8	3.12	2.79	2.41	2.50
22-71- 6	9.57	18.27	.01244	.02764	.00481	.00430	5.00	1.35	1.34	.704	.0522	.852	199.1	120.5	207.7	125.6	3.27	2.92	2.40	2.50
22-71- 7	11.27	21.81	.01237	.02772	.00465	.00413	5.16	1.33	1.32	.705	.0518	.855	235.3	146.2	244.8	152.1	3.23	2.90	2.40	2.50
22-71- 8	2.23	3.85	.01430	.02901	.00593	.00519	3.84	1.29	1.26	.703	.0561	.825	47.0	31.4	48.7	32.5	3.31	3.04	2.42	2.50
22-71- 9	8.90	17.07	.01257	.02795	.00489	.00432	4.97	1.31	1.30	.705	.0522	.852	187.1	119.1	194.3	123.7	3.22	2.91	2.41	2.50
22-71- 10	15.40	30.62	.01230	.02810	.00448	.00393	5.53	1.29	1.28	.703	.0509	.862	325.1	211.8	337.0	219.5	3.12	2.83	2.40	2.50
22-71- 11	22.44	45.96	.01217	.02850	.00416	.00364	6.00	1.28	1.27	.702	.0499	.869	479.7	314.8	496.9	326.1	3.02	2.73	2.39	2.50
22-71- 12	7.43	14.76	.01353	.03006	.0	.0	5.06	1.00	1.00	.710	.0516	.856	164.9	164.9	164.9	164.9	2.88	2.88	2.41	2.50
22-71- 13	5.65	11.06	.01385	.03032	.0	.0	4.82	1.00	1.00	.711	.0522	.851	125.9	125.9	125.9	125.9	2.88	2.88	2.41	2.50
22-71- 14	4.09	7.79	.01388	.02948	.0	.0	4.39	1.00	1.00	.710	.0533	.843	90.0	90.0	90.0	90.0	3.06	3.06	2.42	2.50
22-71- 15	3.23	6.07	.01428	.02997	.0	.0	4.24	1.00	1.00	.710	.0539	.839	71.6	71.6	71.6	71.6	3.04	3.04	2.42	2.50
22-71- 16	2.32	4.23	.01439	.02920	.0	.0	3.85	1.00	1.00	.710	.0554	.830	50.8	50.8	50.8	50.8	3.25	3.25	2.42	2.50
22-71- 17	2.40	4.44	.01477	.03048	.0	.0	4.03	1.00	1.00	.710	.0547	.834	53.7	53.7	53.7	53.7	3.04	3.04	2.42	2.50
22-71- 18	1.72	3.07	.01494	.02974	.0	.0	3.65	1.00	1.00	.710	.0561	.825	38.0	38.0	38.0	38.0	3.20	3.20	2.43	2.50
22-71- 19	23.96	50.33	.01233	.02885	.0	.0	6.09	1.00	1.00	.707	.0494	.872	521.6	521.6	521.6	521.6	2.94	2.94	2.39	2.50
22-71- 20	17.30	35.78	.01258	.02903	.0	.0	5.77	1.00	1.00	.707	.0509	.868	377.7	377.7	377.7	377.7	2.94	2.94	2.40	2.50
22-71- 21	12.78	25.84	.01253	.02822	.0	.0	5.31	1.00	1.00	.708	.0509	.861	275.1	275.1	275.1	275.1	3.11	3.11	2.40	2.50
22-71- 22	9.18	18.39	.01319	.02952	.0	.0	5.19	1.00	1.00	.709	.0512	.858	202.0	202.0	202.0	202.0	2.94	2.94	2.40	2.50

VERS.NR.	RE*E4	Q<KW/M2>	ST1+/ ST1*	STT+/ STT*	STIF/ STIF*	H+	G+	GPRI	G	G*	G*R	GT	GTR	GTF	GTR	X	YR	YG		
22-71- 1	2.18	6.2	1.10	1.10	1.11	1.12	1.20	45.2	13.6	13.0	13.3	13.6	17.1	13.4	16.9	12.0	15.5	2.01	8.46	17.1
22-71- 2	3.18	9.0	1.09	1.10	1.11	1.11	1.18	66.9	14.3	13.6	13.9	14.3	17.9	14.1	17.8	12.9	16.4	2.04	8.37	18.0
22-71- 3	3.87	10.9	1.09	1.09	1.10	1.10	1.17	82.0	14.6	13.9	14.2	14.6	18.3	14.4	18.1	13.2	16.9	2.06	8.31	18.4
22-71- 4	5.32	14.5	1.09	1.08	1.10	1.09	1.16	112.5	16.1	15.2	15.4	16.2	20.1	15.9	19.8	14.9	18.7	2.07	8.33	20.1
22-71- 5	6.97	19.8	1.08	1.09	1.10	1.10	1.16	147.6	15.9	14.9	15.2	15.8	19.6	15.6	19.5	14.6	18.3	2.09	8.34	19.8
22-71- 6	9.57	25.8	1.08	1.08	1.09	1.09	1.14	199.1	17.4	16.3	16.5	17.4	21.3	17.2	21.2	16.1	20.0	2.10	8.51	21.4
22-71- 7	11.27	27.4	1.08	1.08	1.09	1.09	1.14	235.3	18.2	17.1	17.4	18.2	22.4	18.0	22.2	17.0	21.1	2.11	8.49	22.3
22-71- 8	2.23	6.1	1.11	1.10	1.12	1.11	1.19	47.0	13.2	12.7	13.0	13.5	17.0	13.0	16.5	12.0	15.5	2.02	8.30	17.0
22-71- 9	8.90	21.2	1.07	1.08	1.08	1.10	1.15	187.1	17.3	16.4	16.8	17.0	21.1	17.1	21.2	15.8	19.9	2.10	8.46	21.1
22-71- 10	15.40	33.2	1.08	1.07	1.09	1.08	1.13	325.1	19.3	18.4	18.9	19.3	24.0	19.0	23.7	18.2	22.8	2.13	8.44	23.5
22-71- 11	22.44	43.9	1.06	1.07	1.07	1.08	1.11	475.7	21.6	20.8	21.4	21.4	26.5	21.4	26.6	20.3	25.4	2.15	8.38	25.7
22-71- 12	7.43	0.0	0.0	0.0	0.0	0.0	0.0	164.9	0.0	0.0	0.0	0.0	0.0	0.0	0.0	0.0	0.0	2.11	8.16	0.0
22-71- 13	5.65	0.0	0.0	0.0	0.0	0.0	0.0	125.9	0.0	0.0	0.0	0.0	0.0	0.0	0.0	0.0	0.0	2.10	8.12	0.0
22-71- 14	4.09	0.0	0.0	0.0	0.0	0.0	0.0	90.0	0.0	0.0	0.0	0.0	0.0	0.0	0.0	0.0	0.0	2.07	8.24	0.0
22-71- 15	3.23	0.0	0.0	0.0	0.0	0.0	0.0	71.6	0.0	0.0	0.0	0.0	0.0	0.0	0.0	0.0	0.0	2.06	8.17	0.0
22-71- 16	2.32	0.0	0.0	0.0	0.0	0.0	0.0	50.8	0.0	0.0	0.0	0.0	0.0	0.0	0.0	0.0	0.0	2.03	8.28	0.0
22-71- 17	2.40	0.0	0.0	0.0	0.0	0.0	0.0	53.7	0.0	0.0	0.0	0.0	0.0	0.0	0.0	0.0	0.0	2.05	8.10	0.0
22-71- 18	1.72	0.0	0.0	0.0	0.0	0.0	0.0	38.0	0.0	0.0	0.0	0.0	0.0	0.0	0.0	0.0	0.0	2.02	8.20	0.0
22-71- 19	23.96	0.0	0.0	0.0	0.0	0.0	0.0	521.6	0.0	0.0	0.0	0.0	0.0	0.0	0.0	0.0	0.0	2.16	8.33	0.0
22-71- 20	17.30	0.0	0.0	0.0	0.0	0.0	0.0	377.7	0.0	0.0	0.0	0.0	0.0	0.0	0.0	0.0	0.0	2.14	8.30	0.0
22-71- 21	12.78	0.0	0.0	0.0	0.0	0.0	0.0	275.1	0.0	0.0	0.0	0.0	0.0	0.0	0.0	0.0	0.0	2.13	8.42	0.0
22-71- 22	9.18	0.0	0.0	0.0	0.0	0.0	0.0	202.0	0.0	0.0	0.0	0.0	0.0	0.0	0.0	0.0	0.0	2.12	8.23	0.0

Table 2 cont.











VERS.NR.	RE#E4	RE1#E4	F	F1	STB	STPR	F1/F2	TW/T8	TW/T1	PR	H/Y	BETA	H+	H+W	H+R	H+RW	RH+	RH+R	AS	AR
22-71- 1	2.18	3.79	.01390	.02640	.00577	.00508	3.19	1.30	1.30	.703	.0575	.817	45.5	28.9	47.2	30.0	5.01	4.68	2.24	1.89
22-71- 2	3.18	5.56	.01370	.02693	.00562	.00496	3.54	1.31	1.31	.704	.0550	.833	68.2	42.6	70.9	44.3	5.08	4.75	2.28	1.76
22-71- 3	3.87	7.45	.01365	.02760	.00558	.00493	3.81	1.31	1.31	.704	.0537	.841	84.0	52.3	87.4	54.4	4.99	4.66	2.30	1.71
22-71- 4	5.32	10.62	.01335	.02759	.00517	.00455	4.10	1.33	1.33	.704	.0524	.850	116.1	70.7	121.0	73.7	5.06	4.72	2.32	1.66
22-71- 5	6.97	14.25	.01305	.02796	.00524	.00467	4.46	1.34	1.34	.704	.0514	.858	153.1	91.6	159.8	95.6	5.04	4.68	2.35	1.62
22-71- 6	9.57	19.90	.01244	.02712	.00481	.00430	4.68	1.35	1.36	.704	.0508	.863	207.2	121.6	216.6	127.1	5.21	4.83	2.37	1.59
22-71- 7	11.27	23.74	.01237	.02724	.00465	.00413	4.87	1.33	1.34	.705	.0503	.866	244.5	147.8	255.0	154.1	5.20	4.84	2.38	1.58
22-71- 8	2.23	3.53	.01430	.02745	.00593	.00519	3.31	1.29	1.28	.703	.0568	.821	47.3	31.0	49.0	32.1	4.83	4.53	2.24	1.88
22-71- 9	8.90	18.51	.01257	.02737	.00489	.00432	4.64	1.31	1.32	.705	.0509	.862	194.0	120.2	201.9	125.1	5.16	4.82	2.37	1.60
22-71-10	15.40	33.31	.01230	.02771	.00448	.00393	5.28	1.25	1.30	.703	.0493	.874	337.4	214.7	350.3	222.9	5.12	4.81	2.40	1.56
22-71-11	22.44	49.98	.01217	.02821	.00416	.00364	5.81	1.28	1.29	.702	.0483	.882	497.5	319.7	516.2	331.7	5.04	4.73	2.41	1.55
22-71-12	7.43	15.55	.01353	.02907	.0	.C	4.63	1.00	1.00	.710	.0506	.863	166.9	166.9	166.9	166.9	4.86	4.86	2.35	1.61
22-71-13	5.65	11.57	.01385	.02916	.0	.0	4.35	1.00	1.00	.711	.0515	.857	127.0	127.0	127.0	127.0	4.81	4.81	2.33	1.65
22-71-14	4.09	8.06	.01388	.02814	.0	.0	3.90	1.00	1.00	.710	.0530	.845	90.3	90.3	90.3	90.3	4.90	4.90	2.30	1.70
22-71-15	3.23	6.22	.01428	.02844	.0	.0	3.71	1.00	1.00	.710	.0540	.859	71.5	71.5	71.5	71.5	4.80	4.80	2.27	1.75
22-71-16	2.32	4.25	.01439	.02742	.0	.0	3.30	1.00	1.00	.710	.0562	.825	50.4	50.4	50.4	50.4	4.85	4.85	2.24	1.86
22-71-17	2.40	4.47	.01477	.02868	.0	.C	3.46	1.00	1.00	.710	.0554	.825	53.3	53.3	53.3	53.3	4.67	4.67	2.24	1.84
22-71-18	1.72	3.01	.01494	.02769	.0	.0	3.07	1.00	1.00	.710	.0578	.814	37.3	37.3	37.3	37.3	4.61	4.61	2.20	1.99
22-71-19	23.96	53.75	.01233	.02835	.0	.0	5.87	1.00	1.00	.707	.0480	.884	531.6	531.6	531.6	531.6	5.01	5.01	2.42	1.55
22-71-20	17.30	38.14	.01258	.02843	.0	.0	5.49	1.00	1.00	.707	.0487	.879	384.5	384.5	384.5	384.5	5.00	5.00	2.40	1.56
22-71-21	12.78	27.46	.01253	.02753	.0	.0	5.00	1.00	1.00	.708	.0497	.871	279.6	279.6	279.6	279.6	5.14	5.14	2.38	1.57
22-71-22	9.18	19.45	.01319	.02865	.0	.C	4.80	1.00	1.00	.709	.0502	.867	204.8	204.8	204.8	204.8	4.94	4.94	2.36	1.60

VERS.NR.	RE#E4	Q<KW/M2>	ST1+/ ST1*/	STT+/ STT*/	ST1F/ ST1F*/	H+	G+	G*	AST	BSI	H+	ARP	RHP	ARI	RHI	G(H+)		
22-71- 1	2.18	6.2	1.04	1.07	1.06	1.09	1.18	45.5	15.3	14.8	2.07	5.50	38.7	2.26	4.05	2.61	3.77	13.3
22-71- 2	3.18	9.0	1.02	1.05	1.04	1.07	1.15	68.2	16.7	16.0	2.13	5.50	58.4	2.30	4.17	2.39	3.75	13.9
22-71- 3	3.87	10.9	1.02	1.05	1.03	1.06	1.13	84.0	17.2	16.5	2.05	5.50	72.3	2.21	4.05	2.30	3.66	14.9
22-71- 4	5.32	14.5	1.01	1.04	1.03	1.05	1.11	116.1	18.9	18.4	2.15	5.50	102.7	2.13	3.89	1.94	3.99	16.6
22-71- 5	6.97	19.8	1.01	1.04	1.02	1.06	1.11	153.1	18.9	18.2	2.12	5.50	136.2	2.07	3.83	1.94	3.87	16.9
22-71- 6	9.57	25.8	1.01	1.04	1.02	1.06	1.10	207.2	20.6	19.8	2.08	5.50	185.3	2.03	3.83	1.89	3.90	18.6
22-71- 7	11.27	27.4	1.01	1.04	1.02	1.05	1.10	244.5	21.5	20.8	2.11	5.50	221.5	2.06	3.74	1.90	3.87	19.7
22-71- 8	2.23	6.1	1.05	1.07	1.07	1.08	1.18	47.3	15.0	14.8	2.11	5.50	41.3	2.22	4.51	2.61	3.41	13.7
22-71- 9	8.90	21.2	1.00	1.05	1.01	1.06	1.11	194.0	20.5	19.5	2.14	5.50	165.3	2.08	4.65	2.56	3.47	16.4
22-71-10	15.40	33.2	1.01	1.04	1.02	1.05	1.09	337.4	22.7	22.0	2.10	5.50	293.1	2.03	4.68	2.57	3.37	18.9
22-71-11	22.44	43.9	1.00	1.04	1.01	1.05	1.08	497.5	25.2	24.2	2.18	5.50	442.6	2.07	4.43	2.47	3.43	21.5
22-71-12	7.43	0.0	0.0	0.0	0.0	0.0	0.0	166.9	0.0	0.0	2.30	5.50	165.6	2.03	4.08	1.83	4.29	0.0
22-71-13	5.65	0.0	0.0	0.0	0.0	0.0	0.0	127.0	0.0	0.0	2.27	5.50	125.8	2.06	4.05	1.89	4.18	0.0
22-71-14	4.09	0.0	0.0	0.0	0.0	0.0	0.0	90.3	0.0	0.0	2.23	5.50	89.1	2.18	4.02	2.07	4.01	0.0
22-71-15	3.23	0.0	0.0	0.0	0.0	0.0	0.0	71.5	0.0	0.0	2.23	5.50	70.3	2.27	4.09	2.26	3.84	0.0
22-71-16	2.32	0.0	0.0	0.0	0.0	0.0	0.0	50.4	0.0	0.0	2.22	5.50	49.7	2.49	3.76	2.26	3.98	0.0
22-71-17	2.40	0.0	0.0	0.0	0.0	0.0	0.0	53.3	0.0	0.0	2.17	5.50	51.4	2.33	4.24	2.48	3.69	0.0
22-71-18	1.72	0.0	0.0	0.0	0.0	0.0	0.0	37.3	0.0	0.0	2.03	5.50	34.8	2.05	5.64	2.77	3.84	0.0
22-71-19	23.96	0.0	0.0	0.0	0.0	0.0	0.0	531.6	0.0	0.0	2.33	5.50	528.9	1.98	4.23	1.68	4.69	0.0
22-71-20	17.30	0.0	0.0	0.0	0.0	0.0	0.0	384.5	0.0	0.0	2.32	5.50	382.2	1.99	4.23	1.70	4.64	0.0
22-71-21	12.78	0.0	0.0	0.0	0.0	0.0	0.0	279.6	0.0	0.0	2.27	5.50	278.3	1.97	4.30	1.70	4.64	0.0
22-71-22	9.18	0.0	0.0	0.0	0.0	0.0	0.0	204.8	0.0	0.0	2.28	5.50	203.7	1.97	4.21	1.73	4.48	0.0

Table 3 cont.







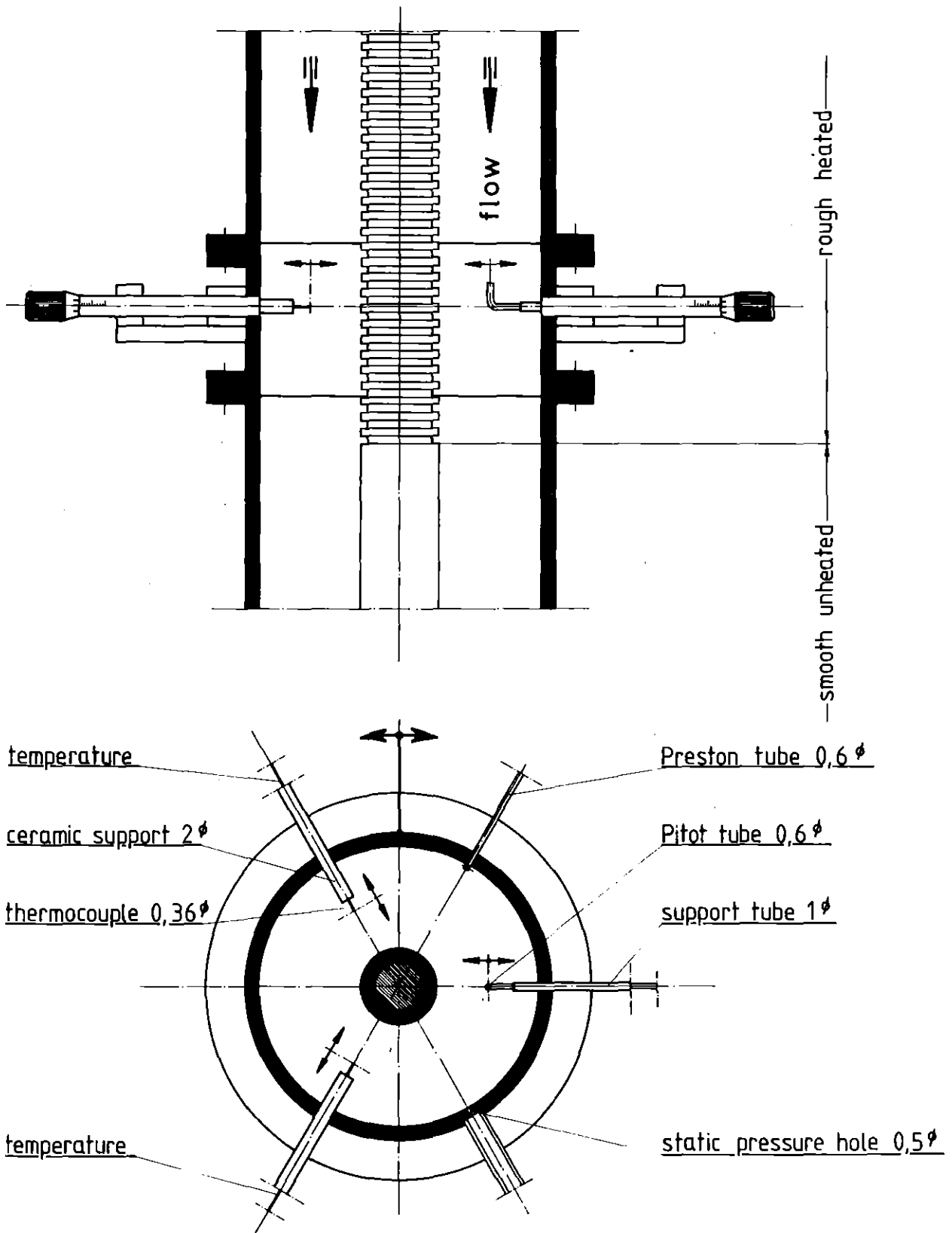


Fig.1: Measuring device

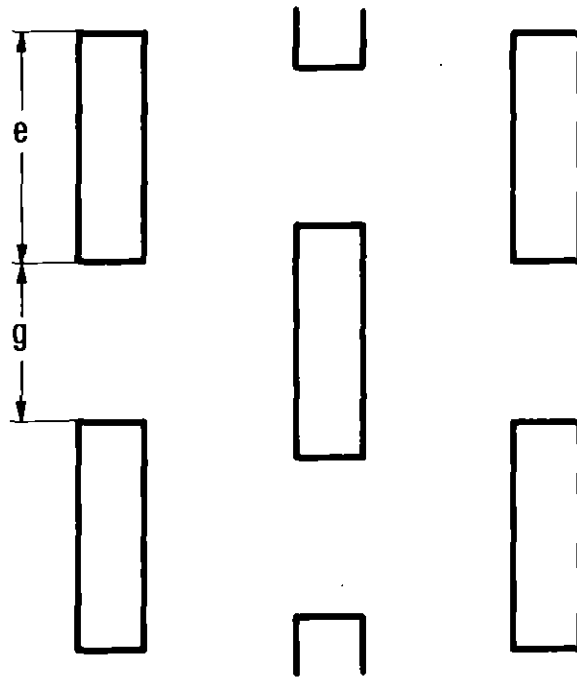
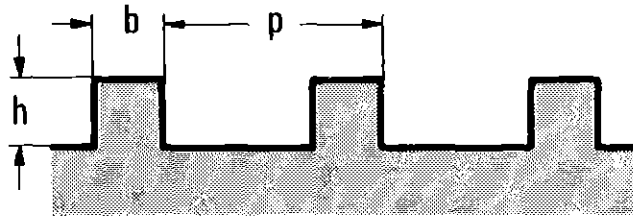


Fig.2: Parameters of the roughnesses

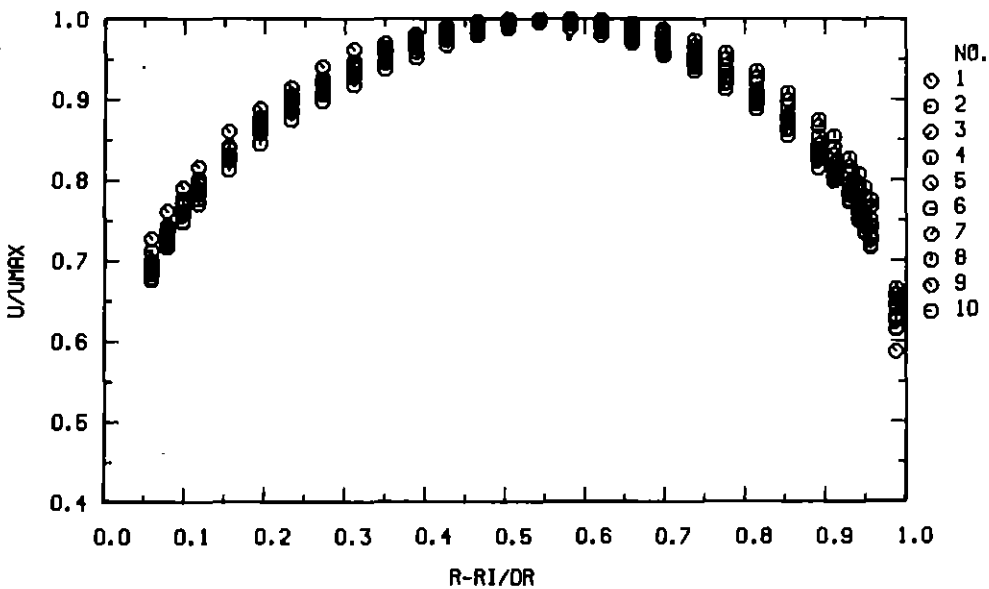
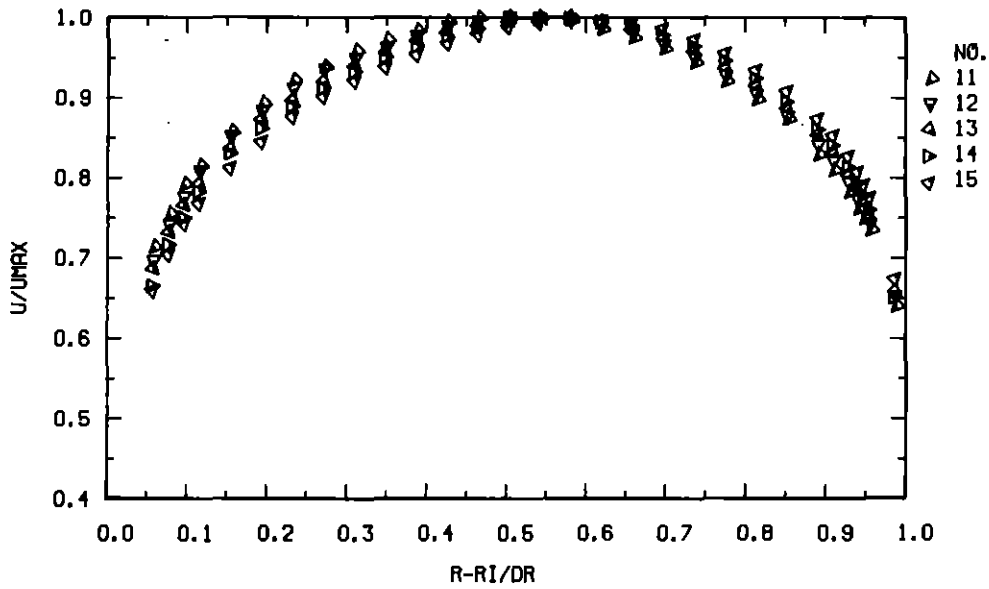
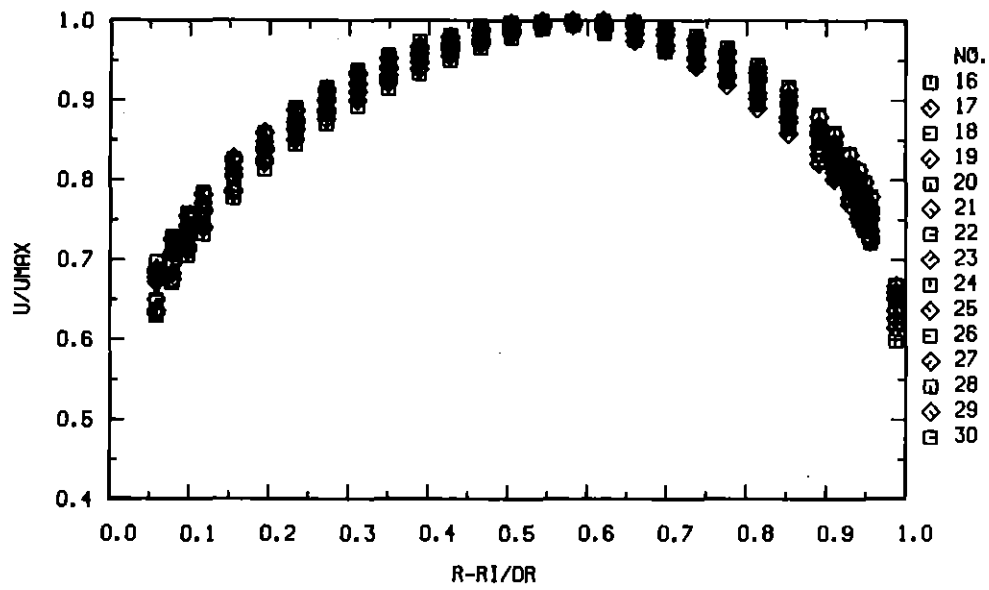


Fig.3: Velocity profiles for test section 23-72 (2-dim. roughness,  $\alpha = 0.262$ )

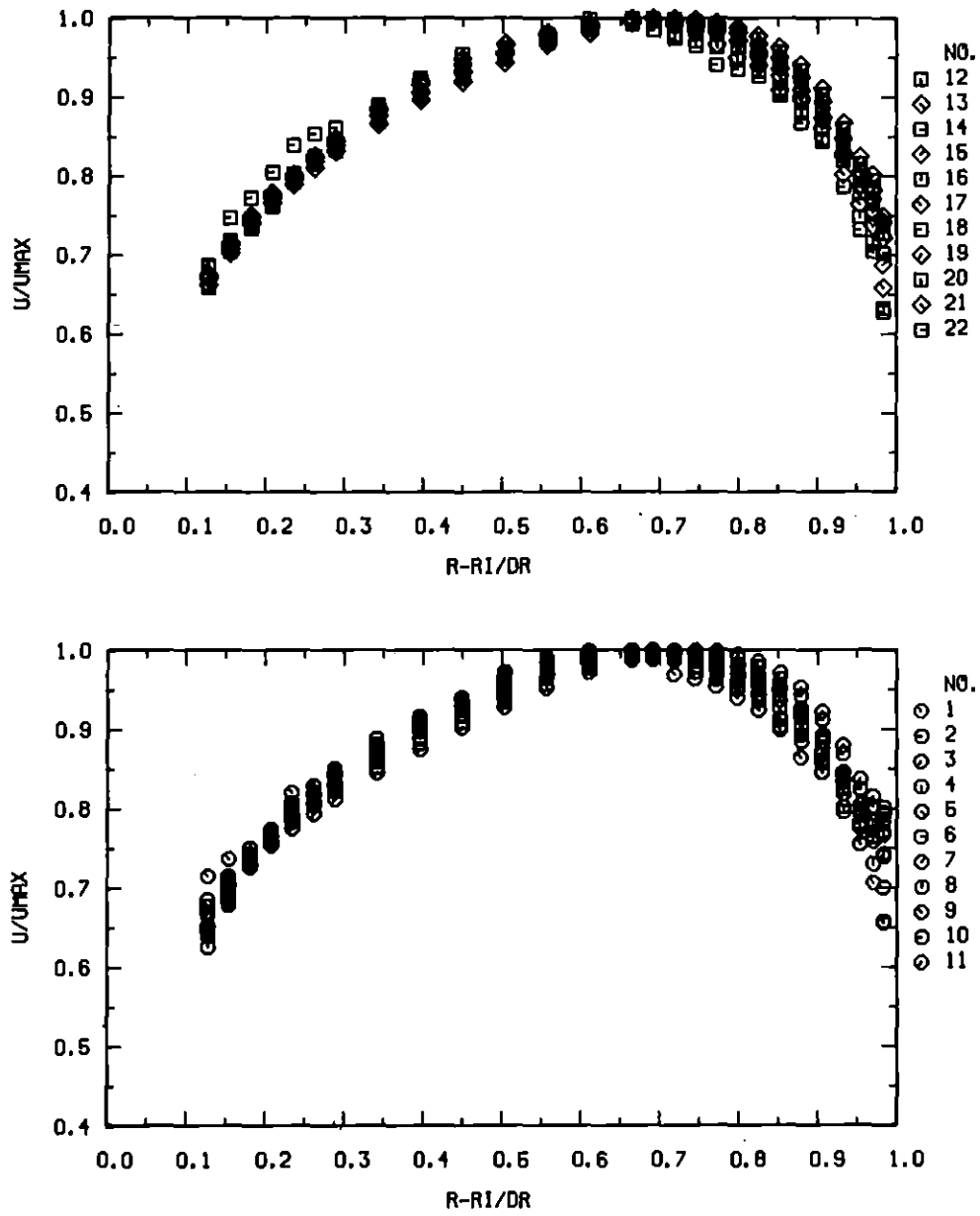


Fig.4: Velocity profiles for test section 22-71 (2-dim. roughness,  $\alpha = 0.468$ )

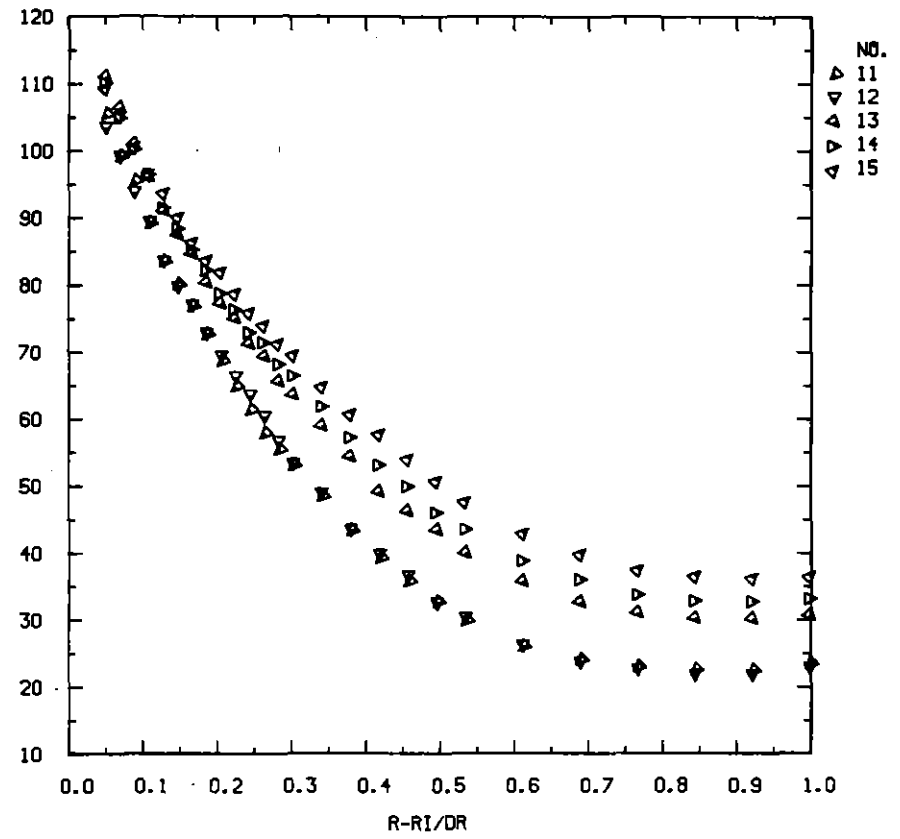
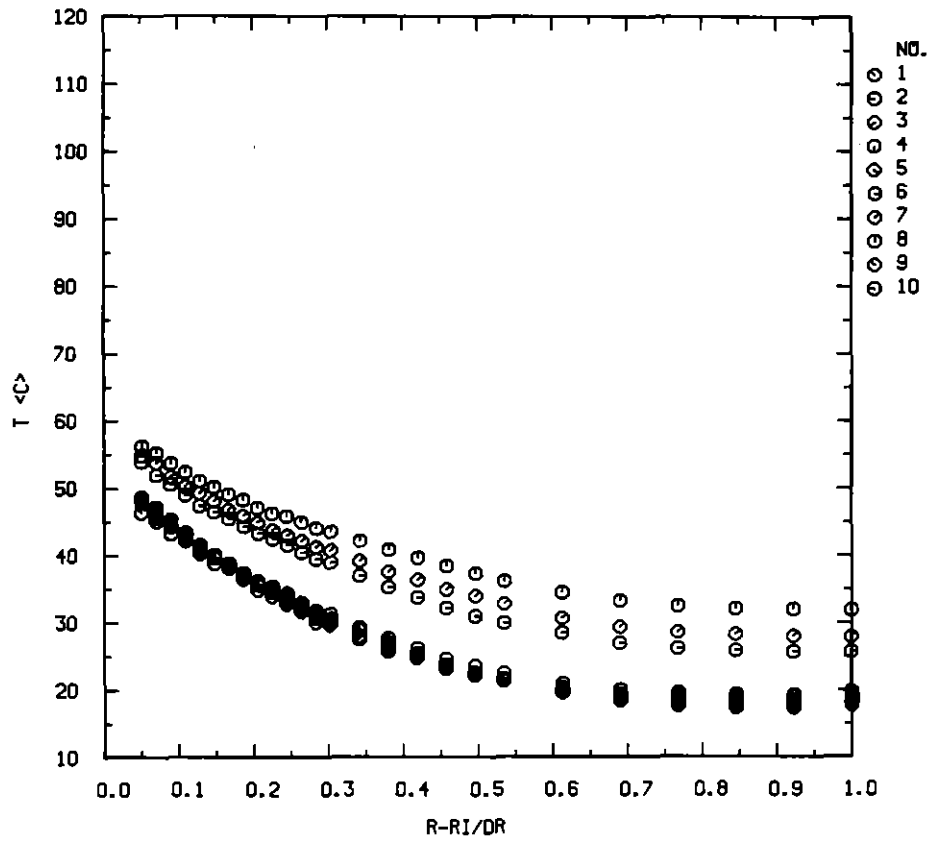


Fig.5: Temperature profiles for test section 23-72 (2-dim. roughness,  $\alpha = 0.262$ )

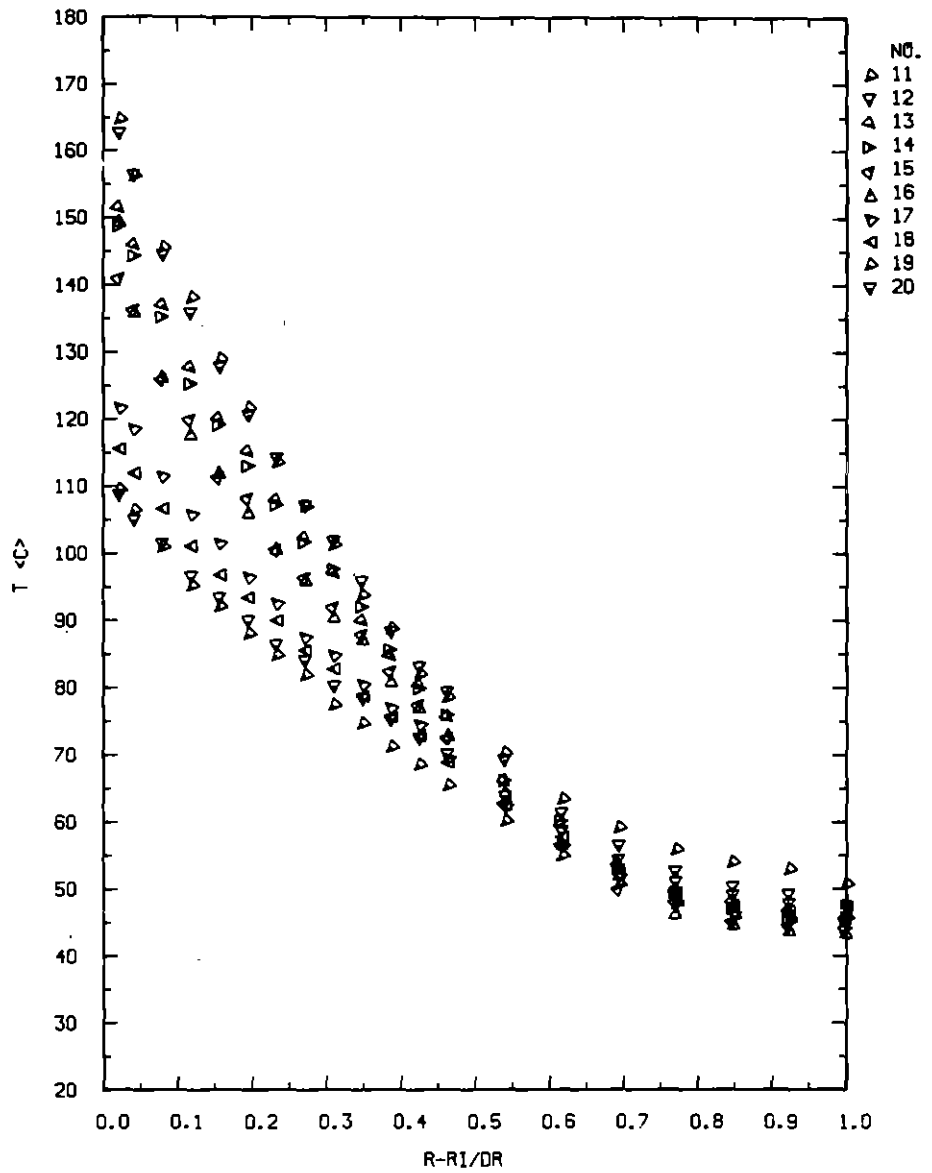
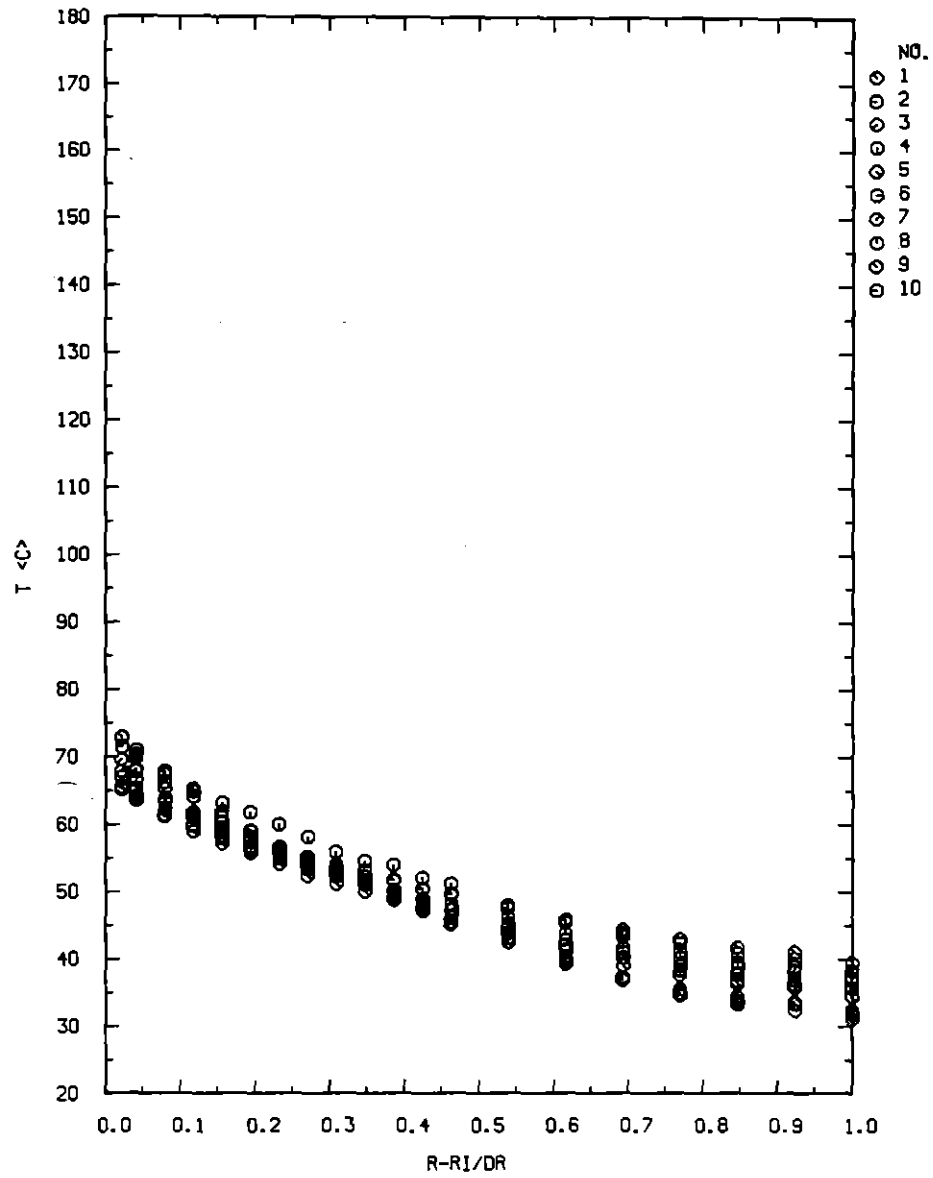


Fig.6: Temperature profiles for test section 22-85 (2-dim. roughness,  $\alpha = 0.386$ )



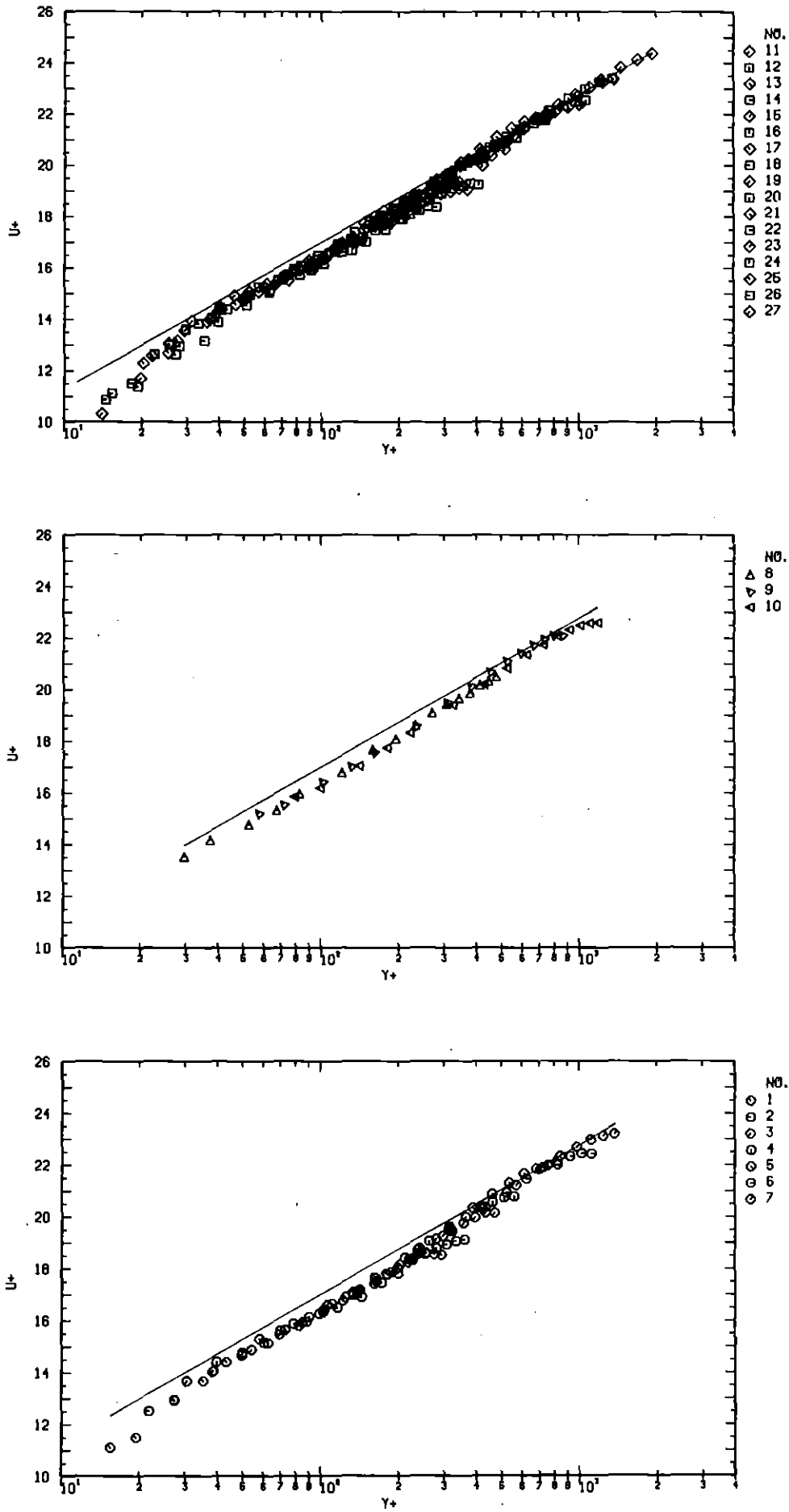


Fig.7: Non-dimensional velocity profiles at the smooth outer tube in test section 23-50 (2-dim. roughness,  $\alpha = 0.0190$ )

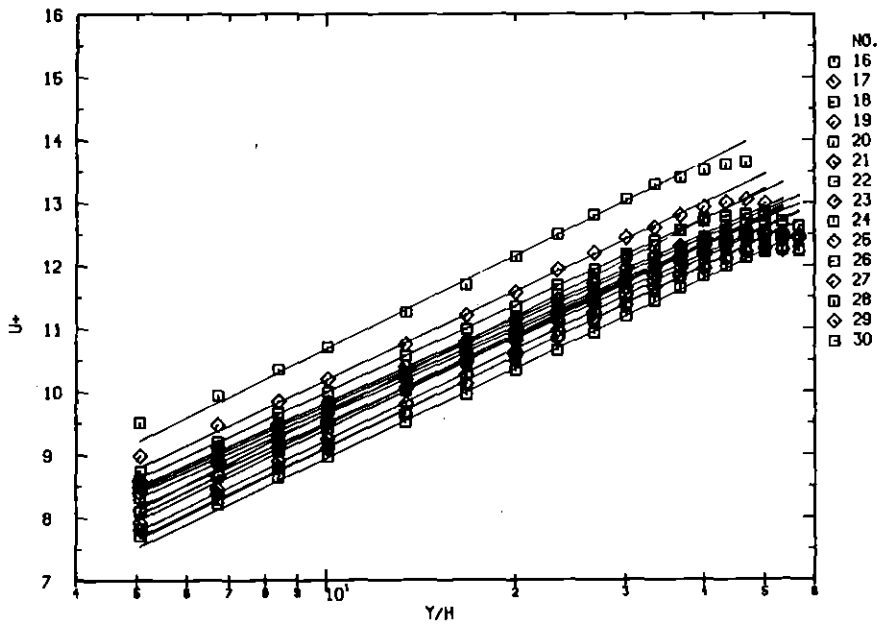
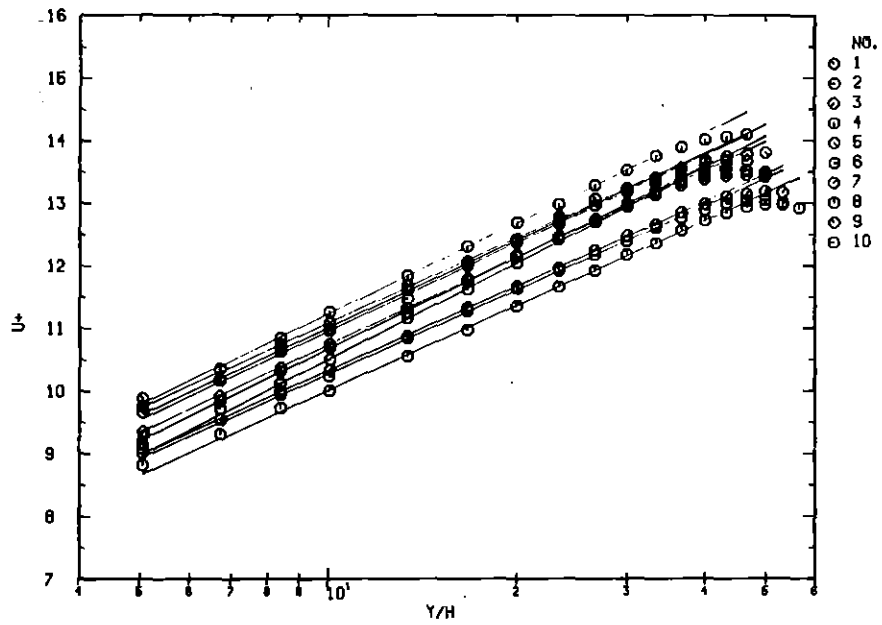
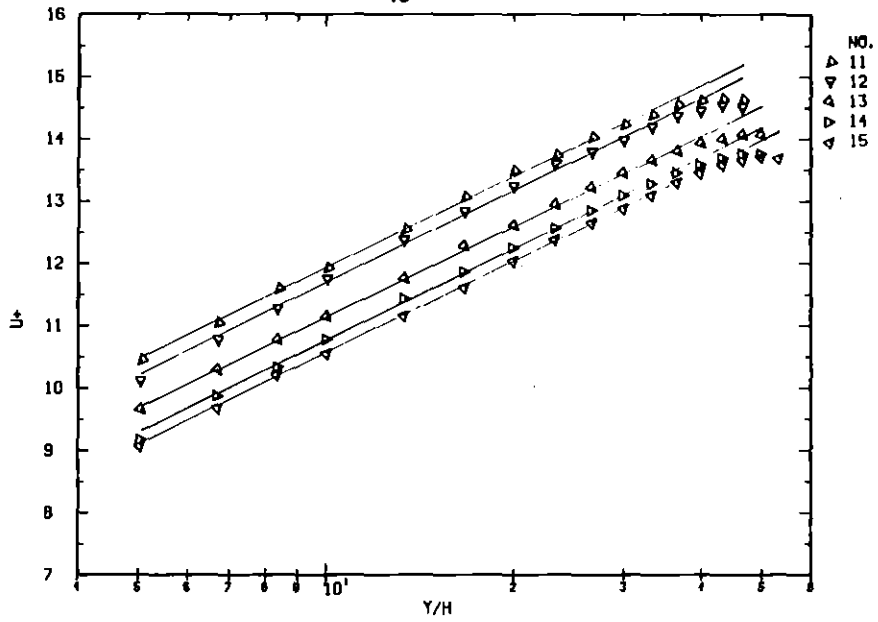


Fig.8: Non-dimensional velocity profiles in the rough zone in test section 23-72 (2-dim. roughness,  $\alpha = 0.262$ )

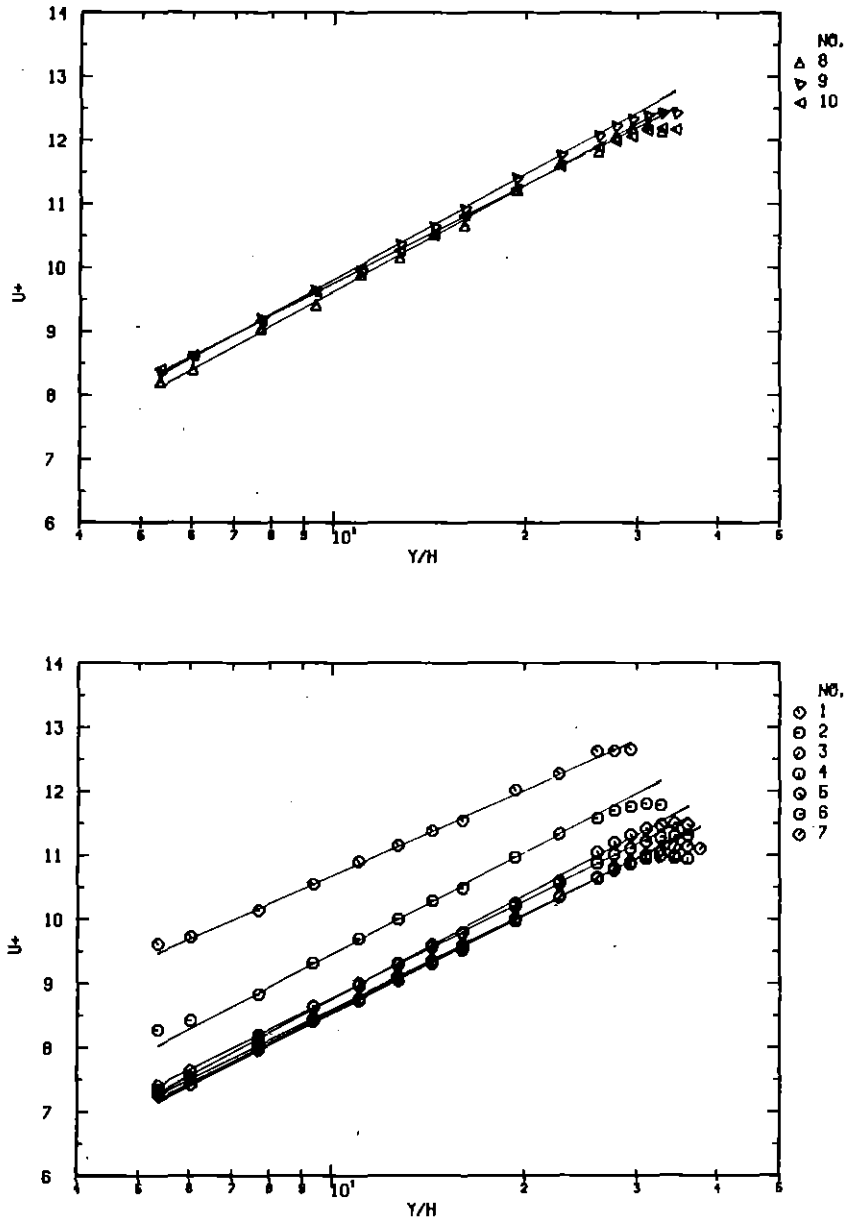


Fig.9: Non-dimensional velocity profiles in the rough zone in test section 23-50 (2-dim. roughness,  $\alpha = 0.190$ )

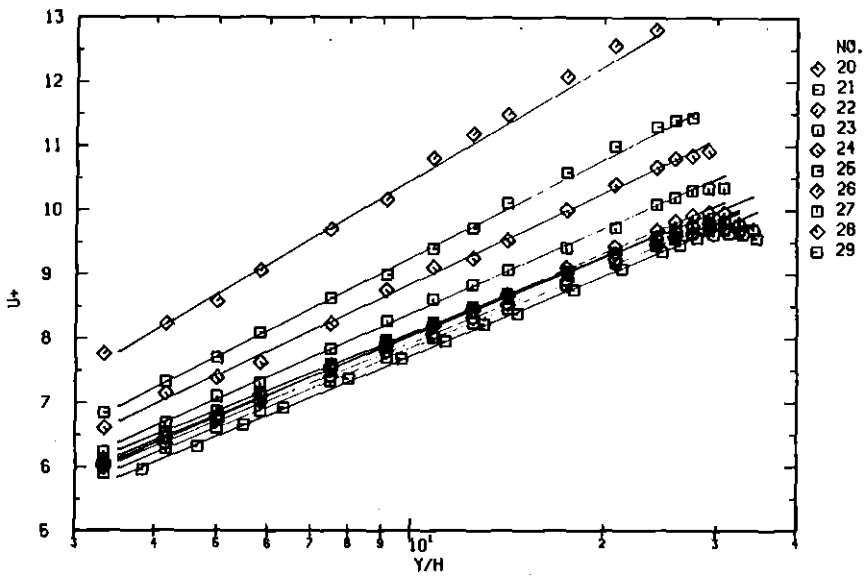
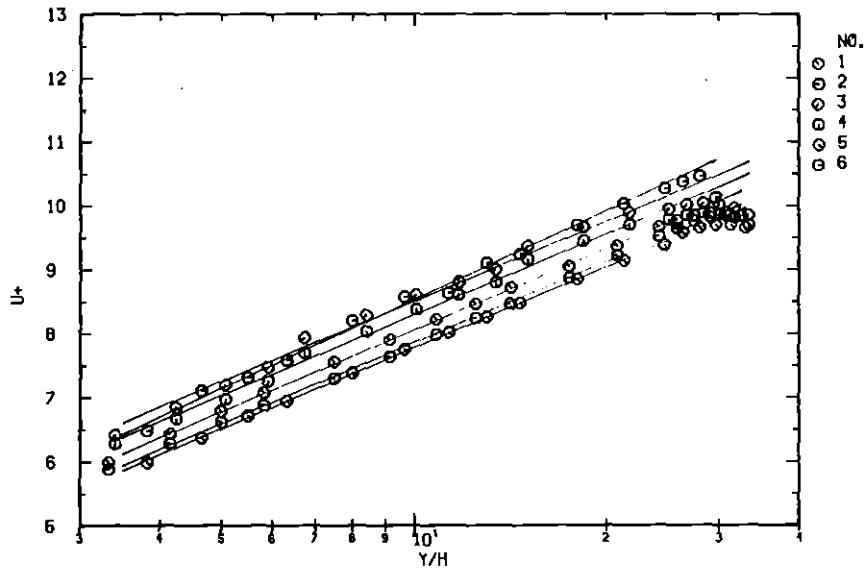
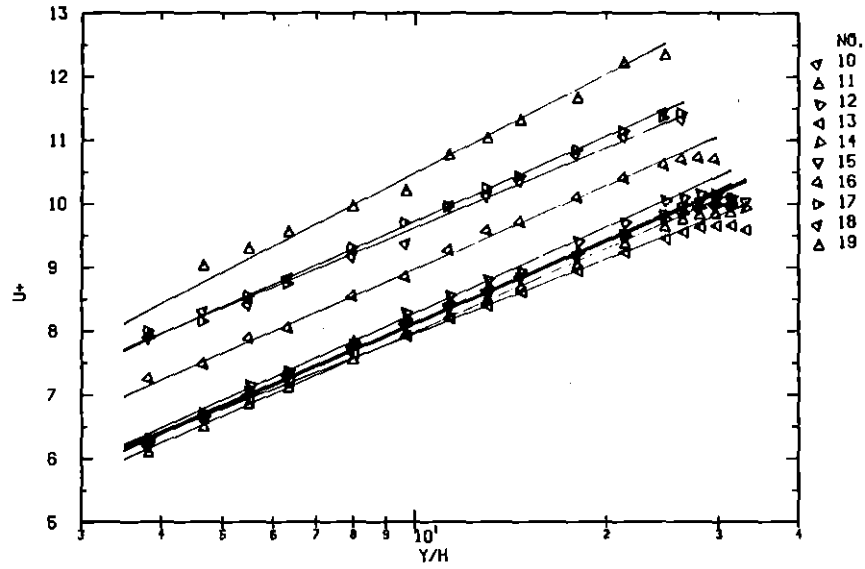


Fig.10: Non-dimensional velocity profiles in the rough zone in test section 12-85 (3-dim. roughness,  $\alpha = 0.386$ )

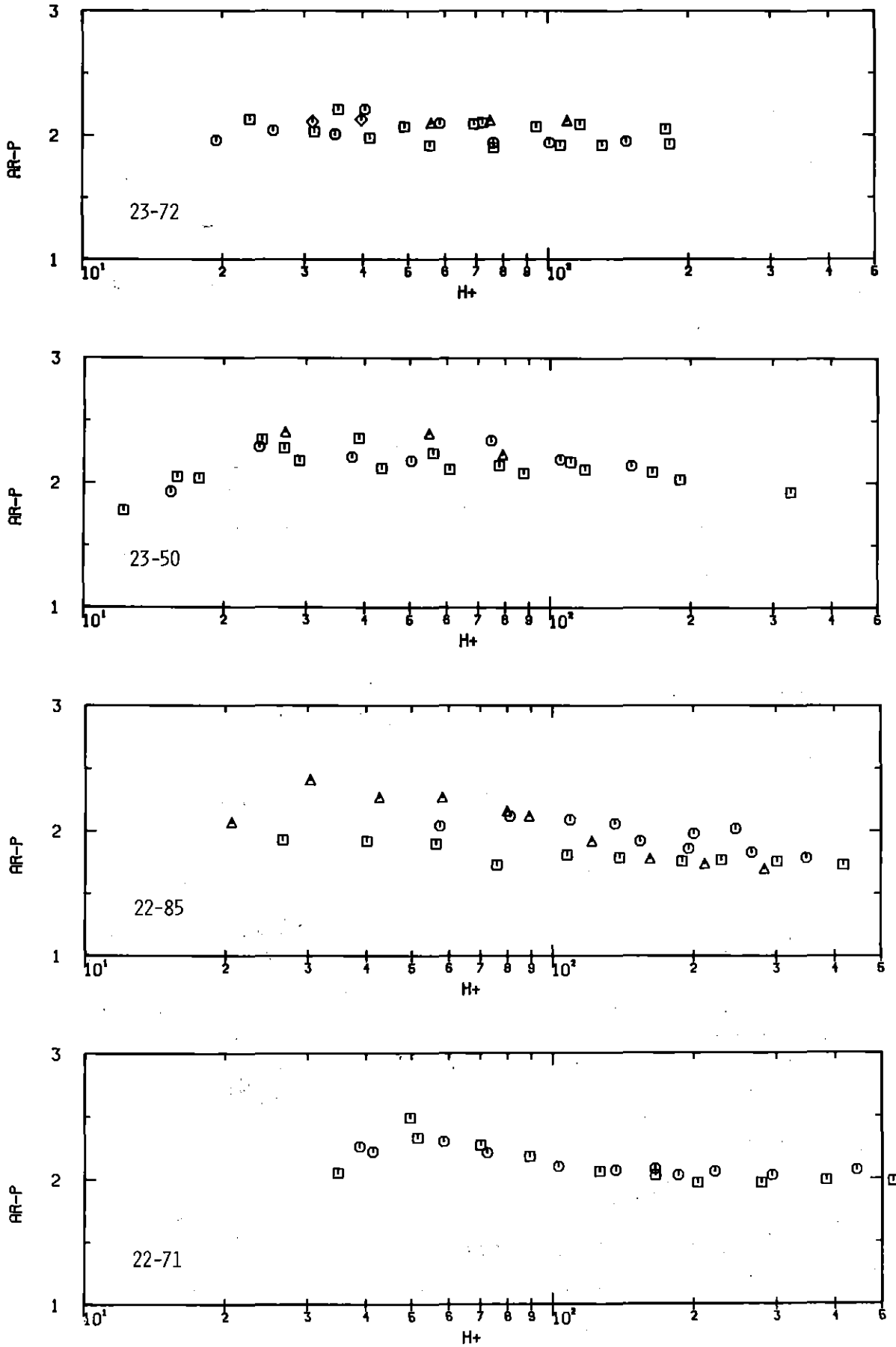


Fig.11: The slope  $A_r$  of the non-dimensional velocity profile in the rough zone with 2-dimensional roughness, determined by a least square fit.

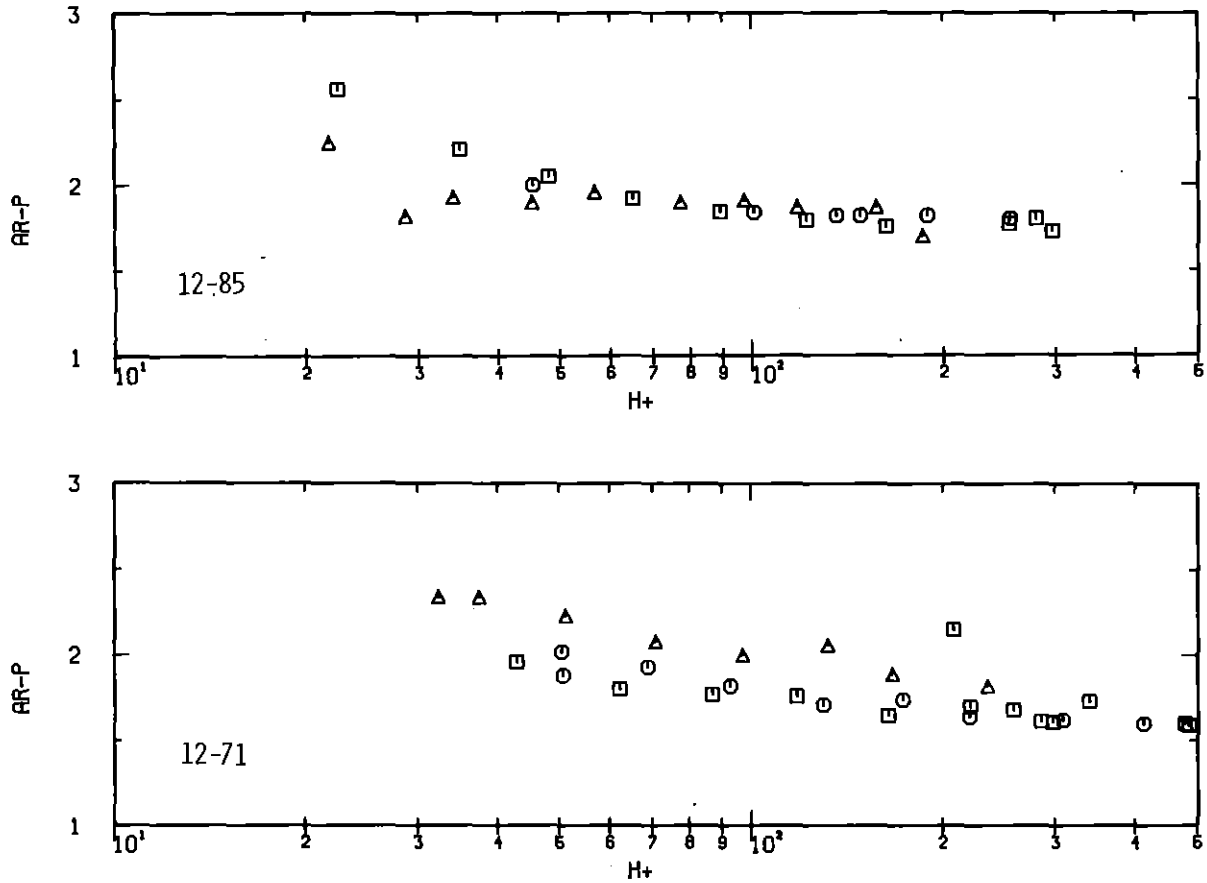


Fig.12: The slope  $A_r$  of the non-dimensional velocity profile in the rough zone with 3-dimensional roughness, determined by a least square fit

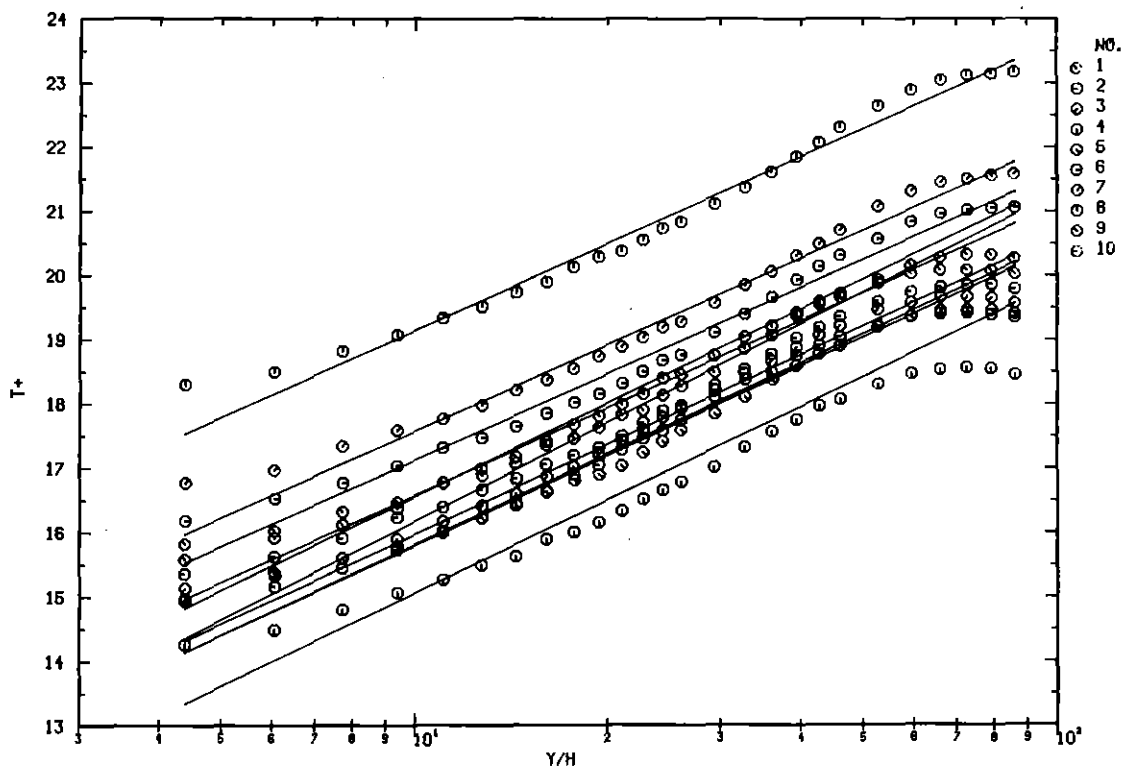
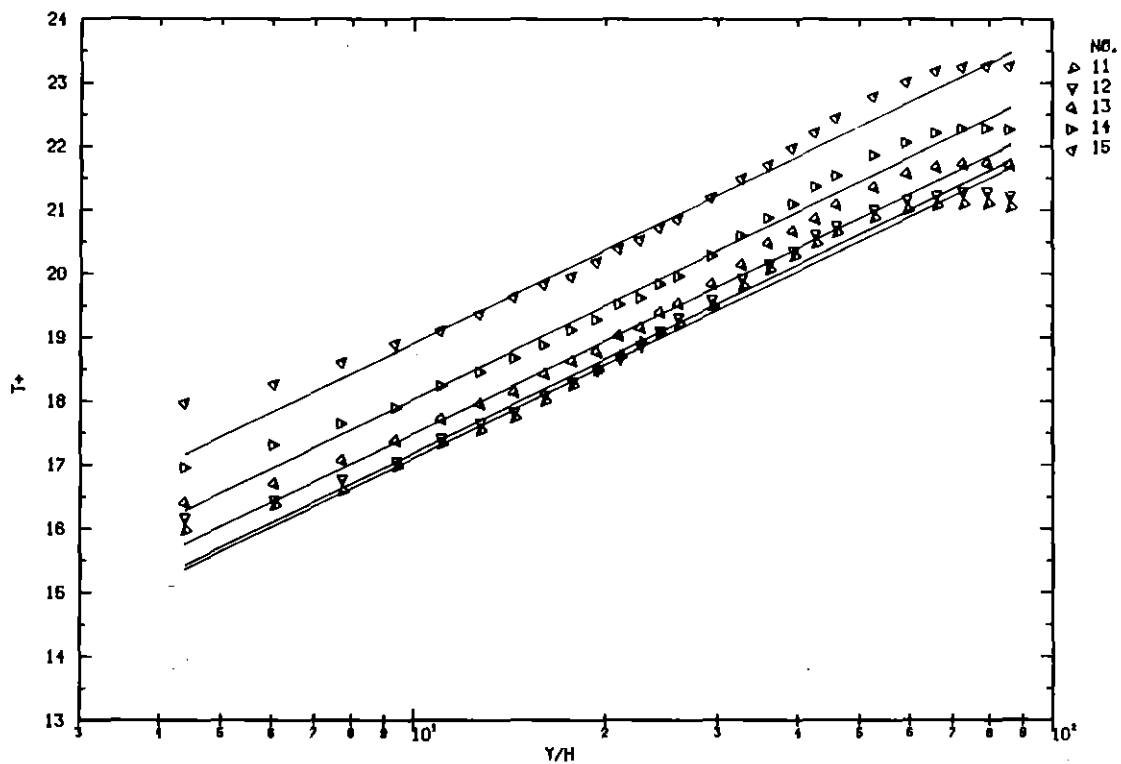


Fig.13: Non-dimensional temperature profiles in test section 23-70

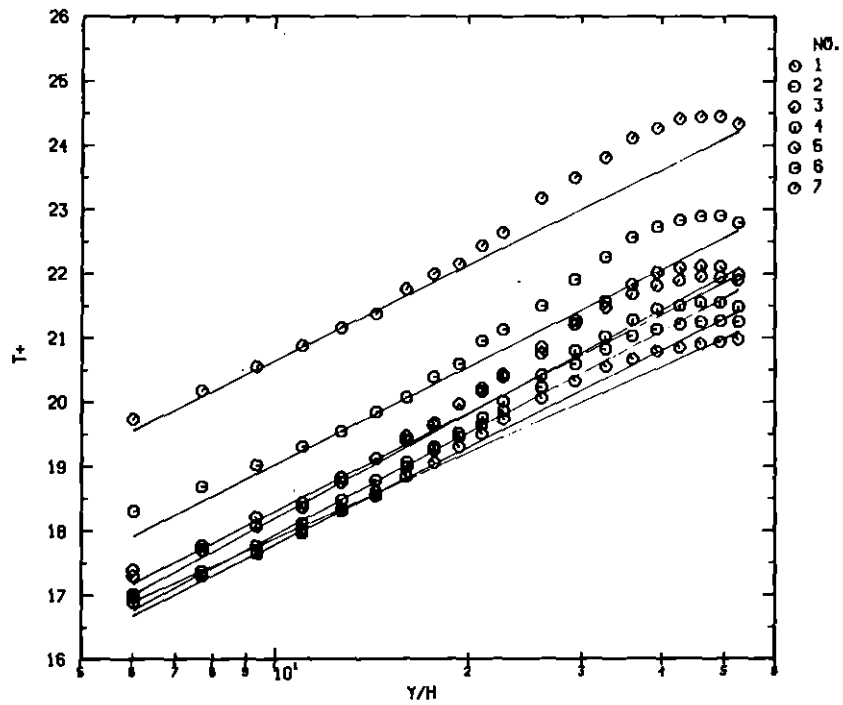
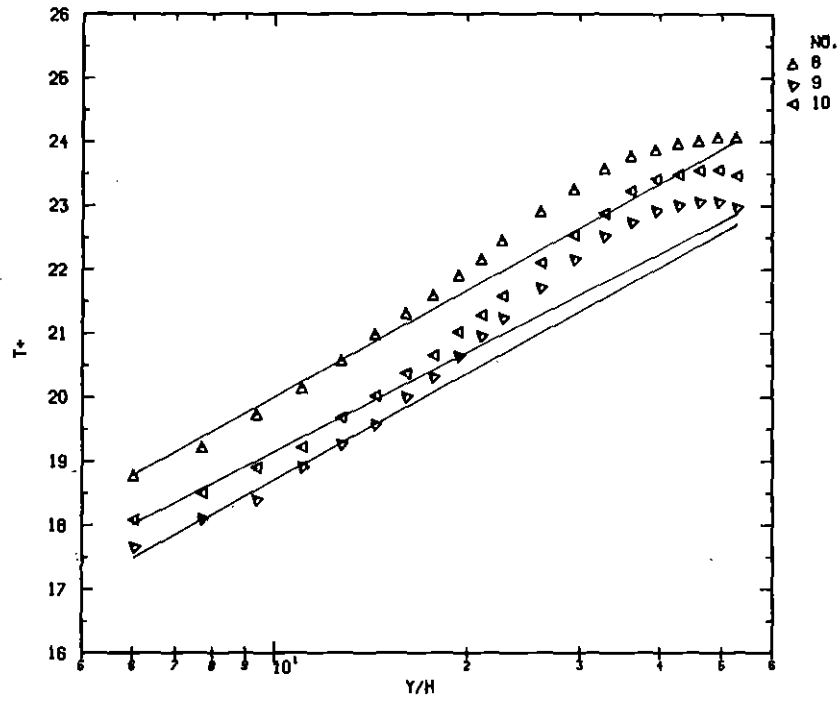


Fig.14: Non-dimensional temperature profiles in test section 23-50



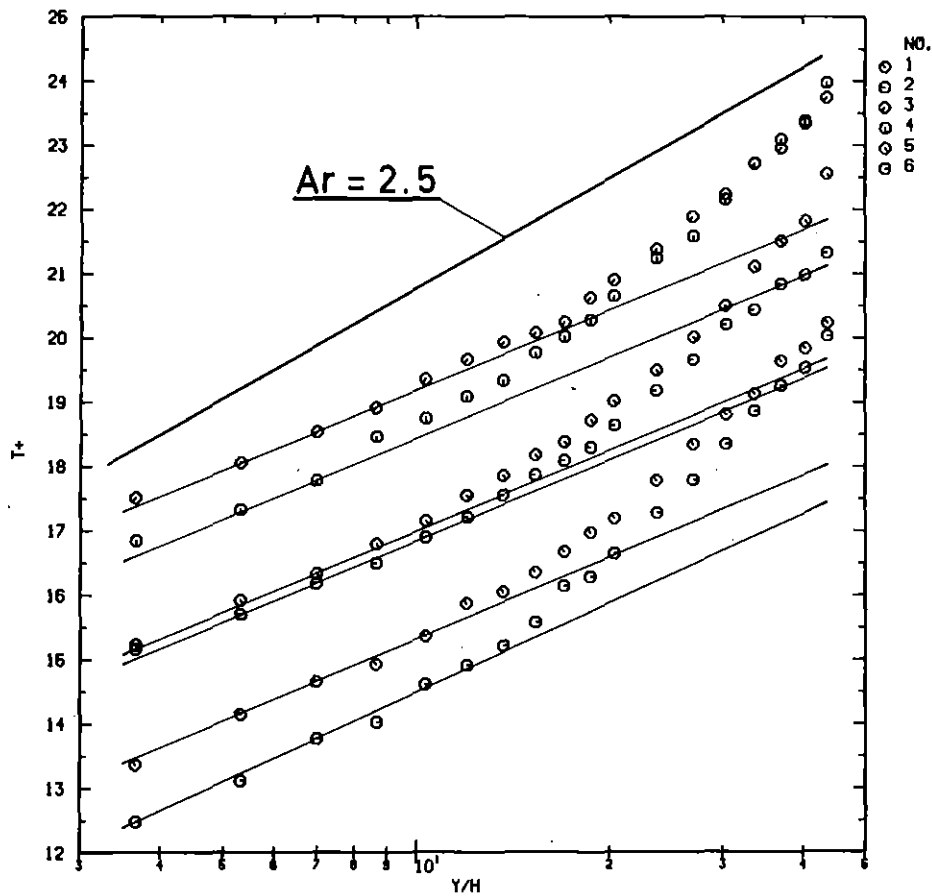
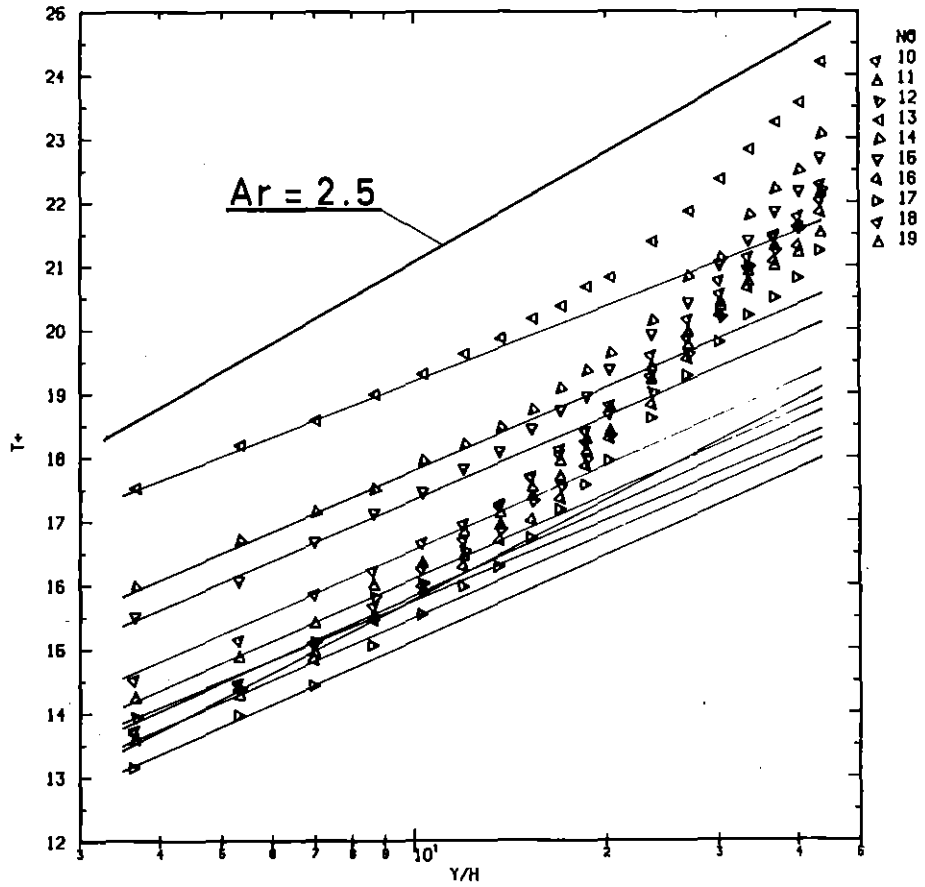


Fig.15: Non-dimensional temperature profiles in test section 12-85

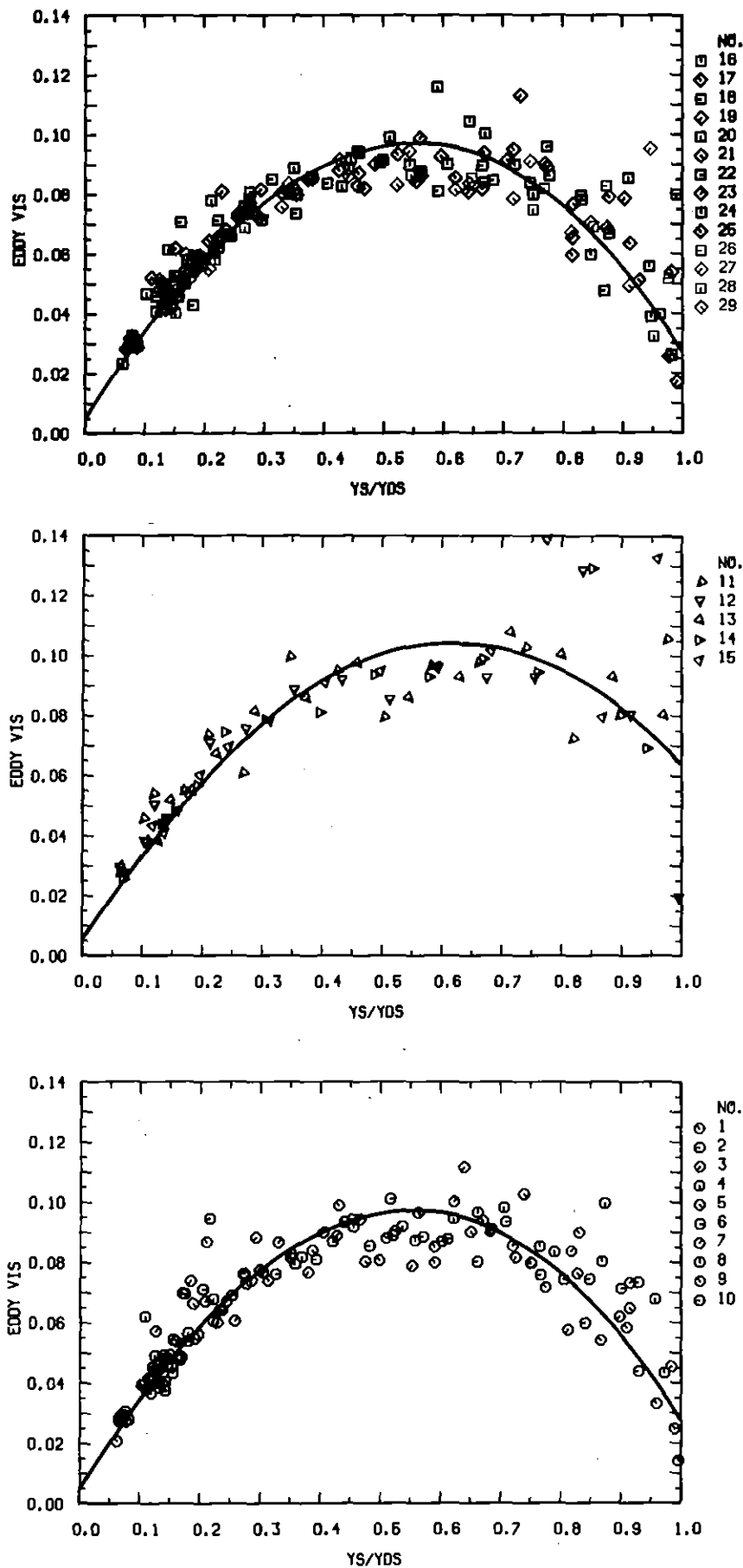


Fig.16: Non-dimensional eddy viscosity  $\epsilon_s^+$  in the smooth zone in test section 23-72, with least square fit line,  $YS/YDS = y_s/\hat{y}_s$

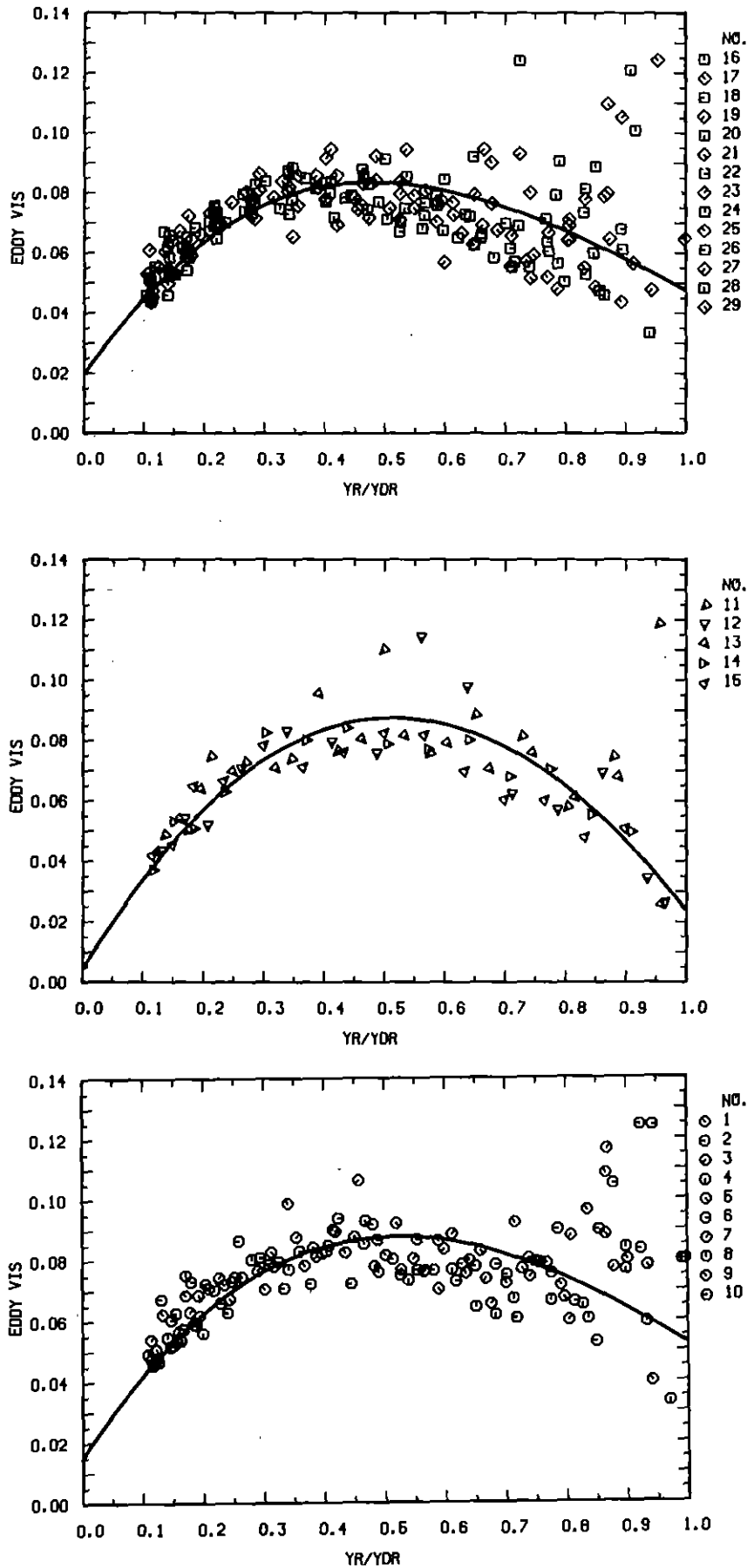


Fig.17: Non-dimensional eddy viscosity  $\epsilon_r^+$  in the rough zone in test section 23-72 with least square fit line,  $YR/YDR = y_r/\hat{Y}_r$

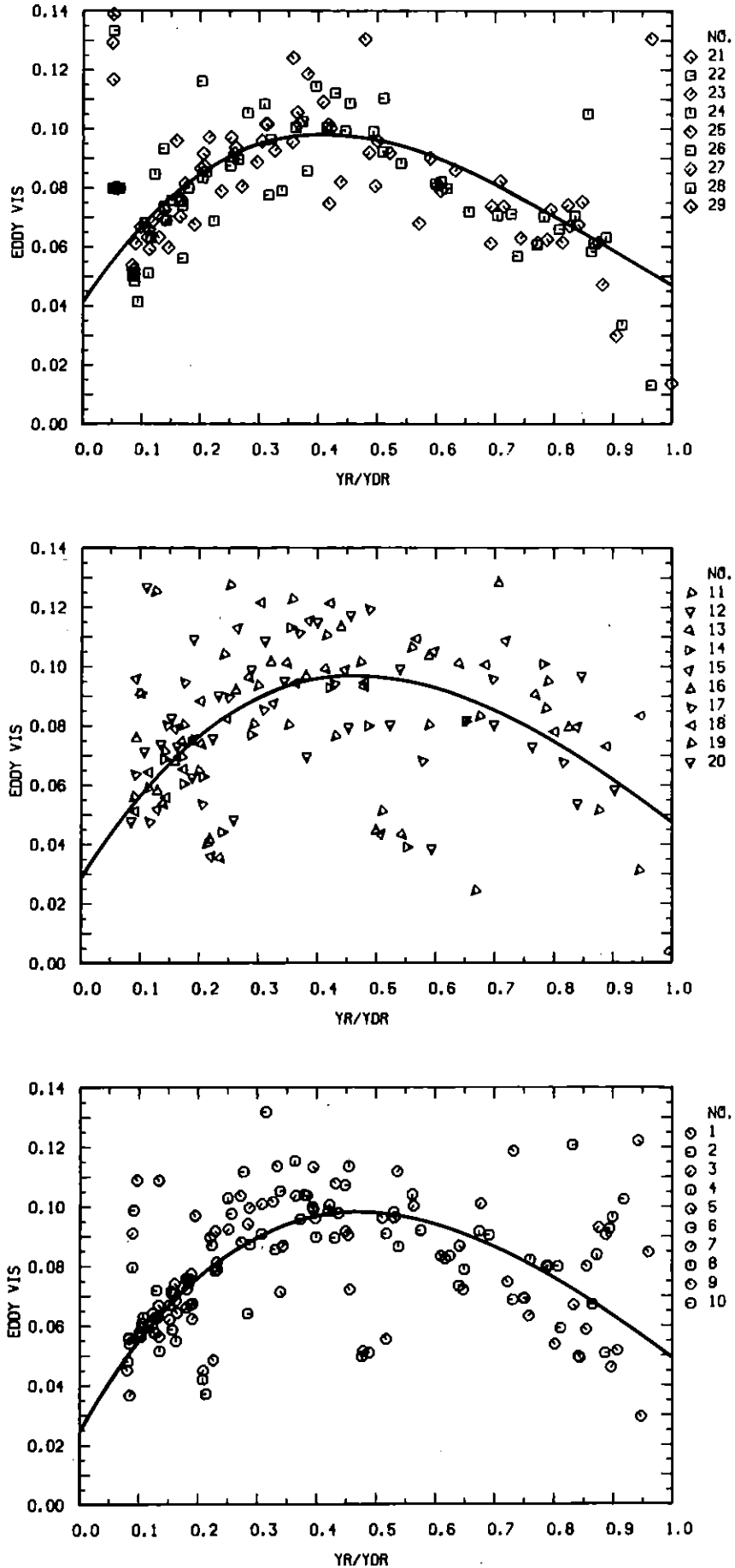


Fig.18: Non-dimensional eddy viscosity  $\epsilon_r^+$  in the rough zone in test section 22-85 with least square fit line

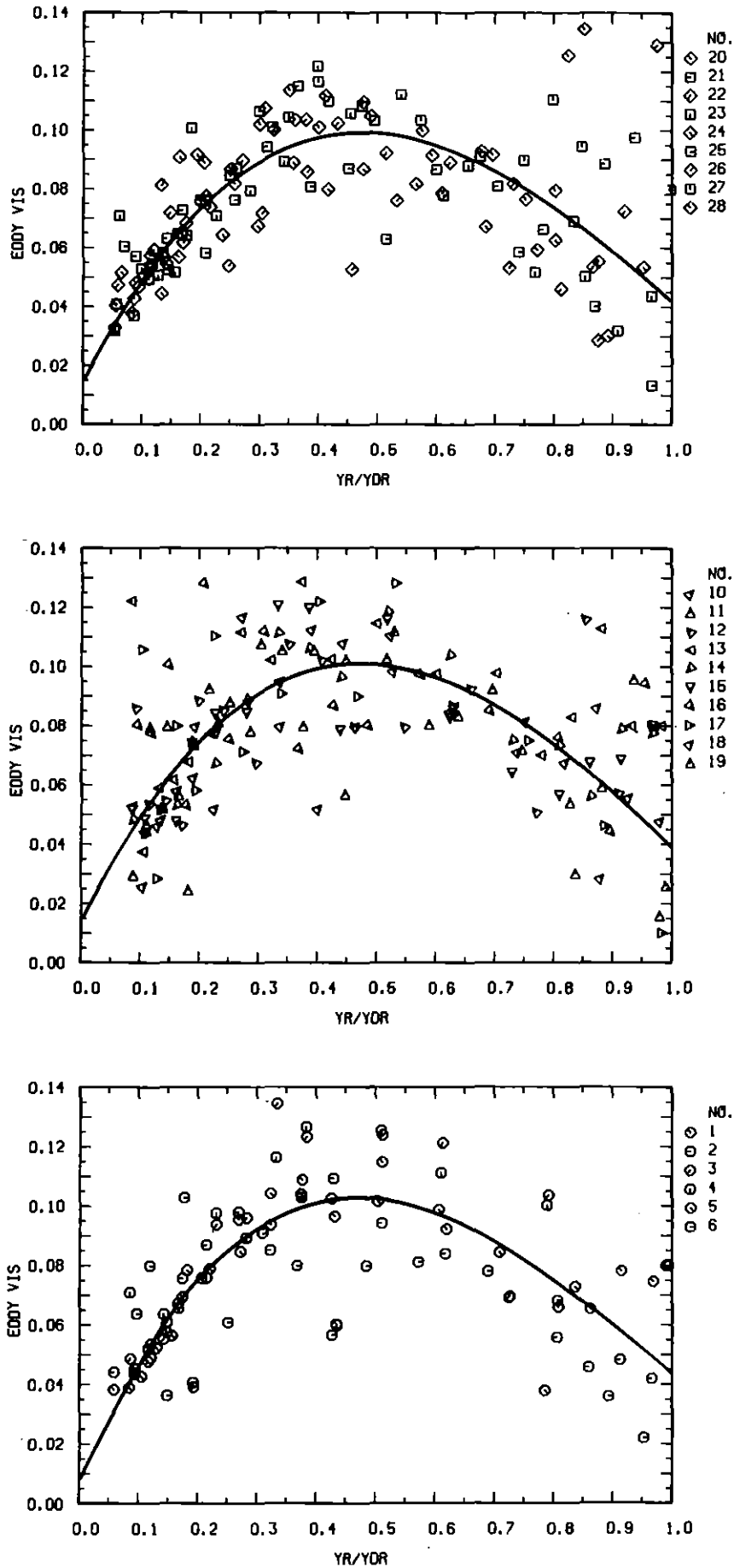


Fig.19: Non-dimensional eddy viscosity  $\epsilon_r^+$  in the rough zone in test section 12-85 with least square fit line

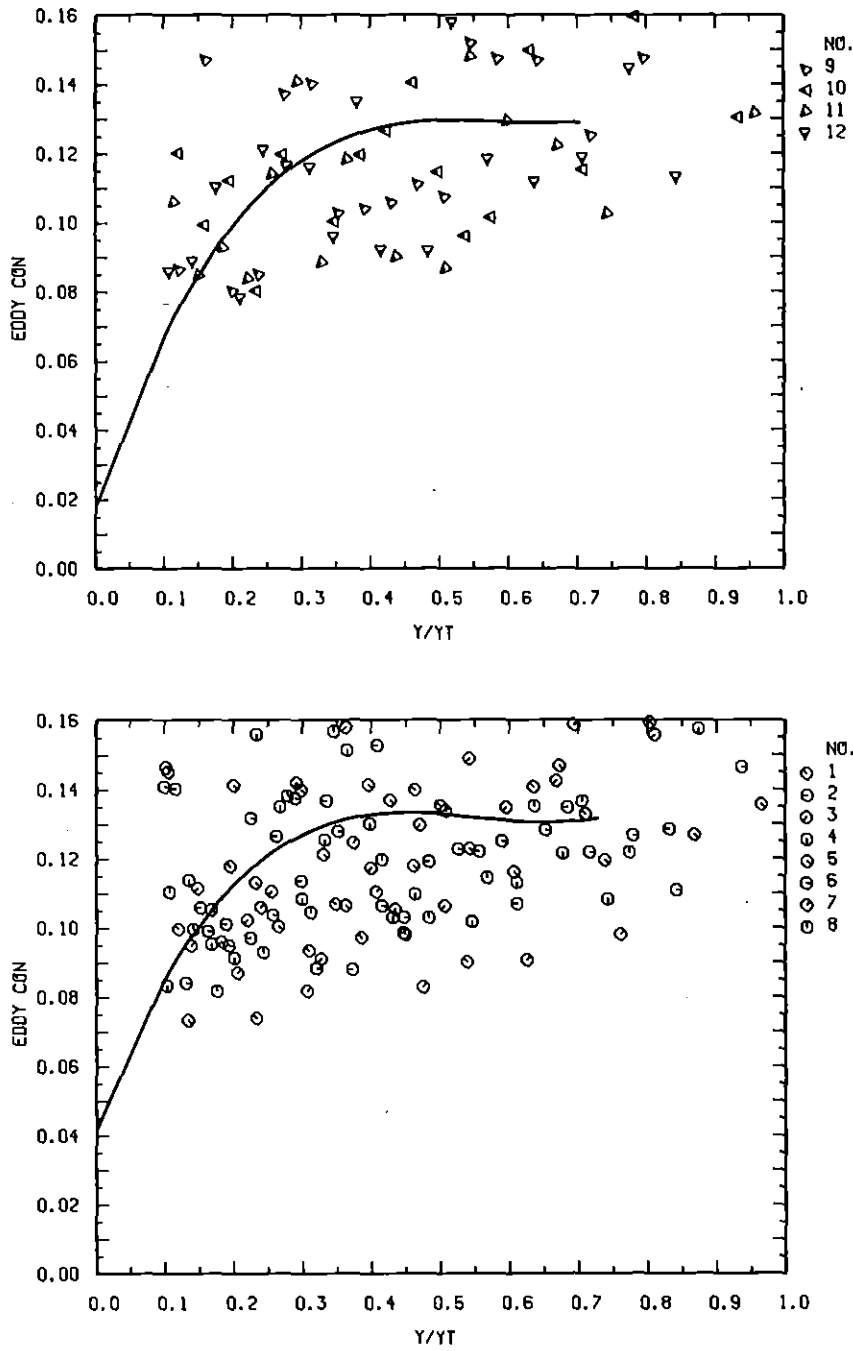


Fig.20: Non-dimensional eddy conductivity  $\epsilon_H^+$  in test section 23-72 with least square fit line,  $Y/YT = y_r/\hat{y}_r$

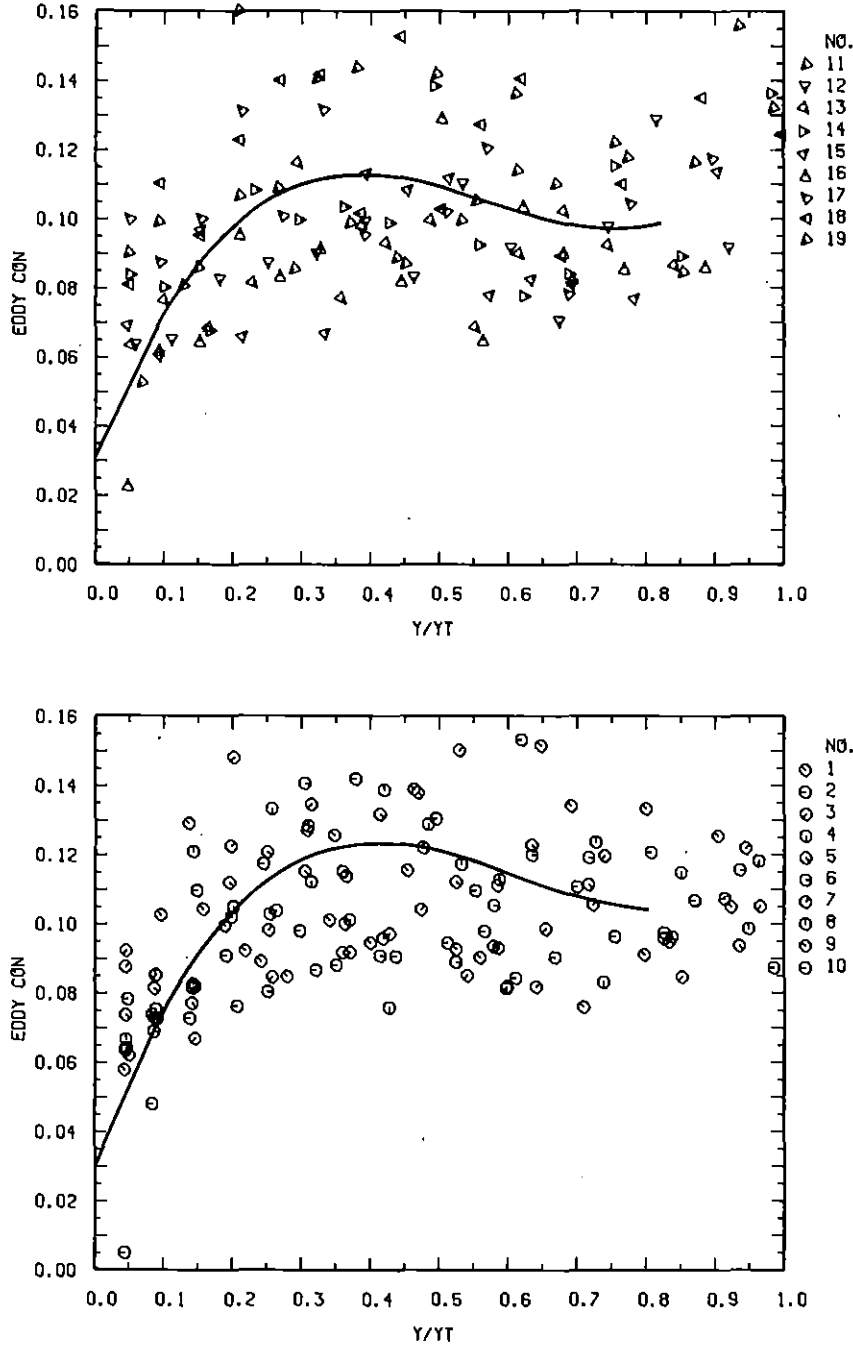


Fig.21: Non-dimensional eddy conductivity  $\epsilon_H^+$  in test section 22-85 with least square fit line.

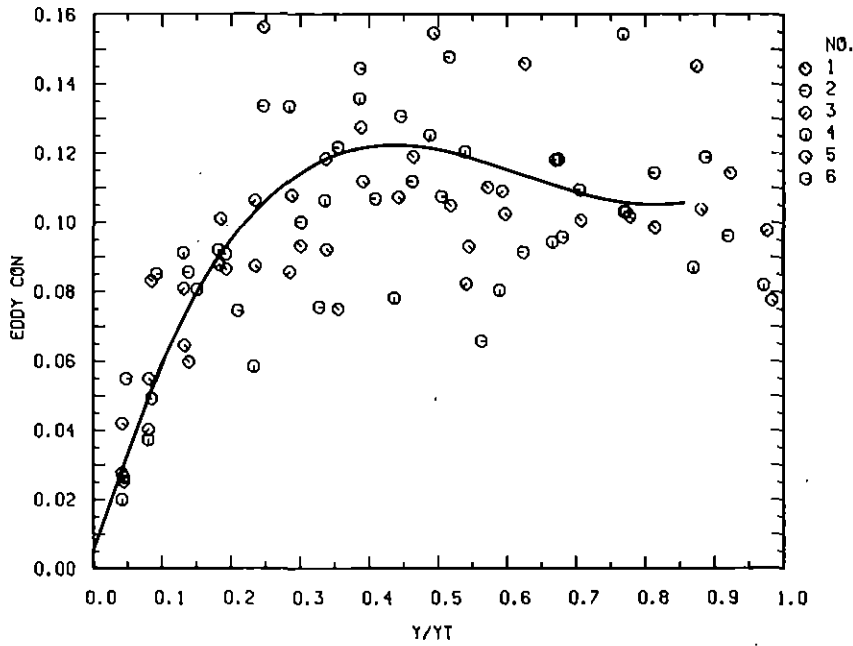
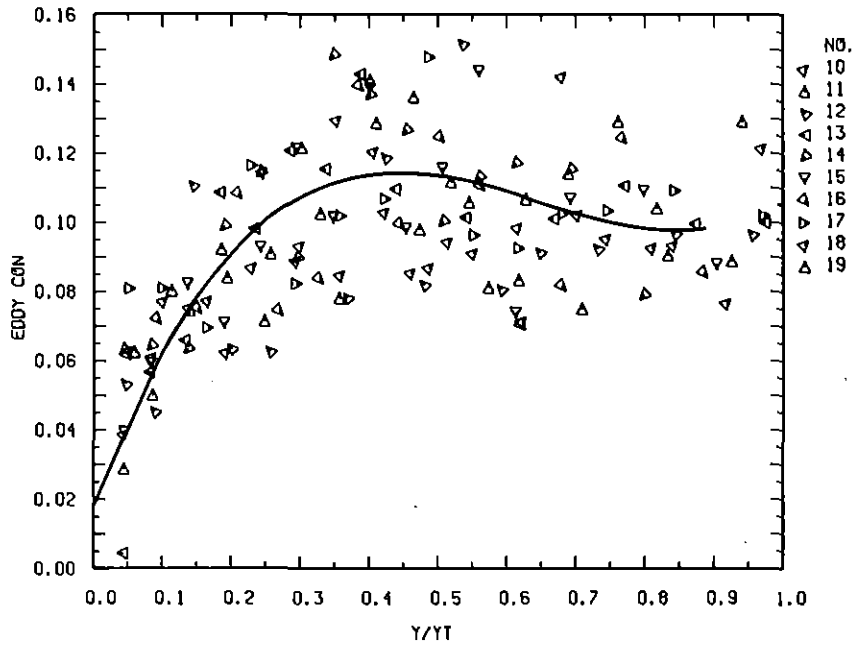


Fig.22: Non-dimensional eddy conductivity  $\epsilon_H^+$  in test section 12-85 with least square fit line



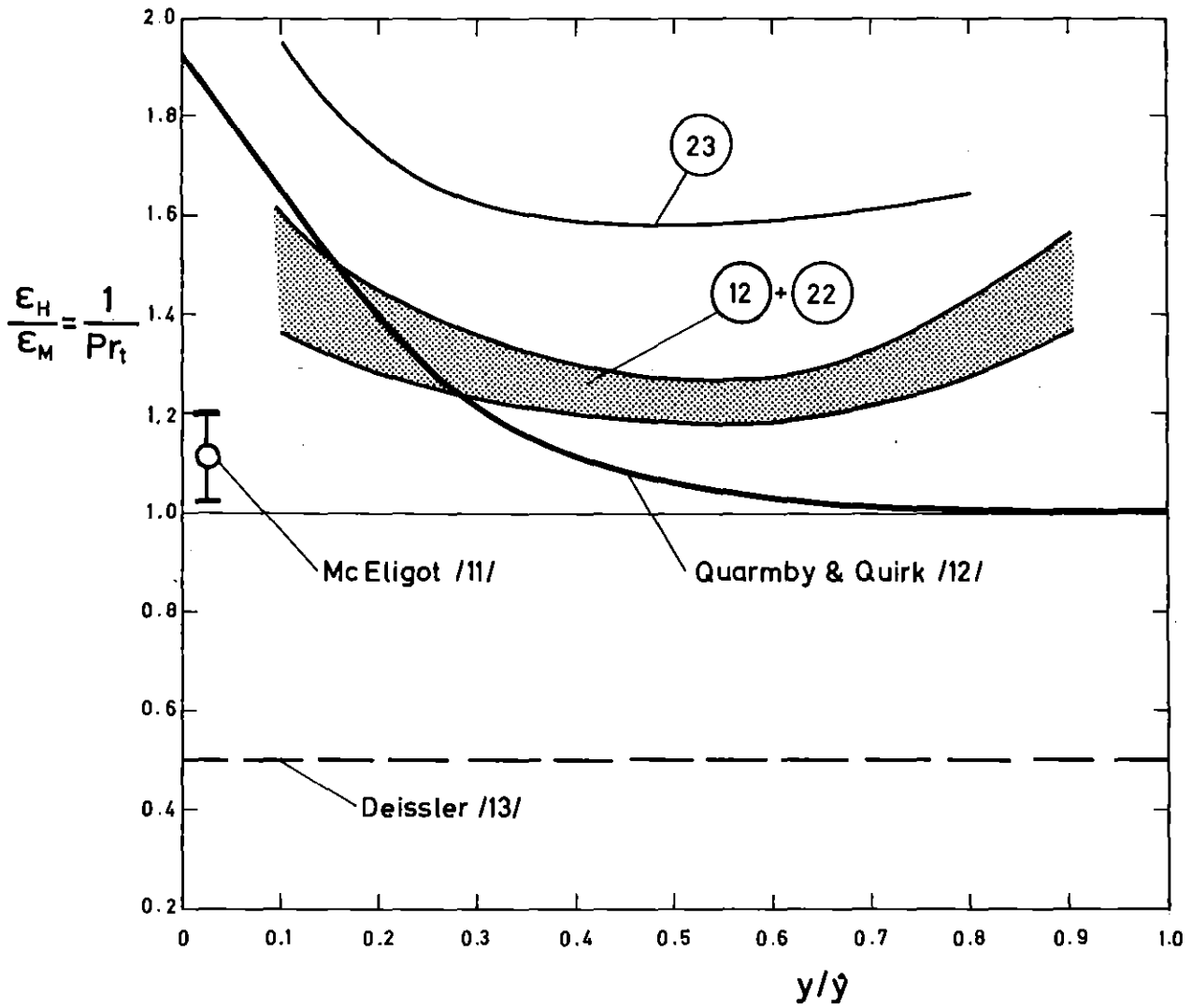


Fig. 23: Variation of  $Pr_t$  in rough annuli compared with data suggested by various authors for gas flow in smooth tubes

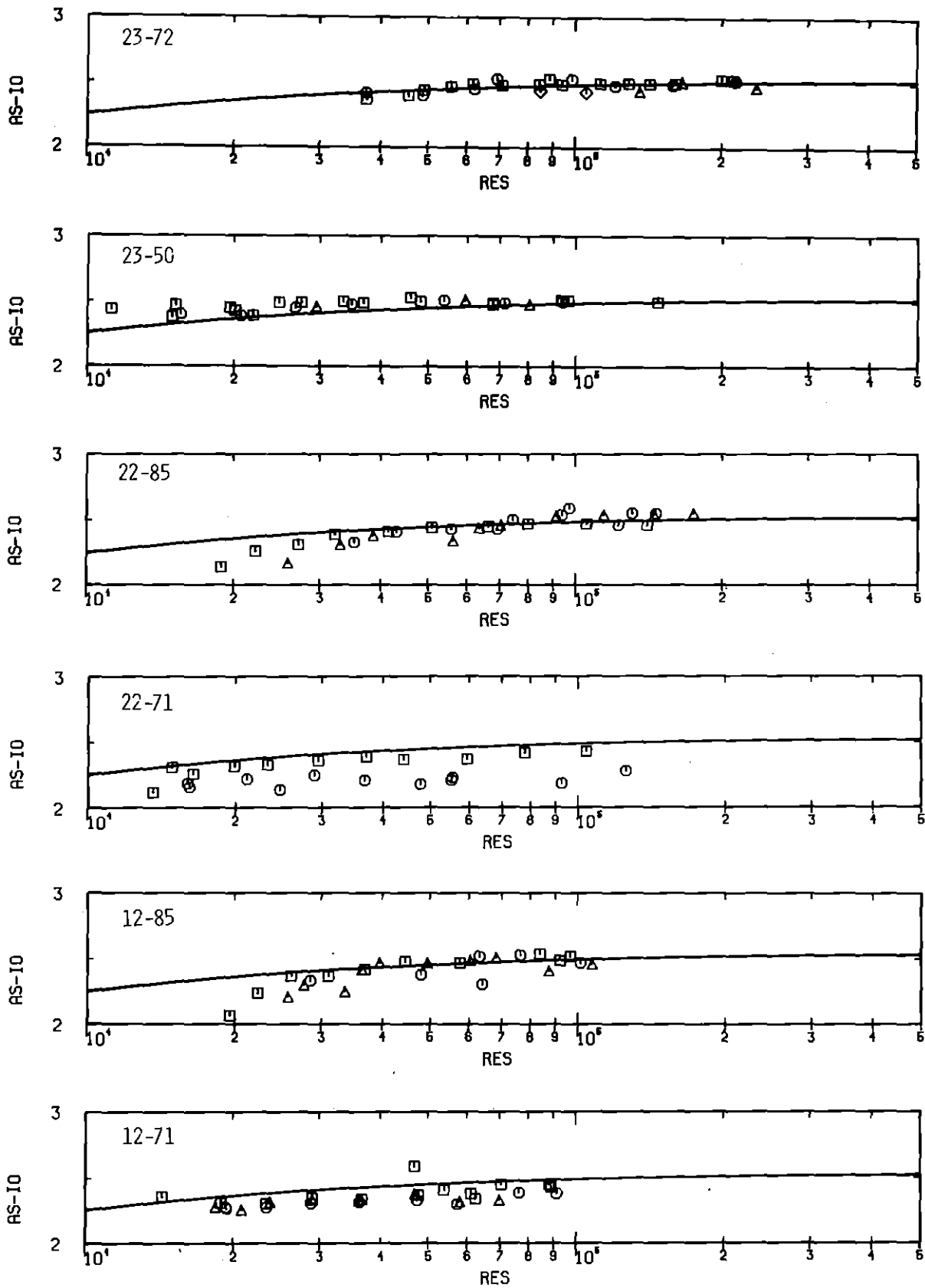


Fig.24: Variation of  $A_{SO}$  with Reynolds number, determined by Eq. (22) and (30), with a line according to Eq. (31)

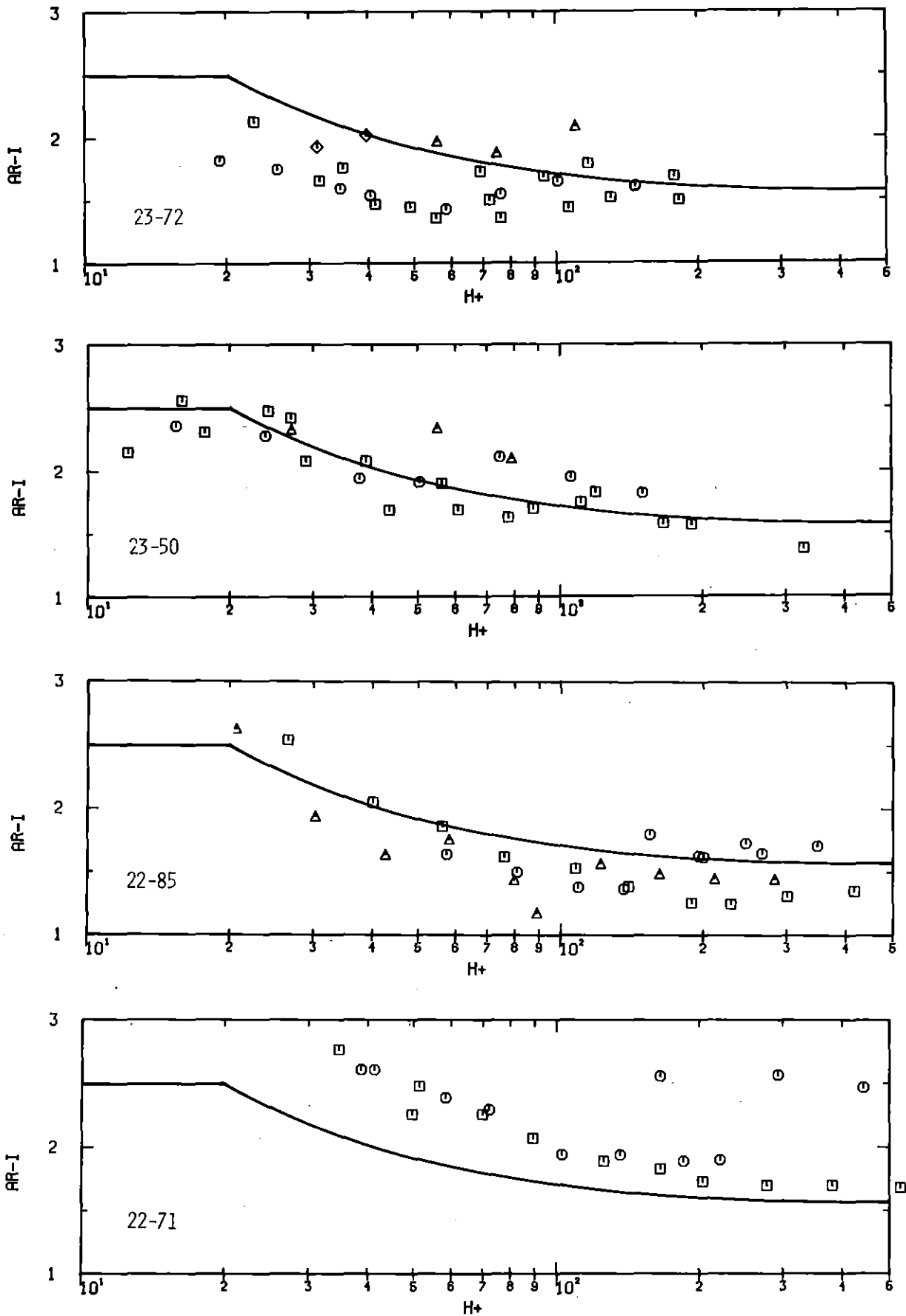


Fig.25a: Variation of  $A_r$  with  $h^+$ , determined by Eq.(23), with a line according to Eq.(32), (2-dimensional roughness)

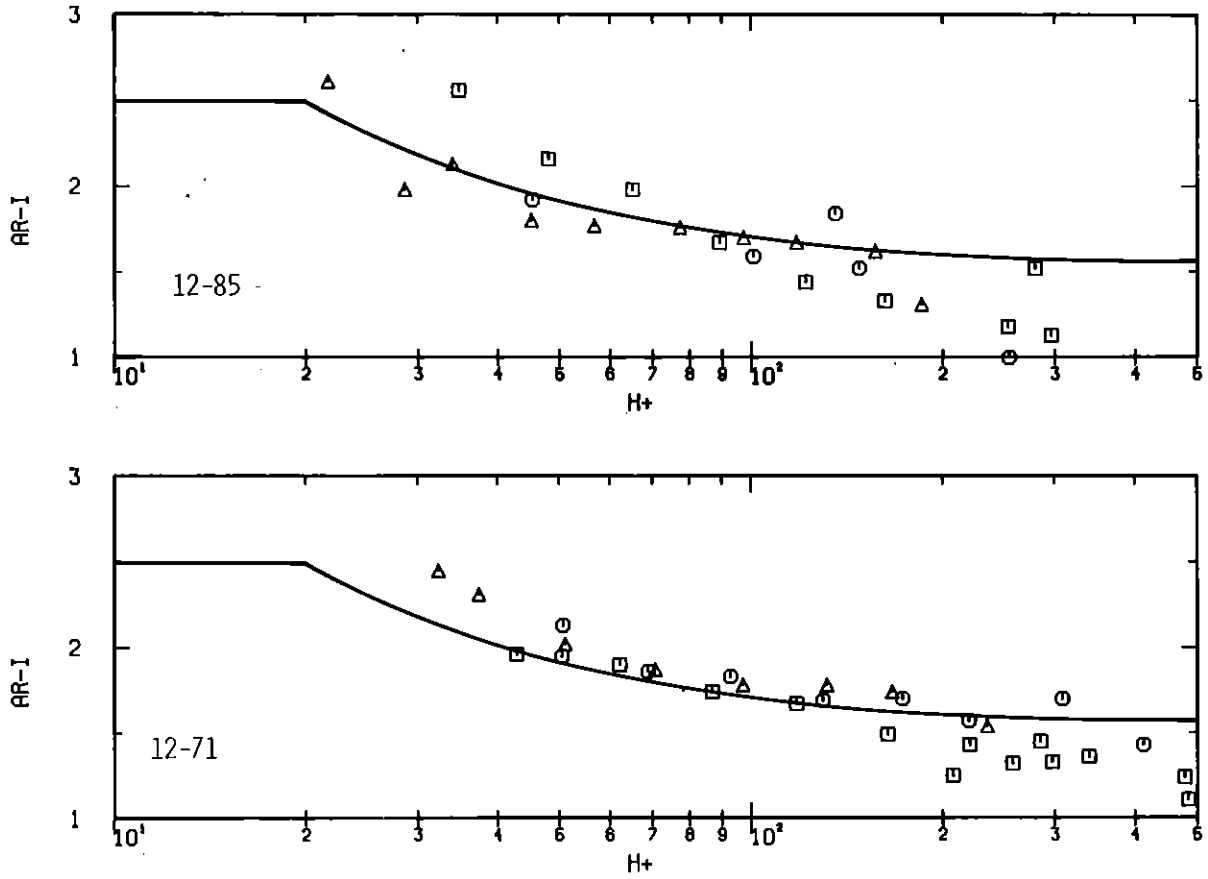


Fig.25b: Variation of  $A_r$  with  $h^+$ , determined by Eq.(23), with a line according to Eq.(32), (3-dimensional roughness)

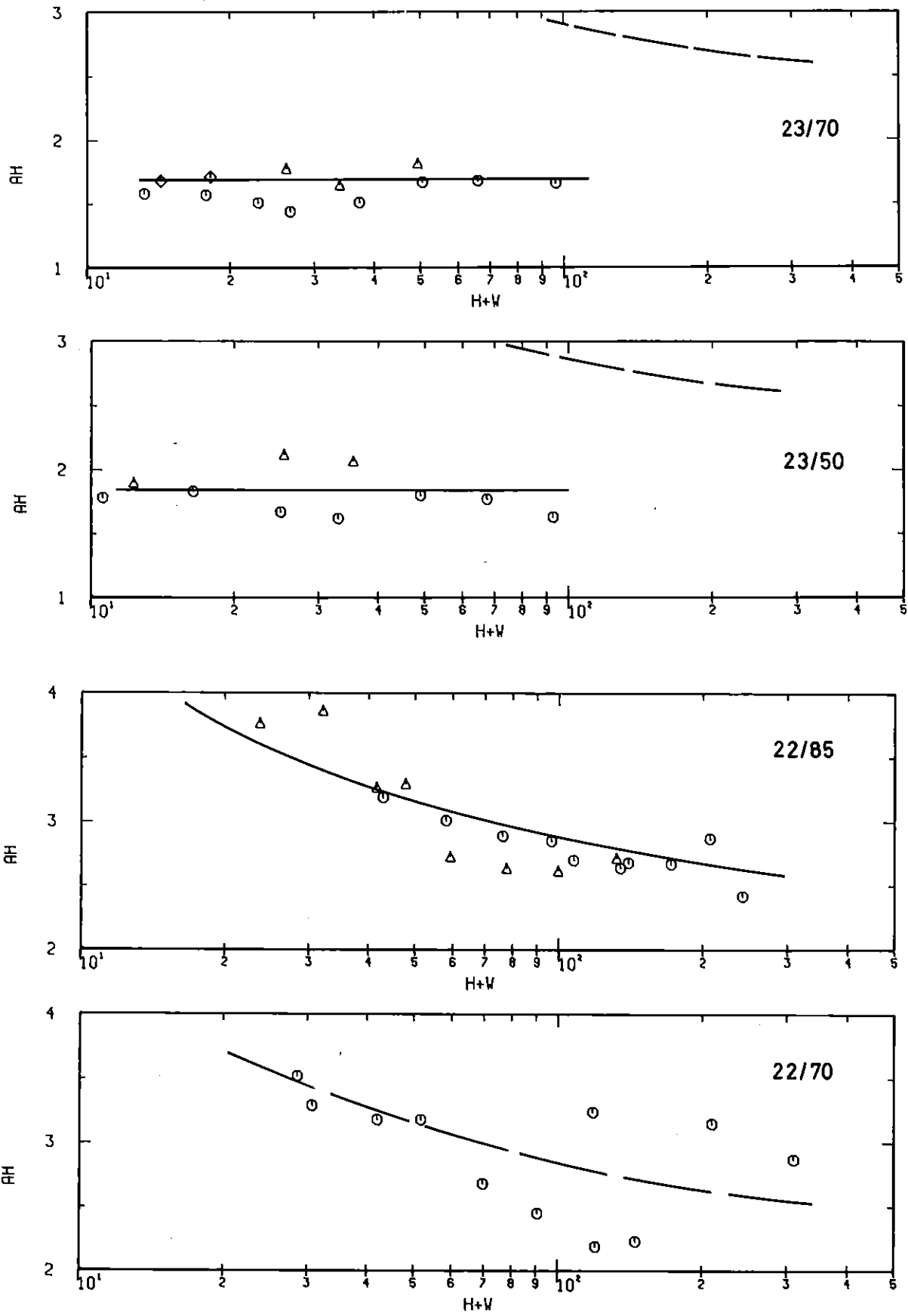


Fig. 25c: The slope of the temperature profile determined by Eq. (27)

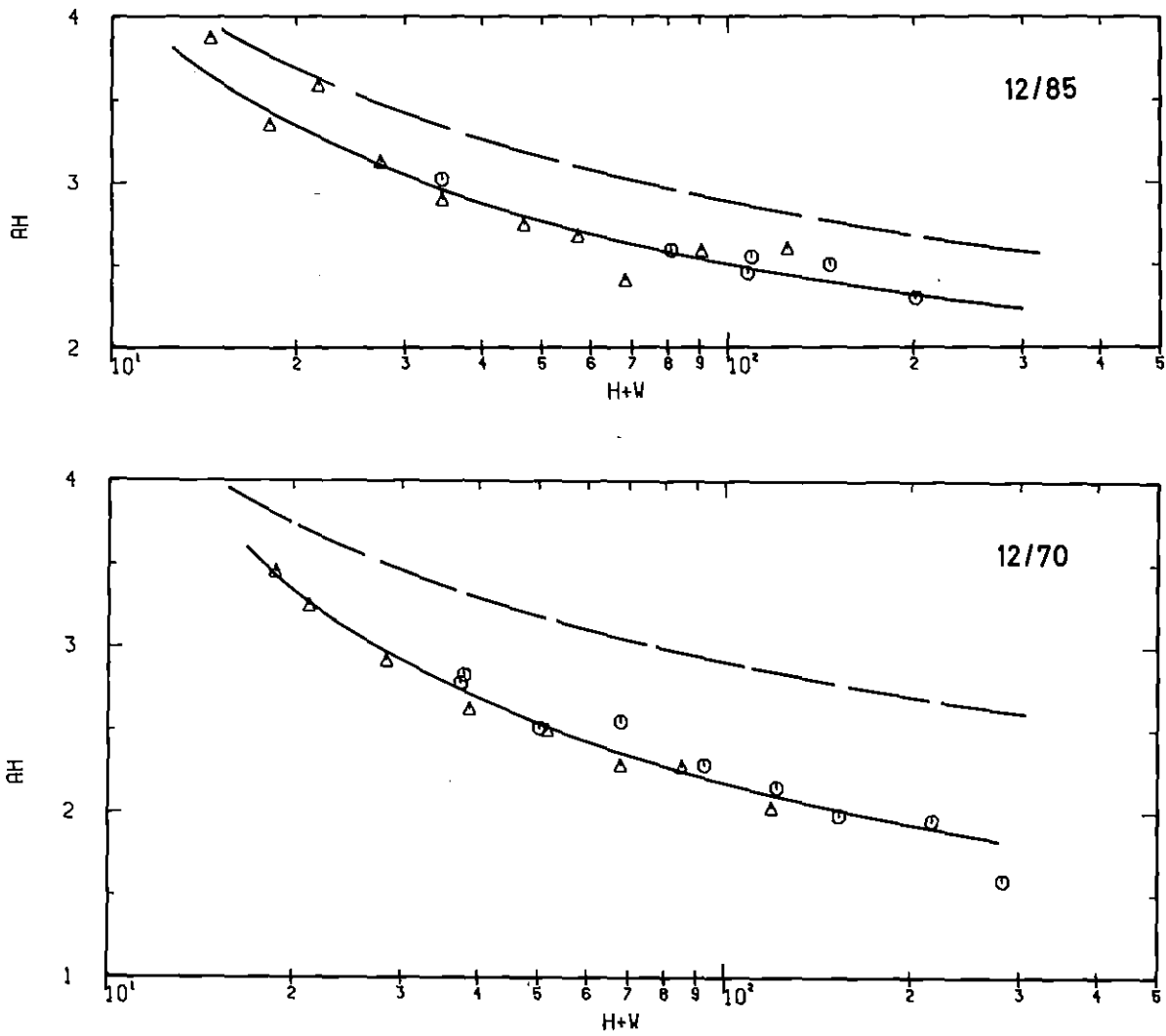


Fig. 25d: The slope of the temperature profile determined by Eq. (27)

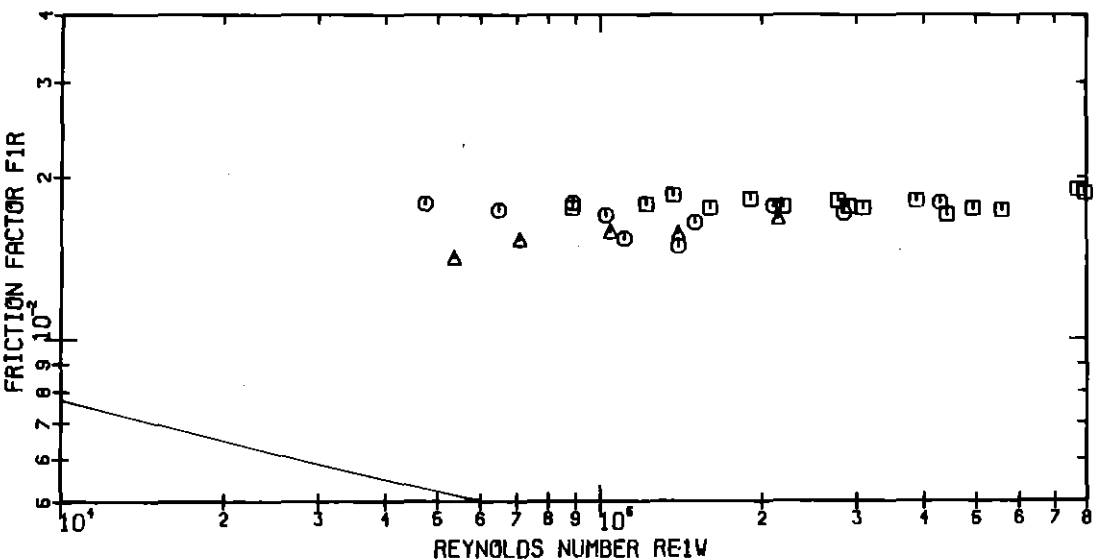
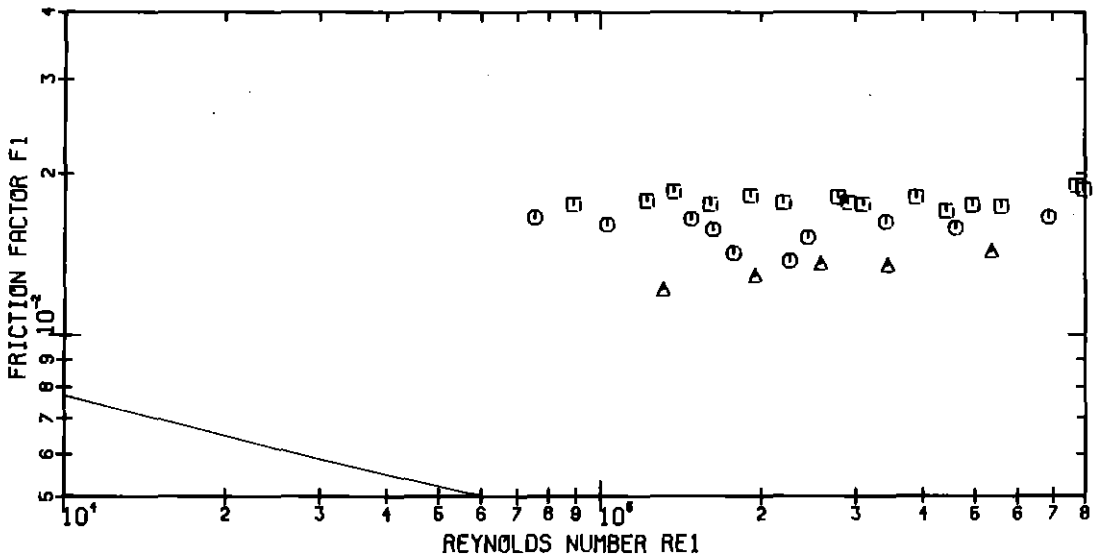
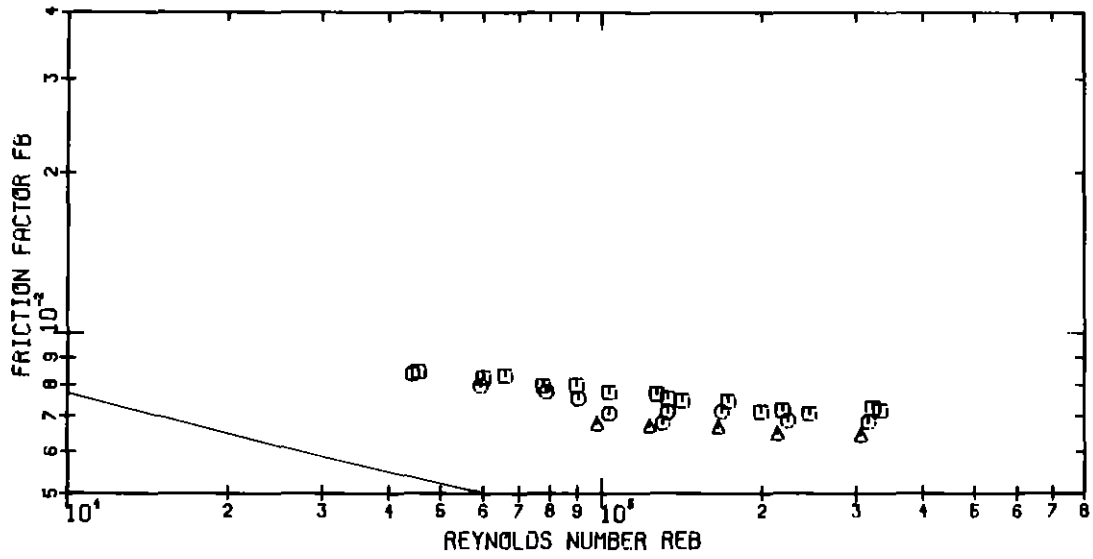


Fig.26: Friction factor versus Reynolds number (23-72)

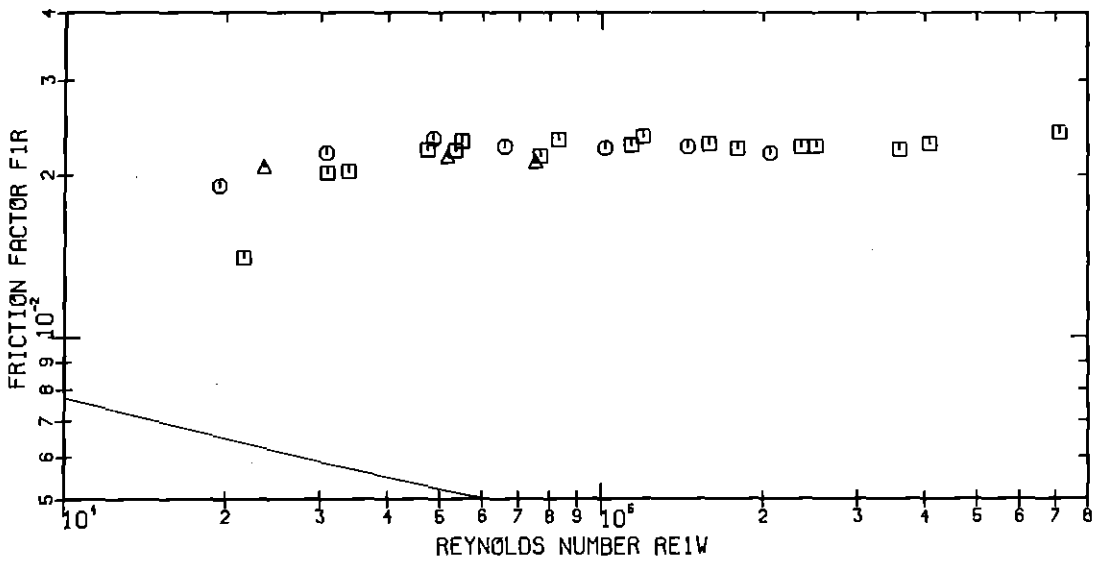
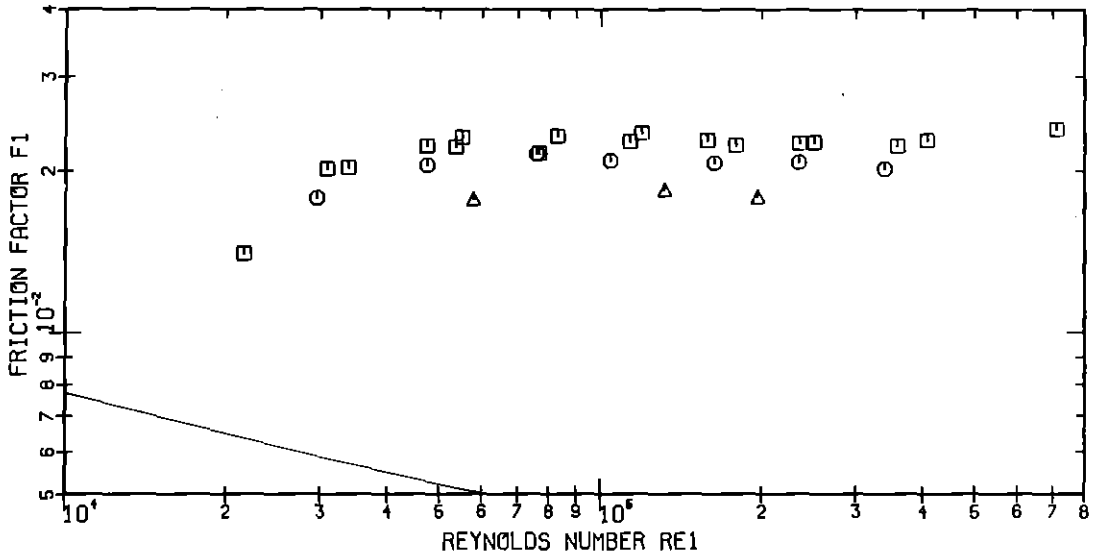
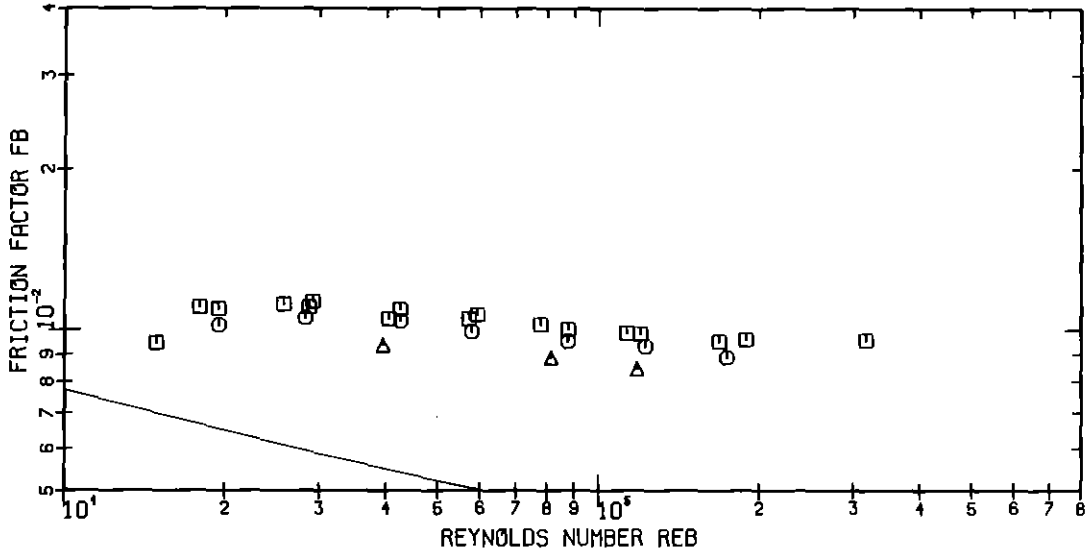


Fig.27: Friction factor versus Reynolds number (23-50)



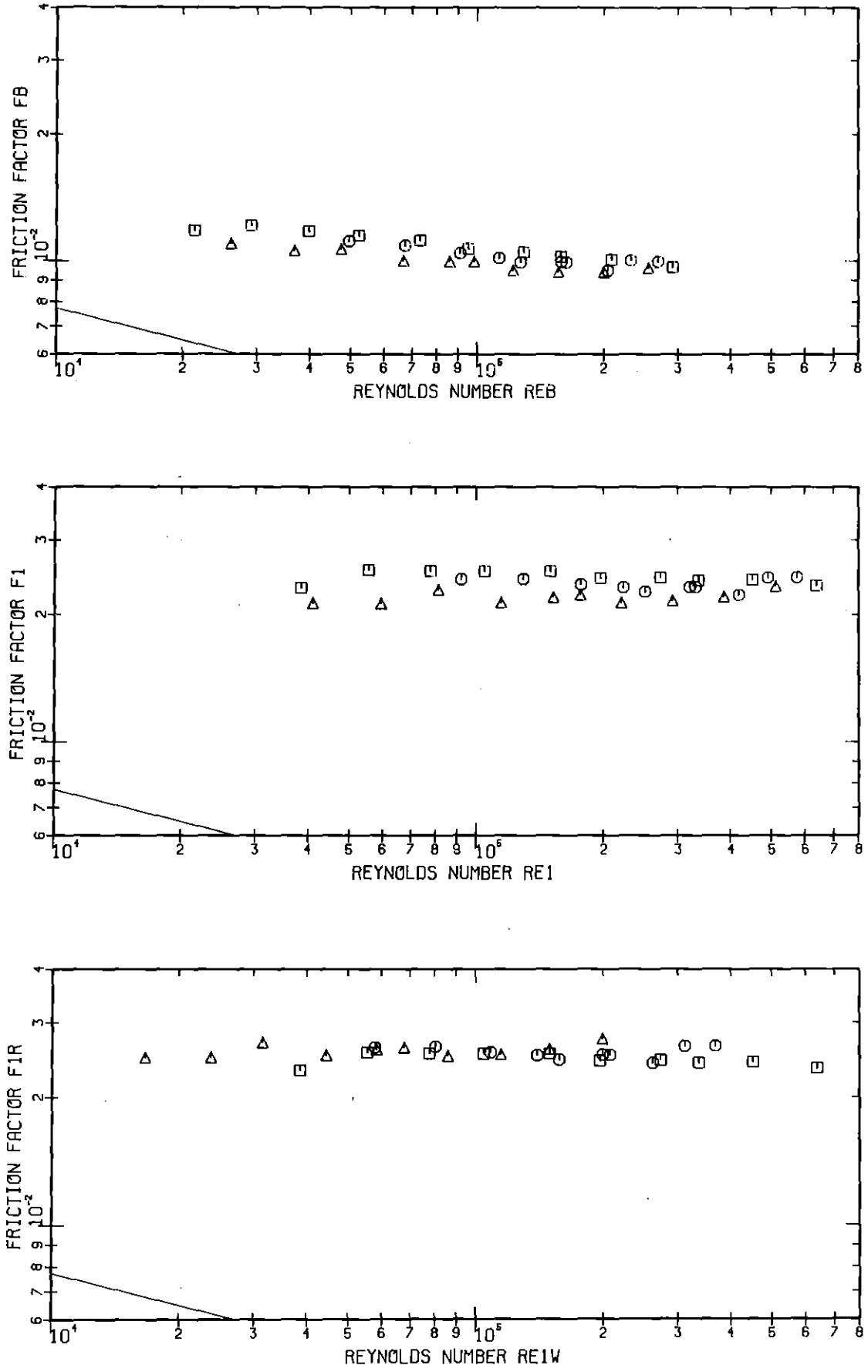


Fig.28: Friction factor versus Reynolds number (22-85)

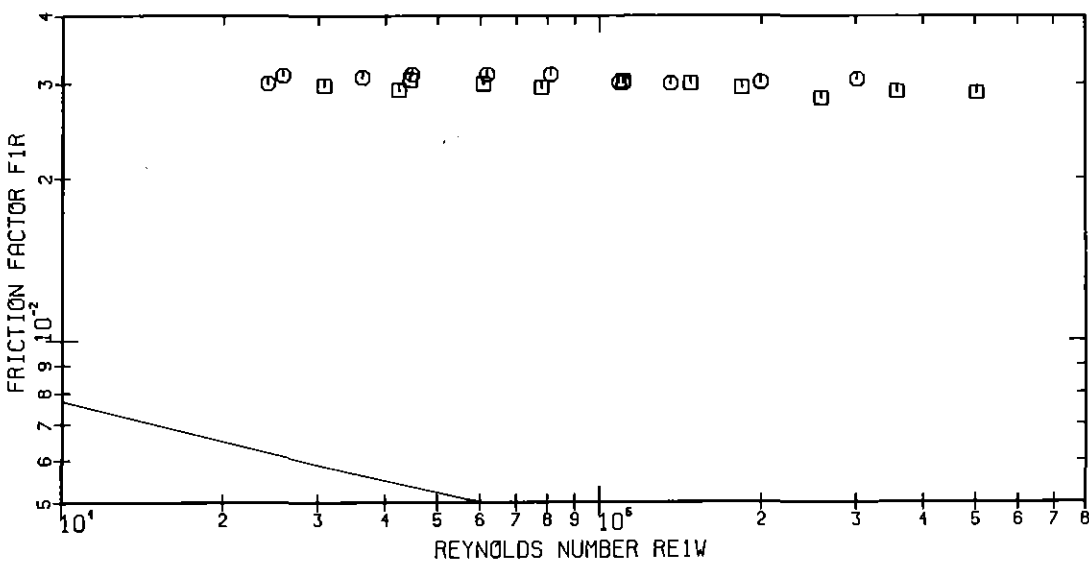
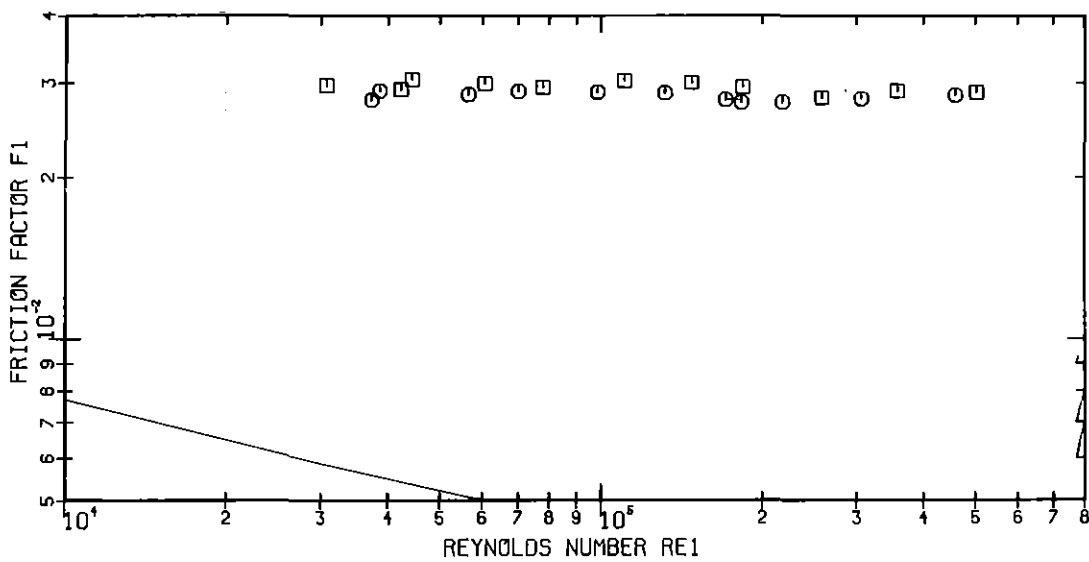
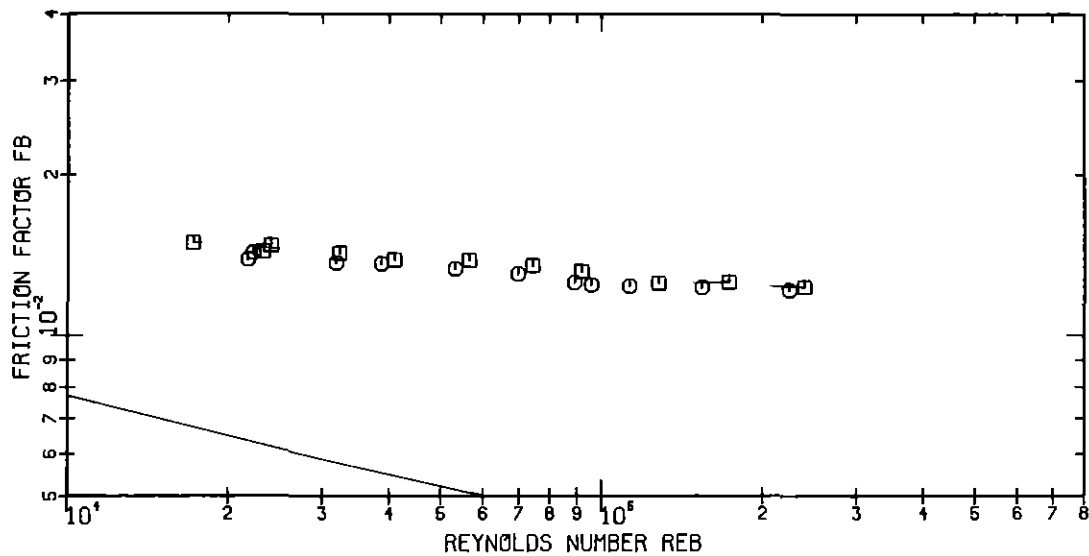


Fig.29: Friction factor versus Reynolds number (22-71)

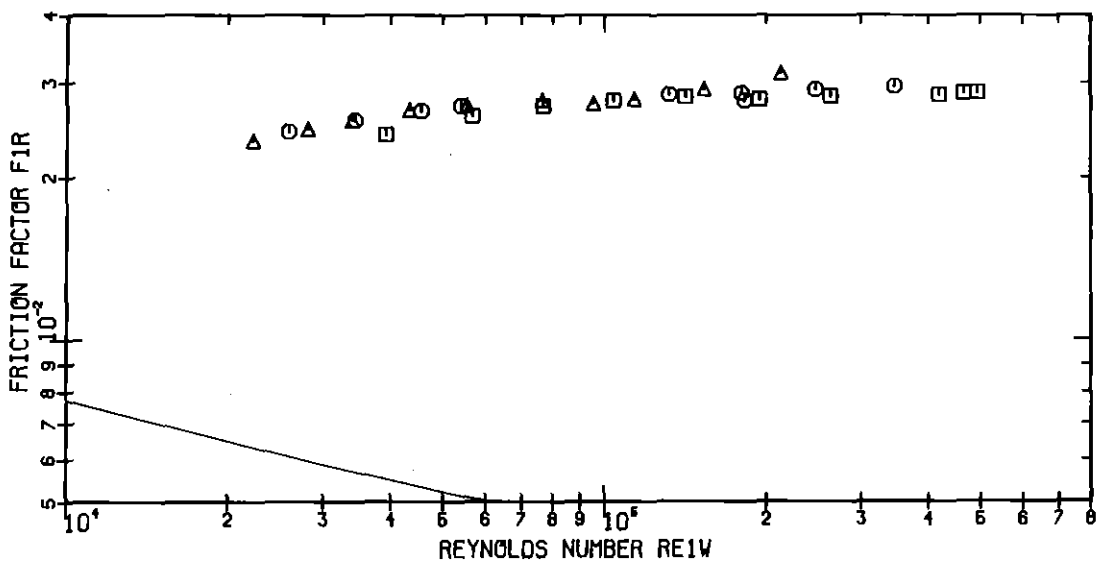
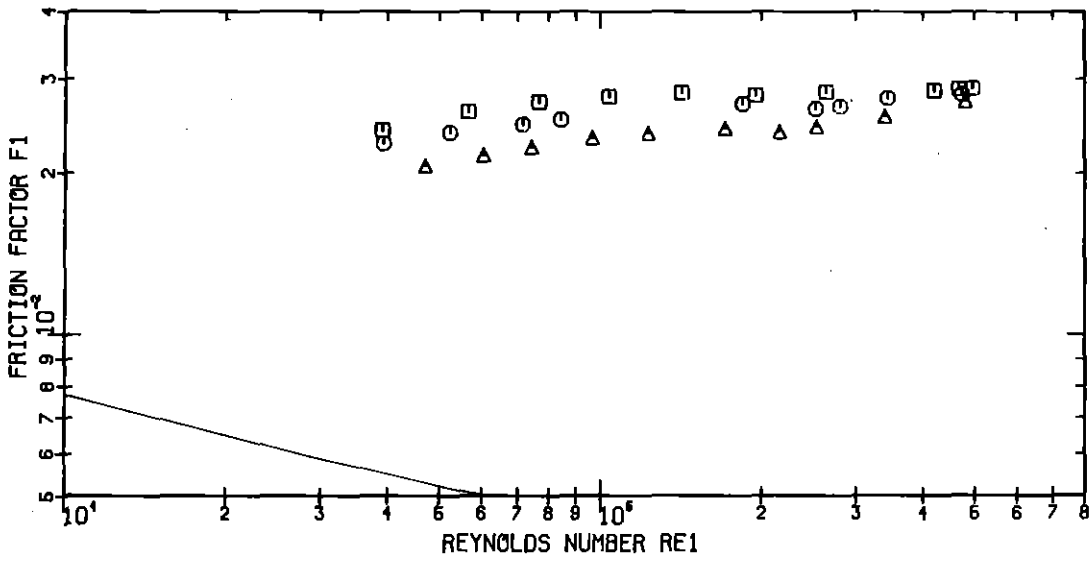
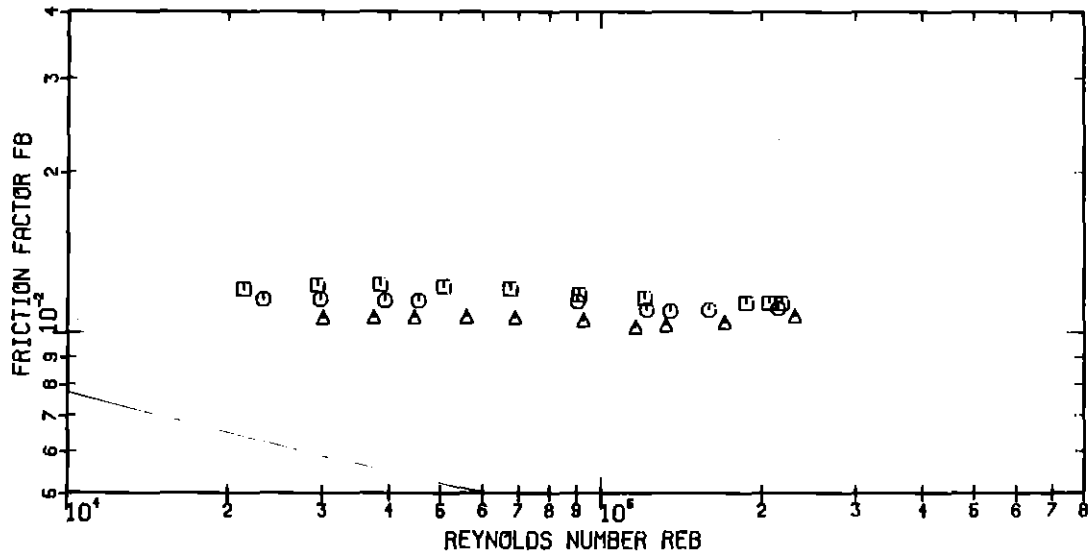


Fig.30: Friction factor versus Reynolds number (12-85)

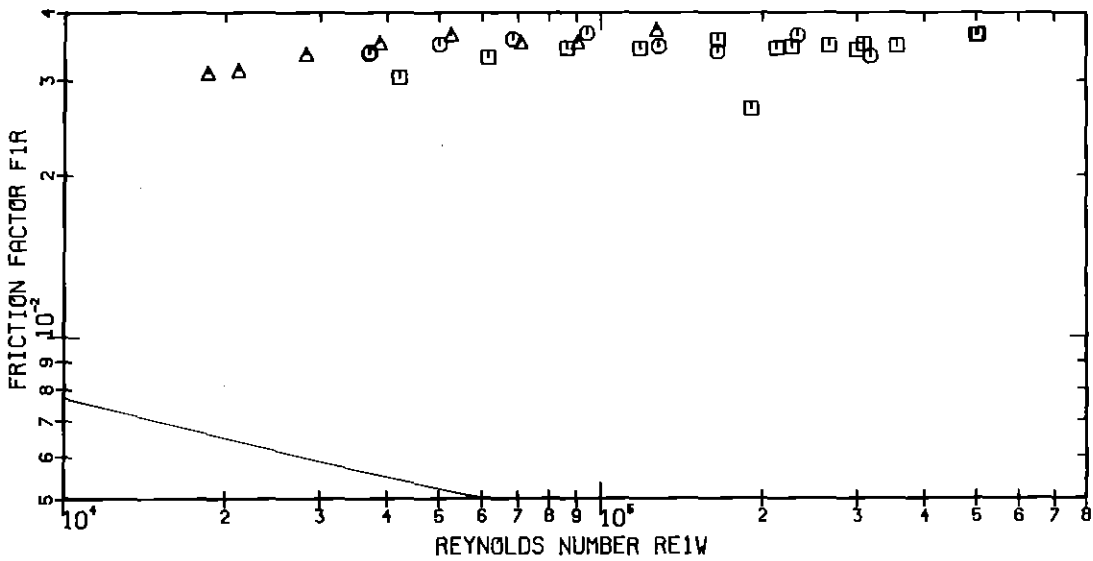
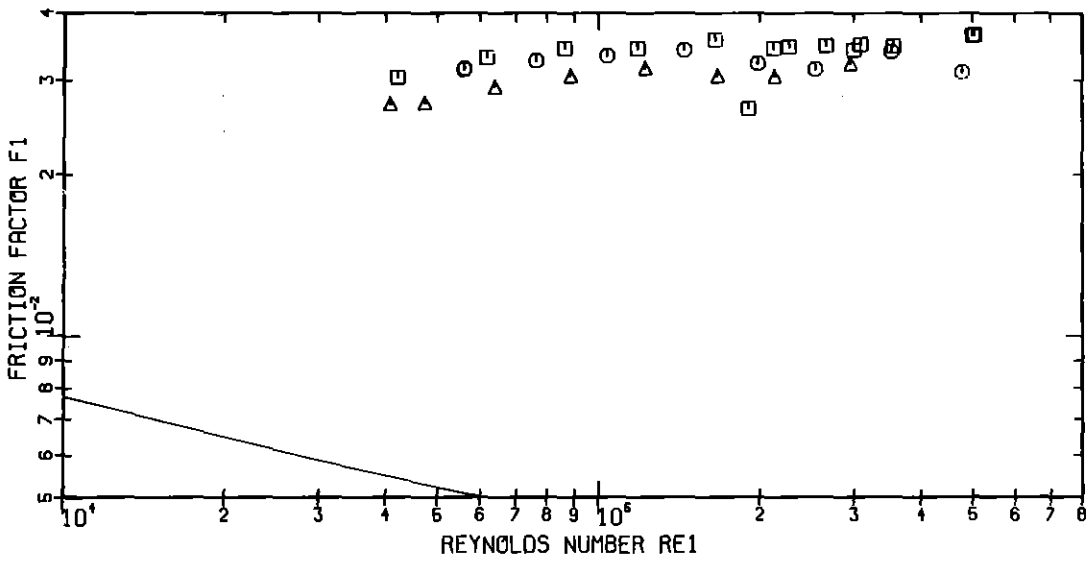
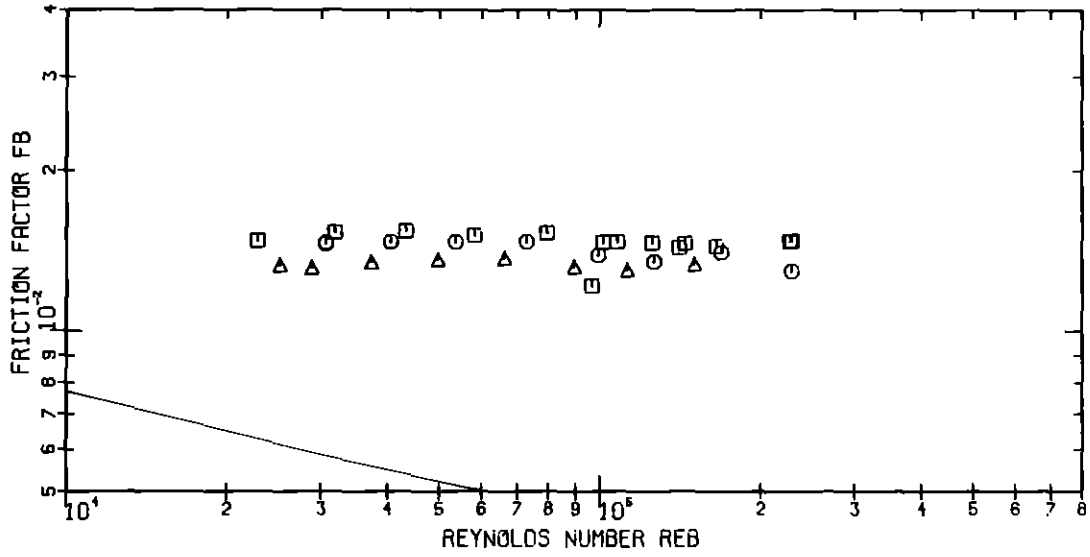


Fig.31: Friction factor versus Reynolds number (12-71)

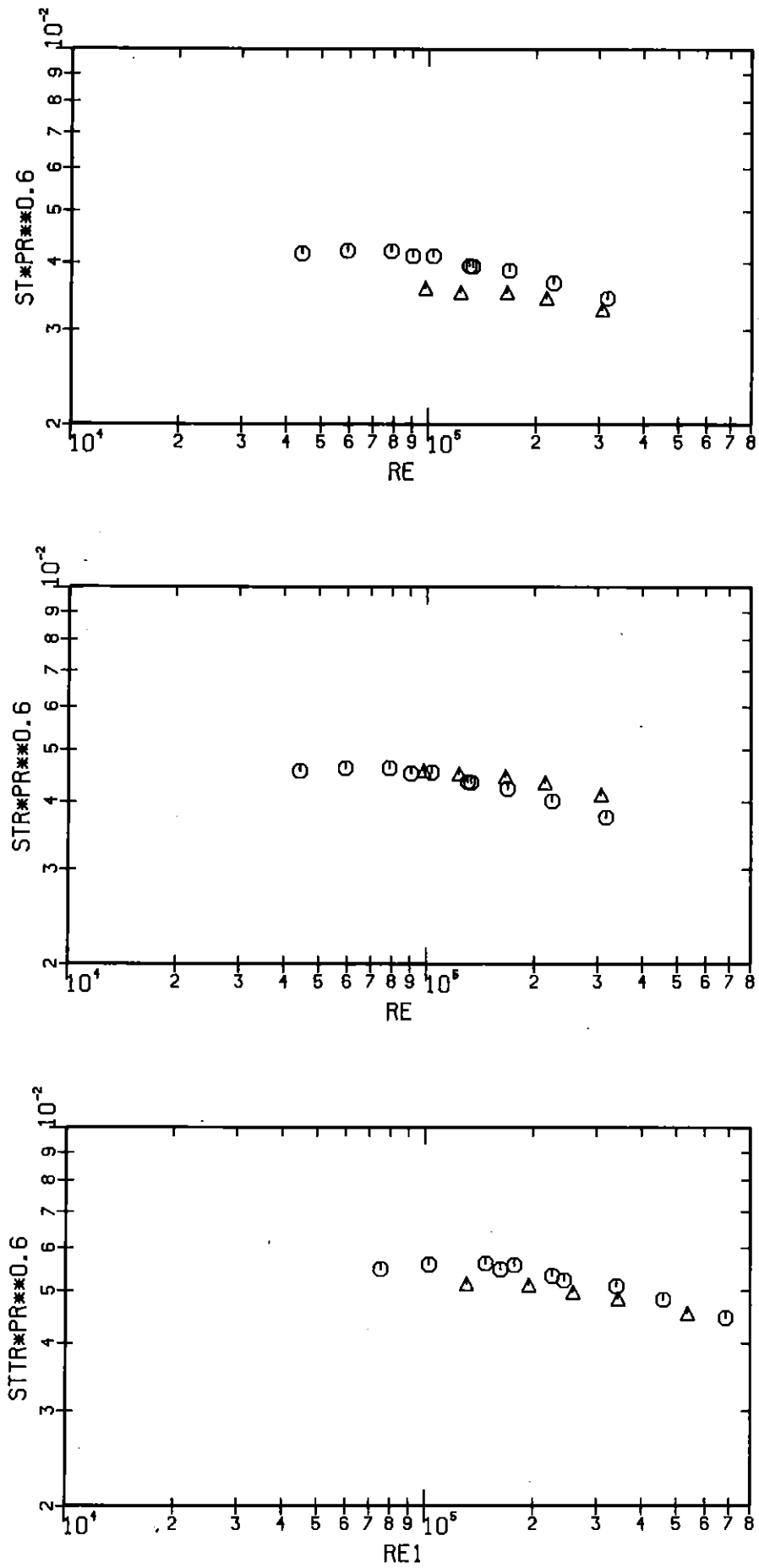


Fig.32: Stanton number versus Reynolds number (23-72)

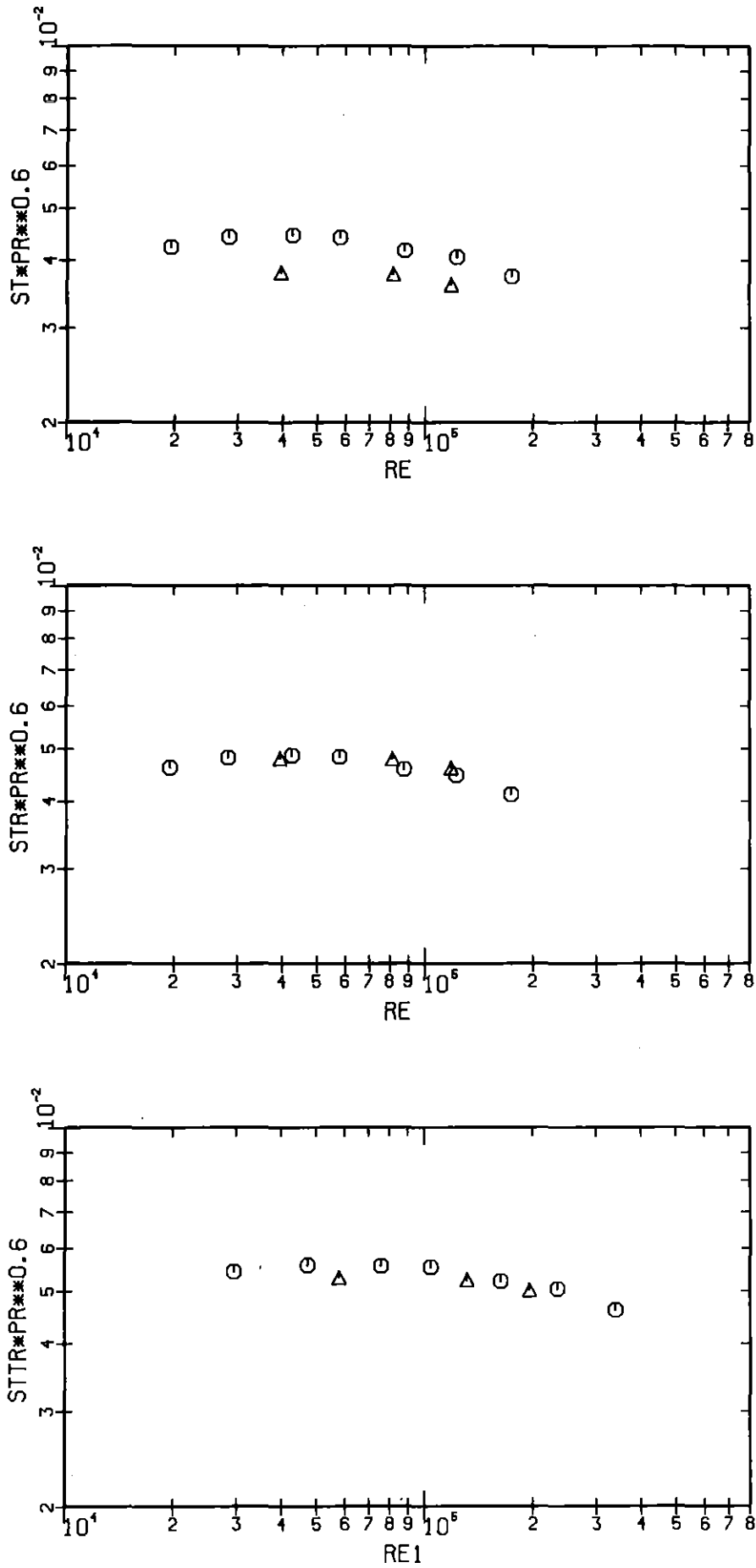


Fig.33: Stanton number versus Reynolds number (23-50)

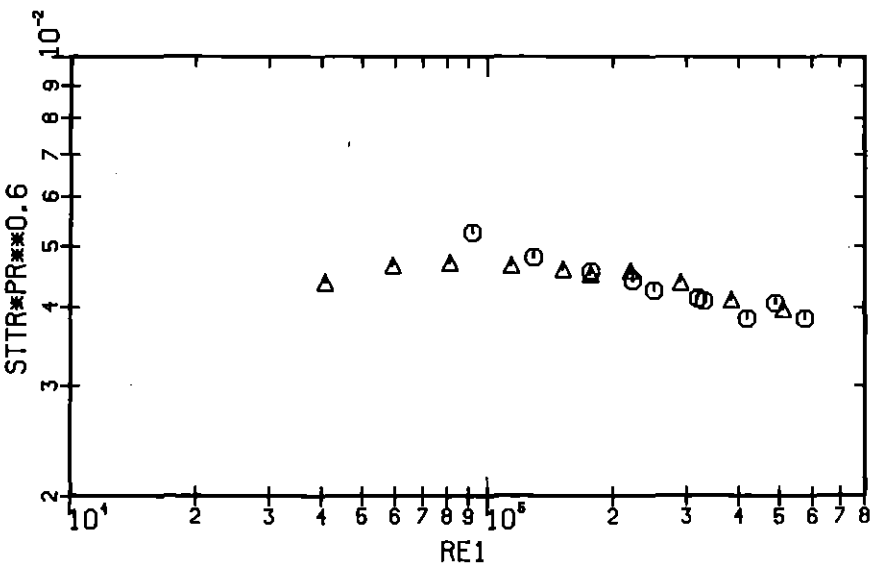
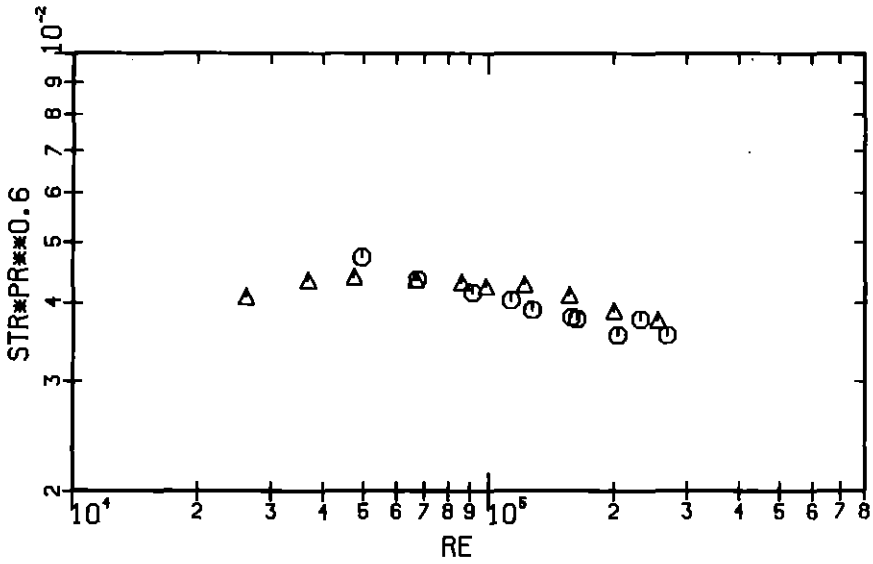
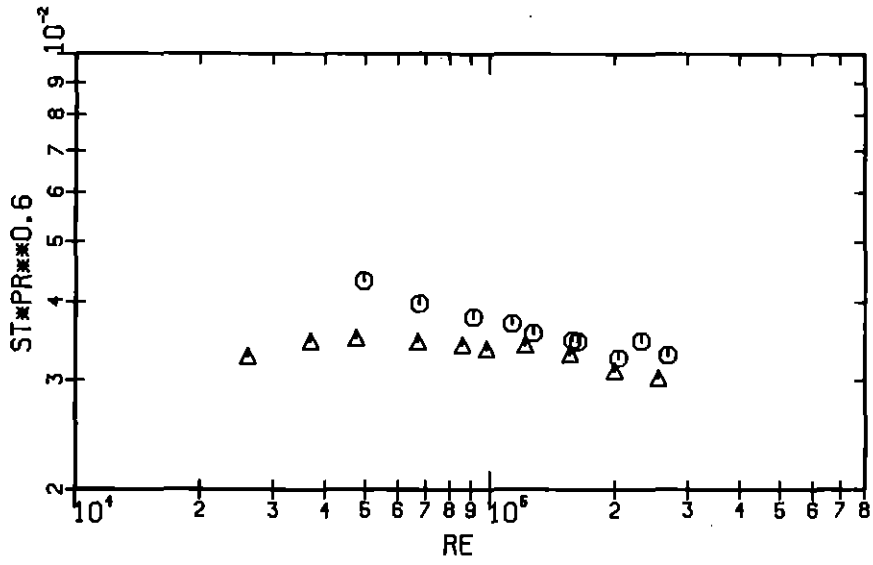


Fig.34: Stanton number versus Reynolds number (22-85)

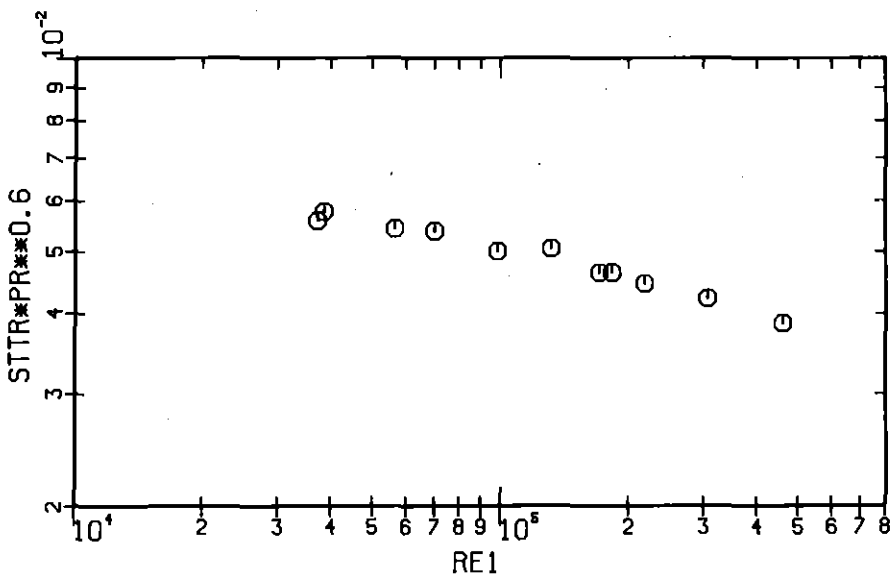
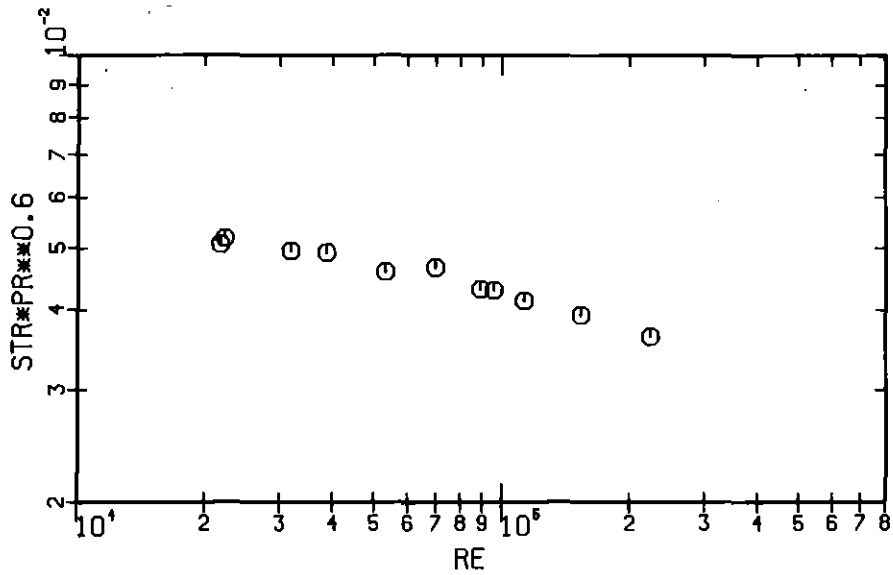
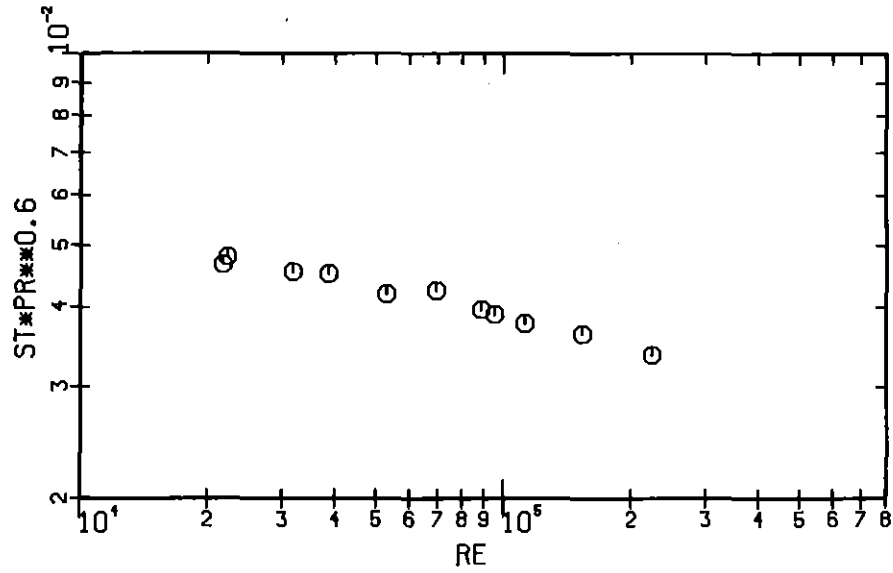


Fig.35: Stanton number versus Reynolds number (22-71)



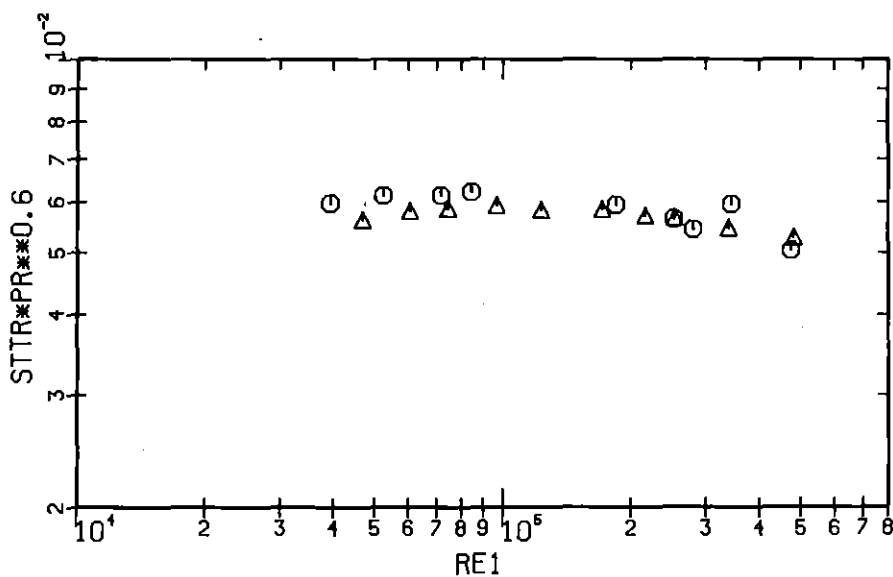
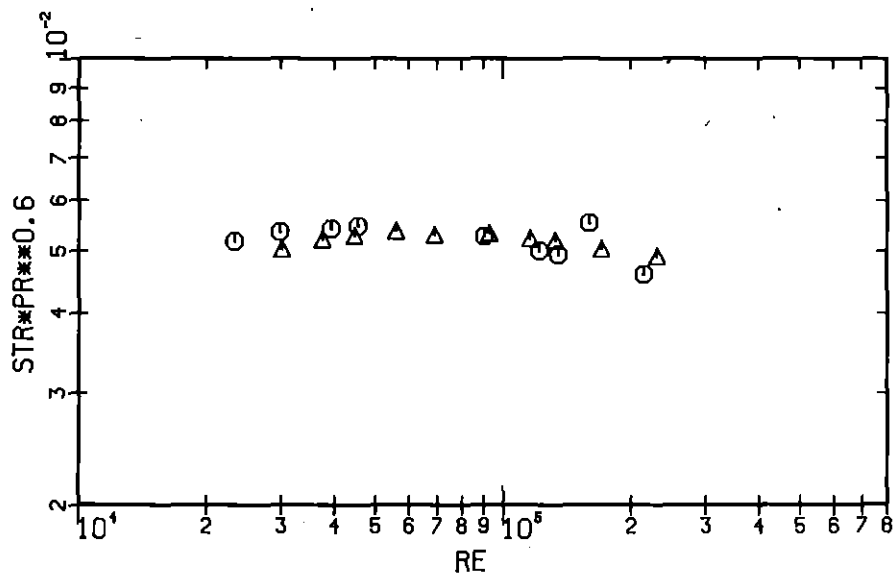
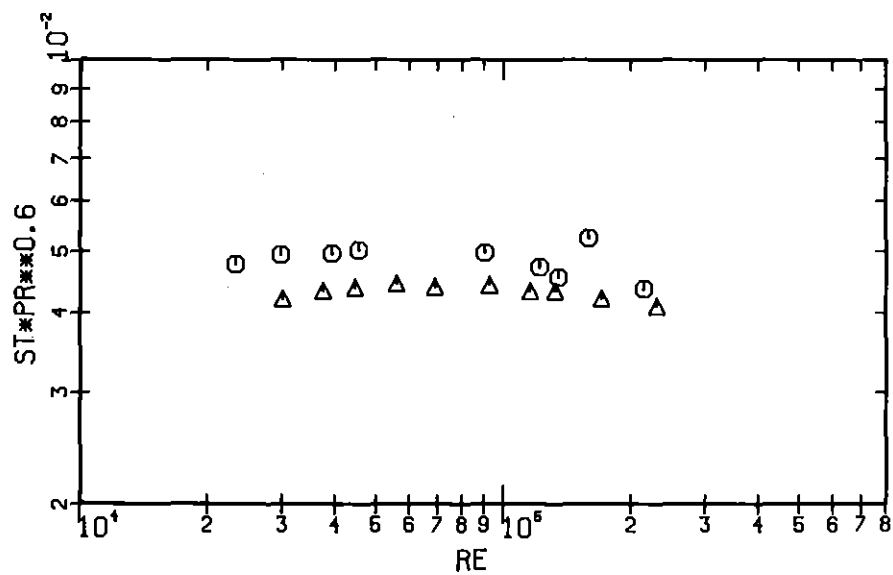


Fig.36: Stanton number versus Reynolds number (12-85)

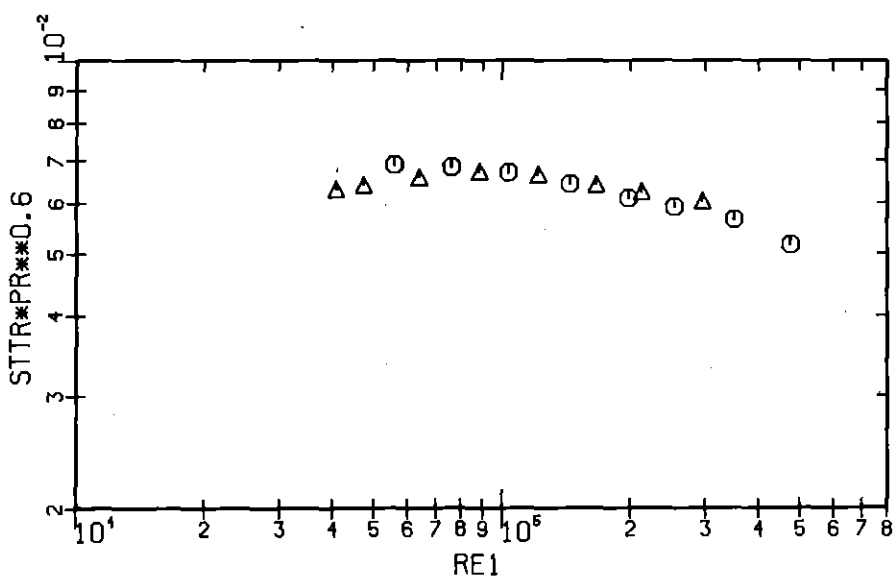
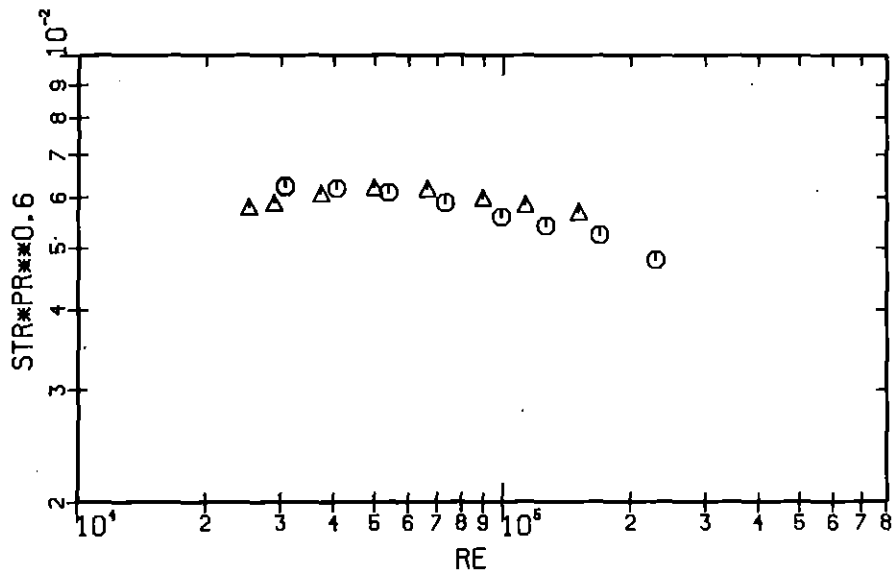
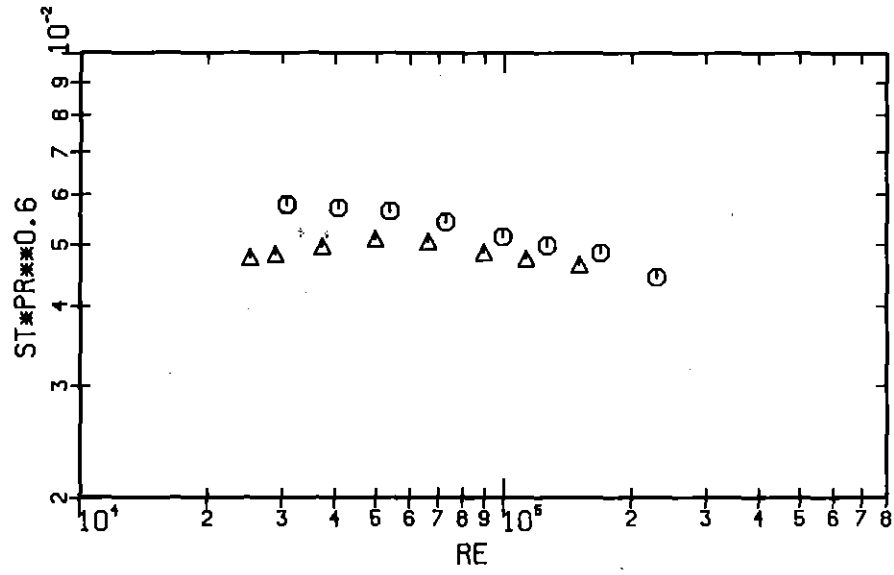


Fig.37: Stanton number versus Reynolds number (12-71)

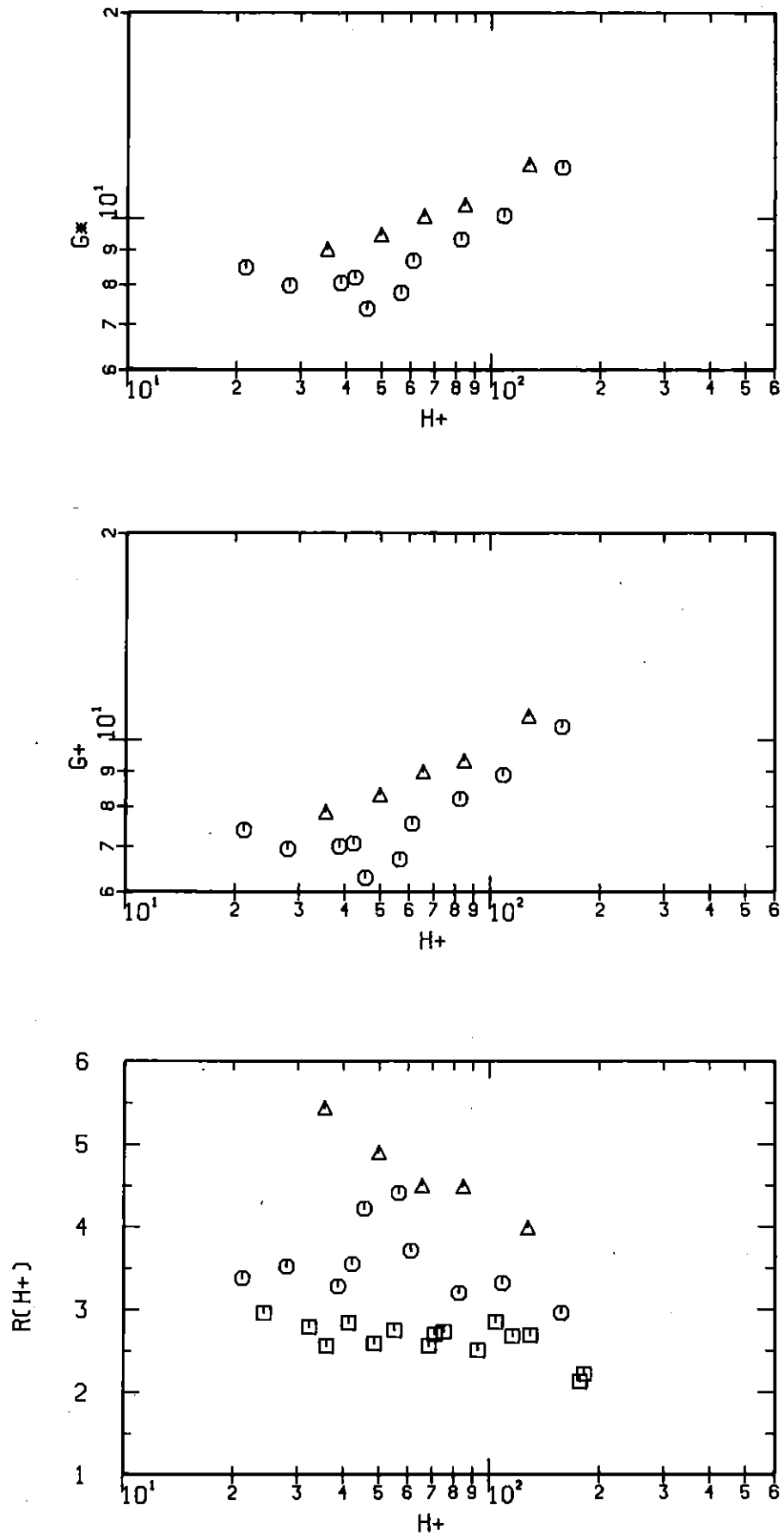


Fig.38: The roughness parameter R and G evaluated from bulk data with  $A_r=2.5$  and  $A_s=\text{function}(f_1/f_2)$  (23-72)

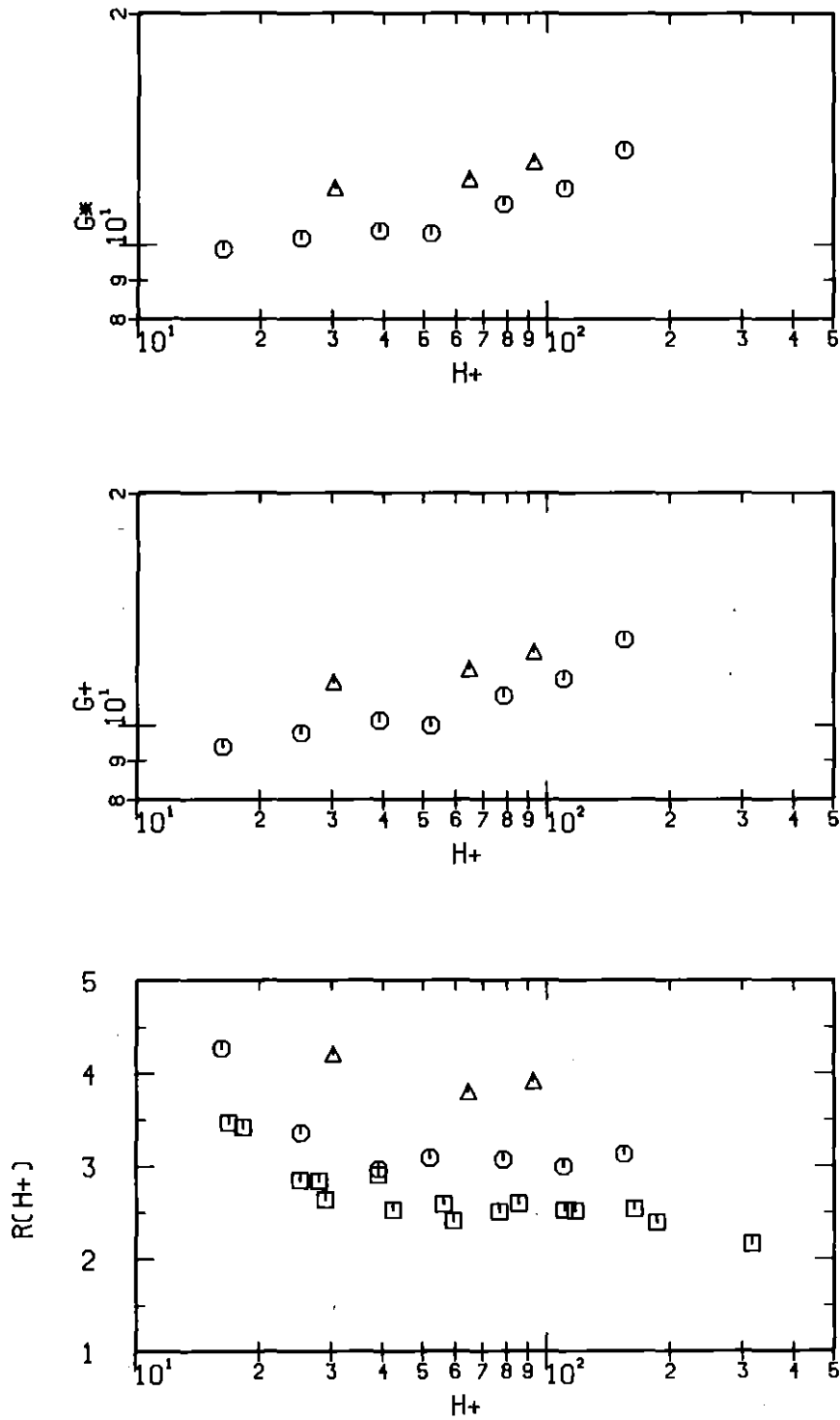


Fig.39: The roughness parameter  $R$  and  $G$  evaluated from bulk data with  $A_r=2.5$  and  $A_s=\text{function}(f_1/f_2)$  (23-50)

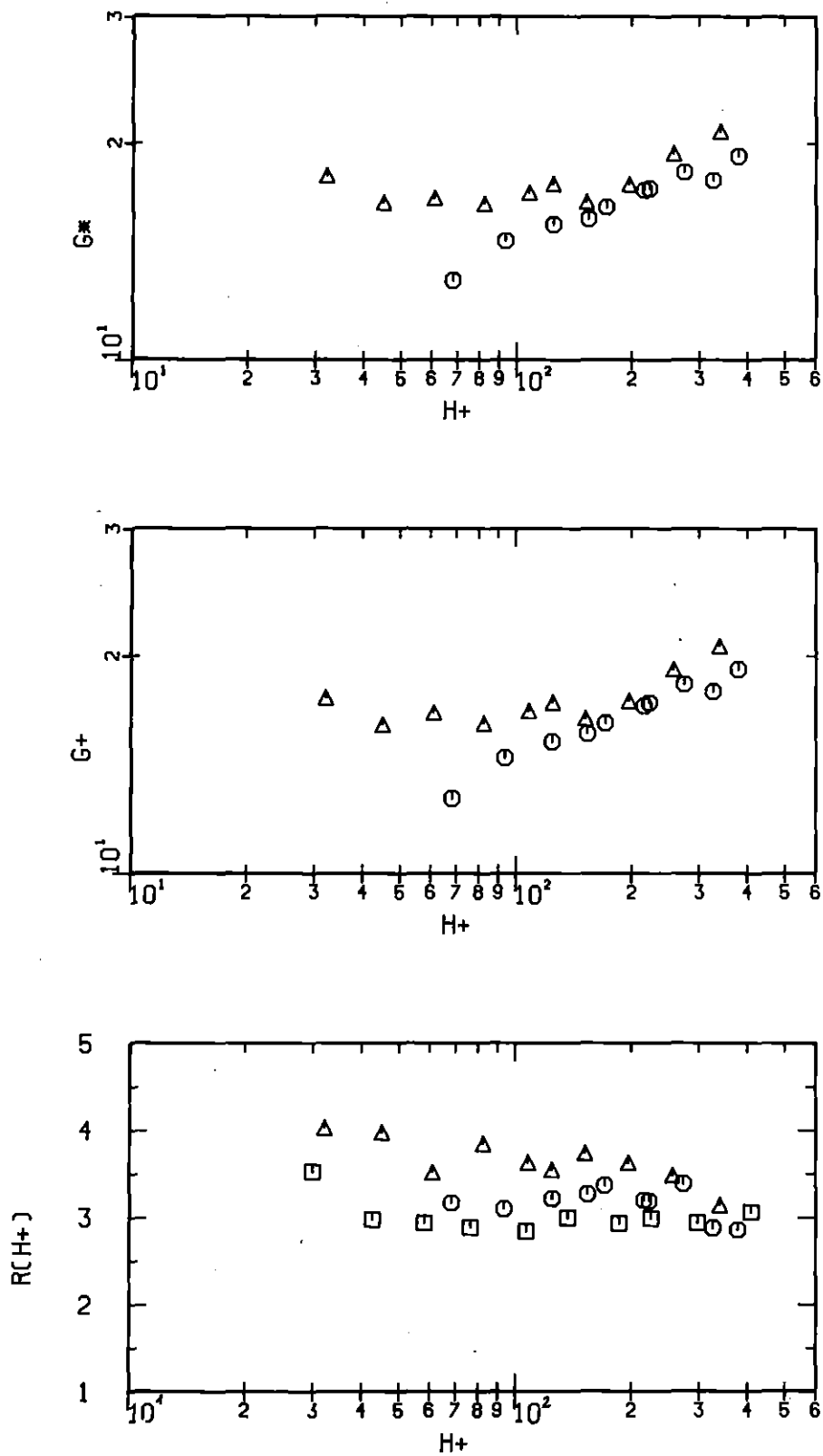


Fig.40: The roughness parameter  $R$  and  $G$  evaluated from bulk data with  $A_r = 2.5$  and  $A_s = \text{function}(f_1/f_2)$  (22-85)

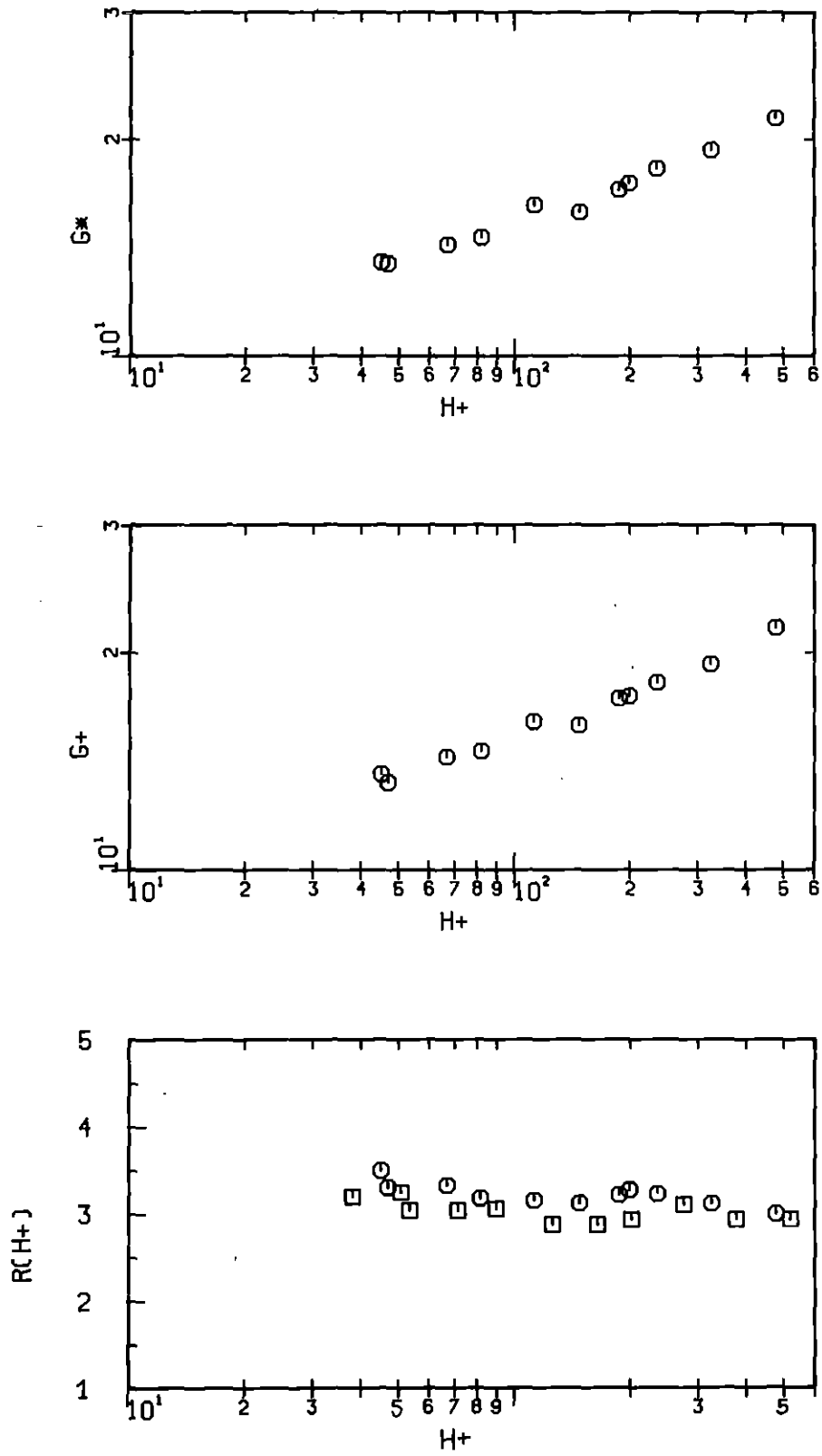


Fig.41: The roughness parameter  $R$  and  $G$  evaluated from bulk data with  $A_r=2.5$  and  $A_s=\text{function}(f_1/f_2)$  (22-71)

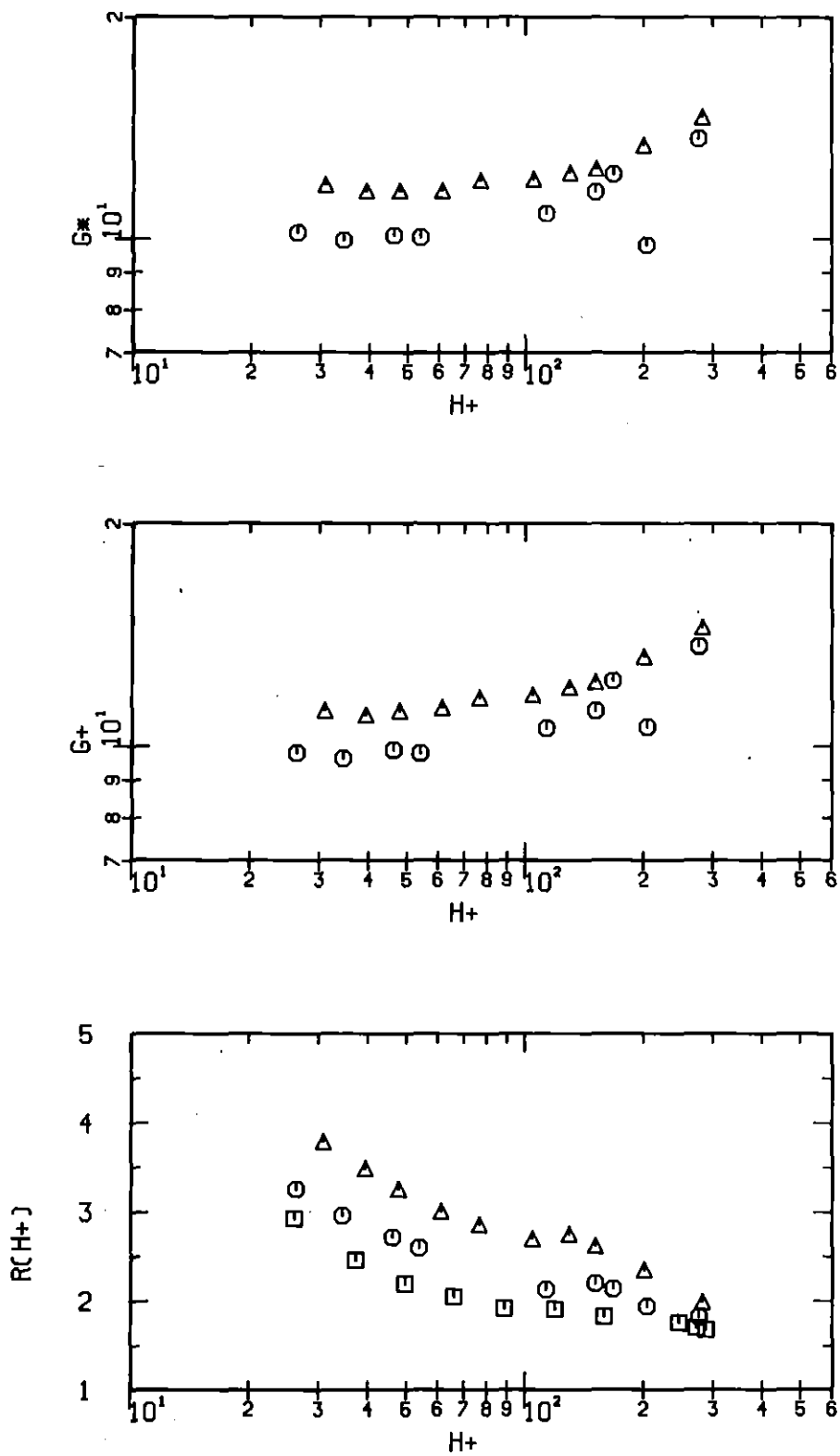


Fig.42: The roughness parameter R and G evaluated from bulk data with  $A_r=2.5$  and  $A_s=\text{function}(f_1/f_2)$  (12-85)

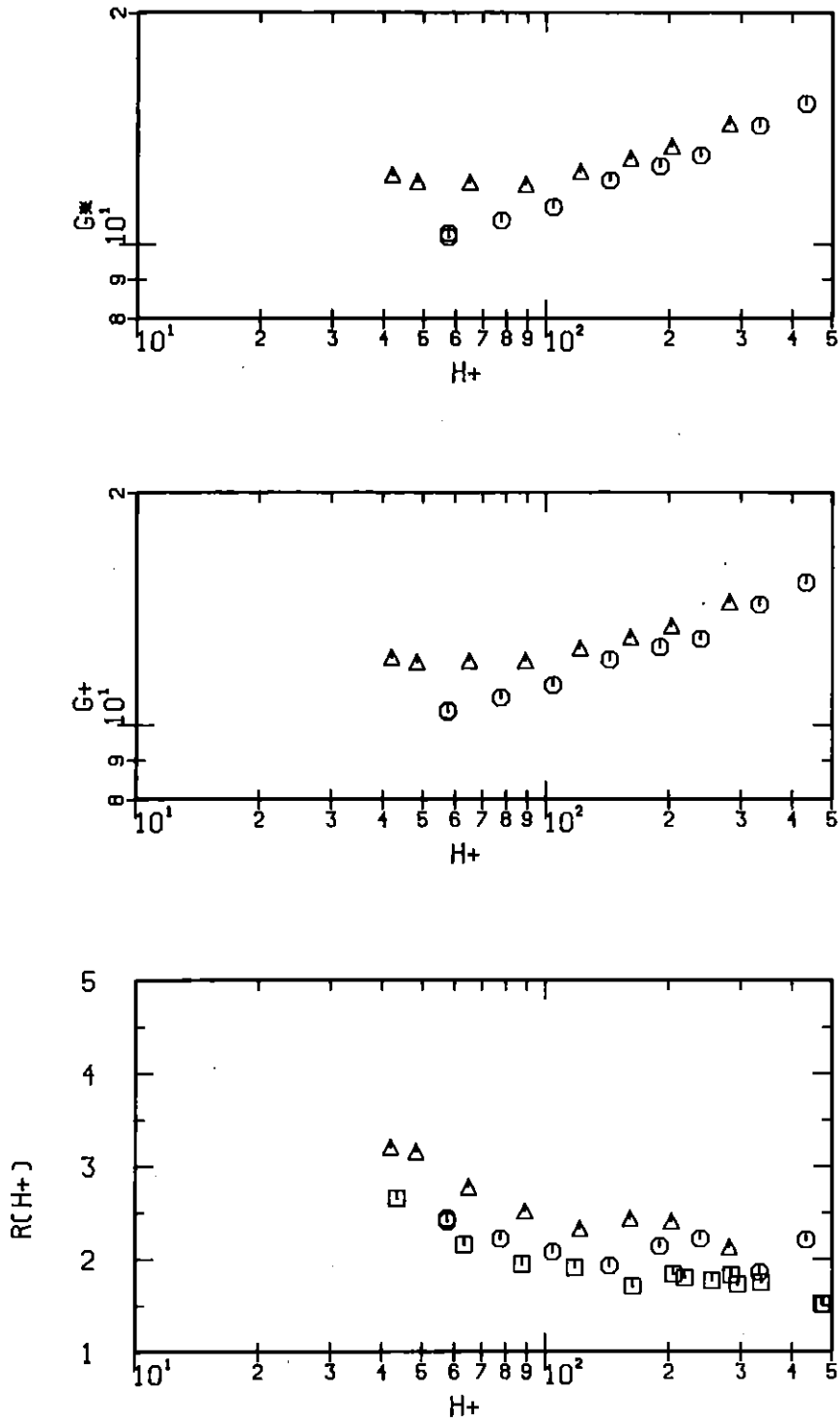


Fig.43: The roughness parameter  $R$  and  $G$  evaluated from bulk data with  $A_r=2.5$  and  $A_s=\text{function}(f_1/f_2)$  (12-71)



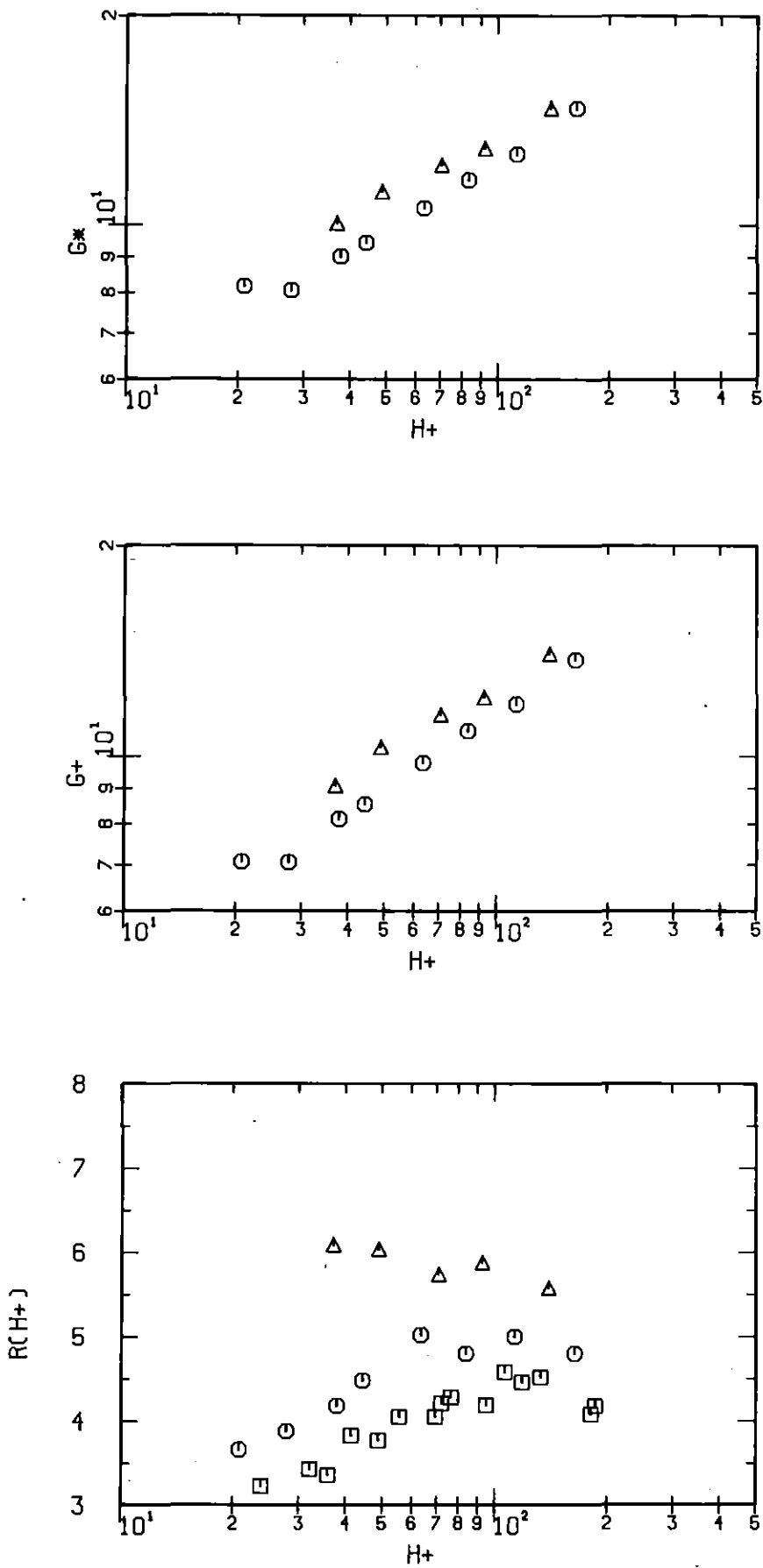


Fig.44: The roughness parameters R and G evaluated from bulk data with  $A_S$  and  $A_R$  by Eq.(35) and (36) (23-72)

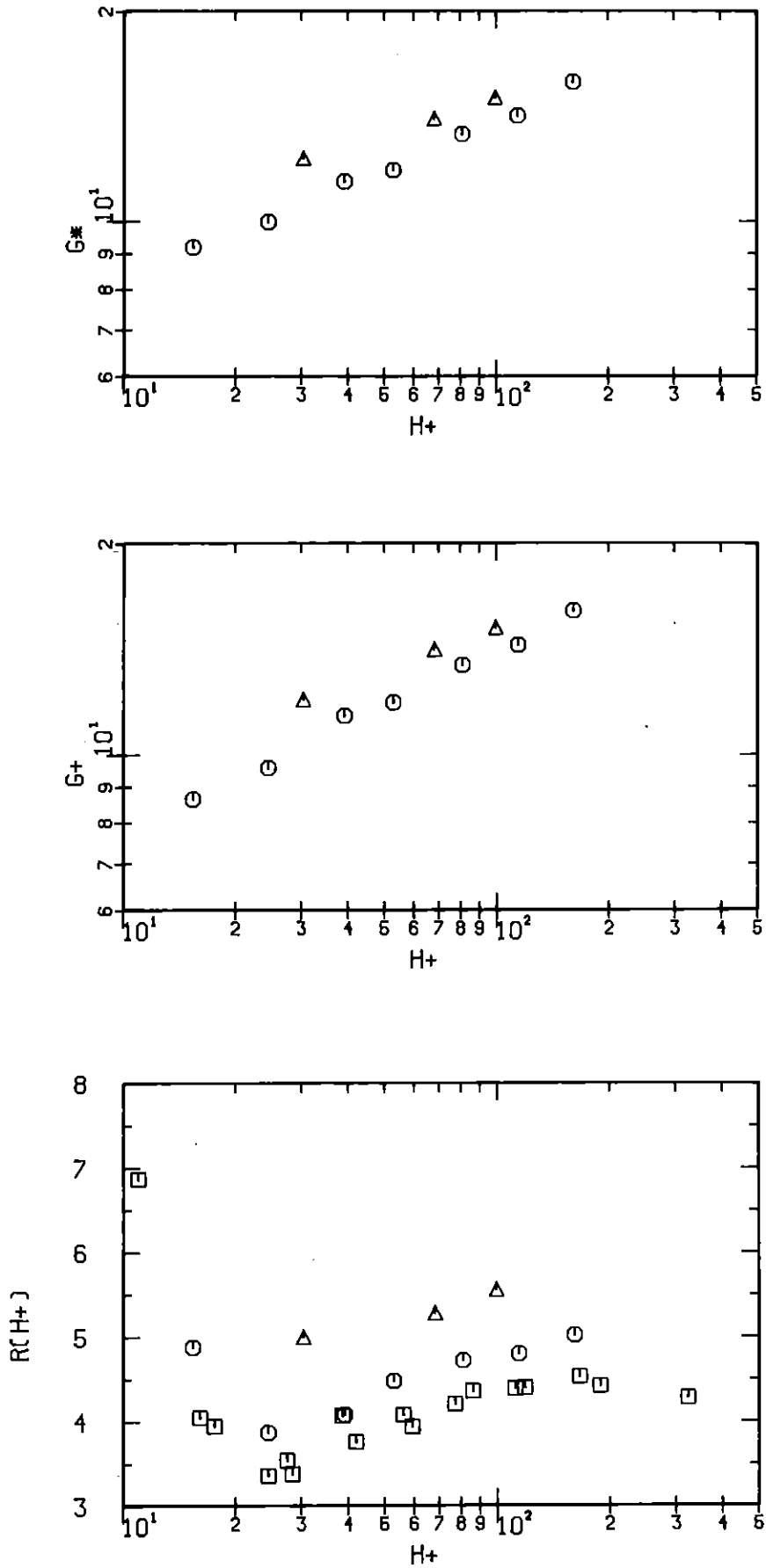


Fig.45: The roughness parameters  $R$  and  $G$  evaluated from bulk data with  $A_S$  and  $A_R$  by Eq.(35) and (36). (23-50)

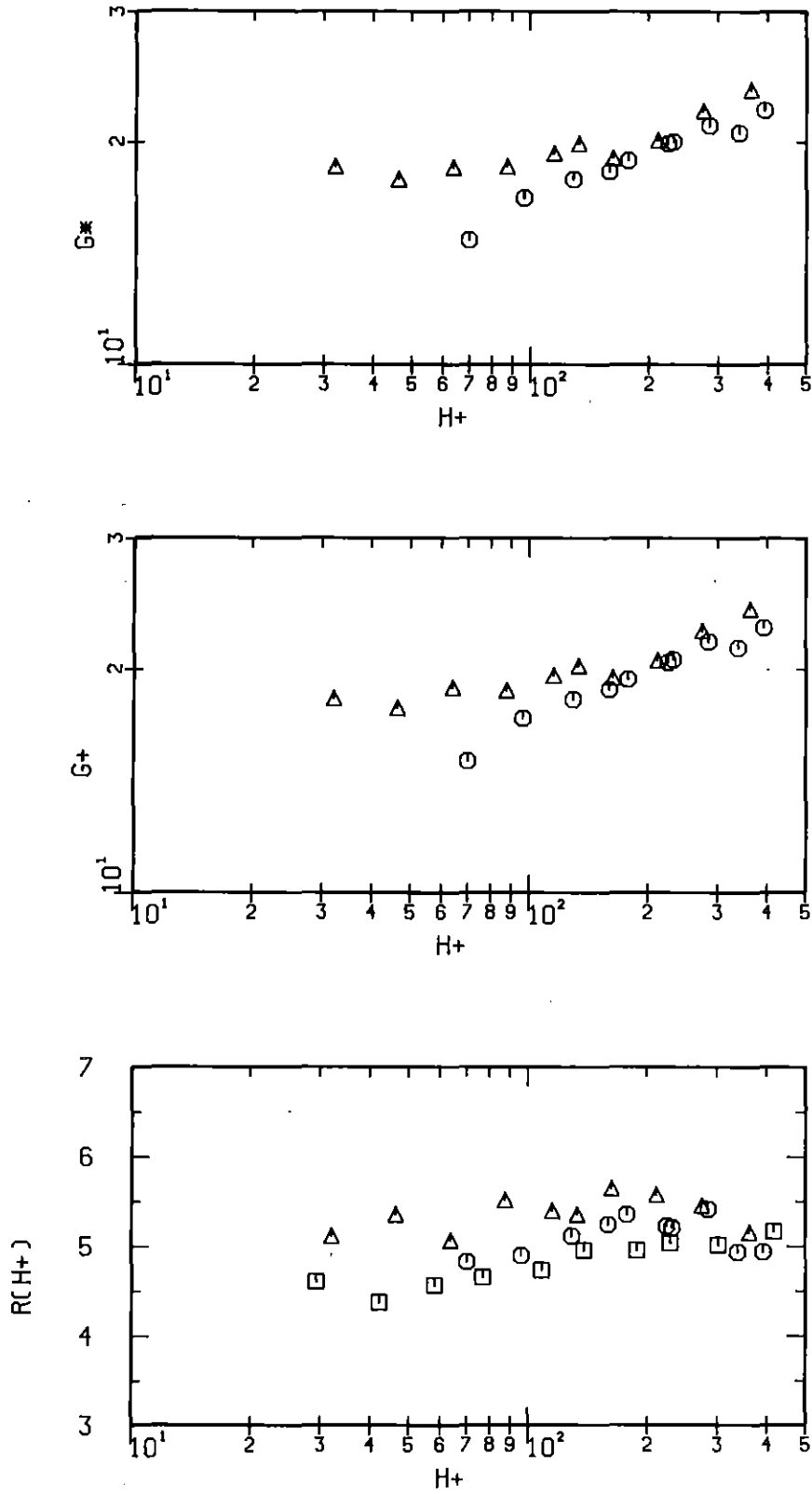


Fig.46: The roughness parameters  $R$  and  $G$  evaluated from bulk data with  $A_S$  and  $A_r$  by Eq.(35) and (36) (22-85)

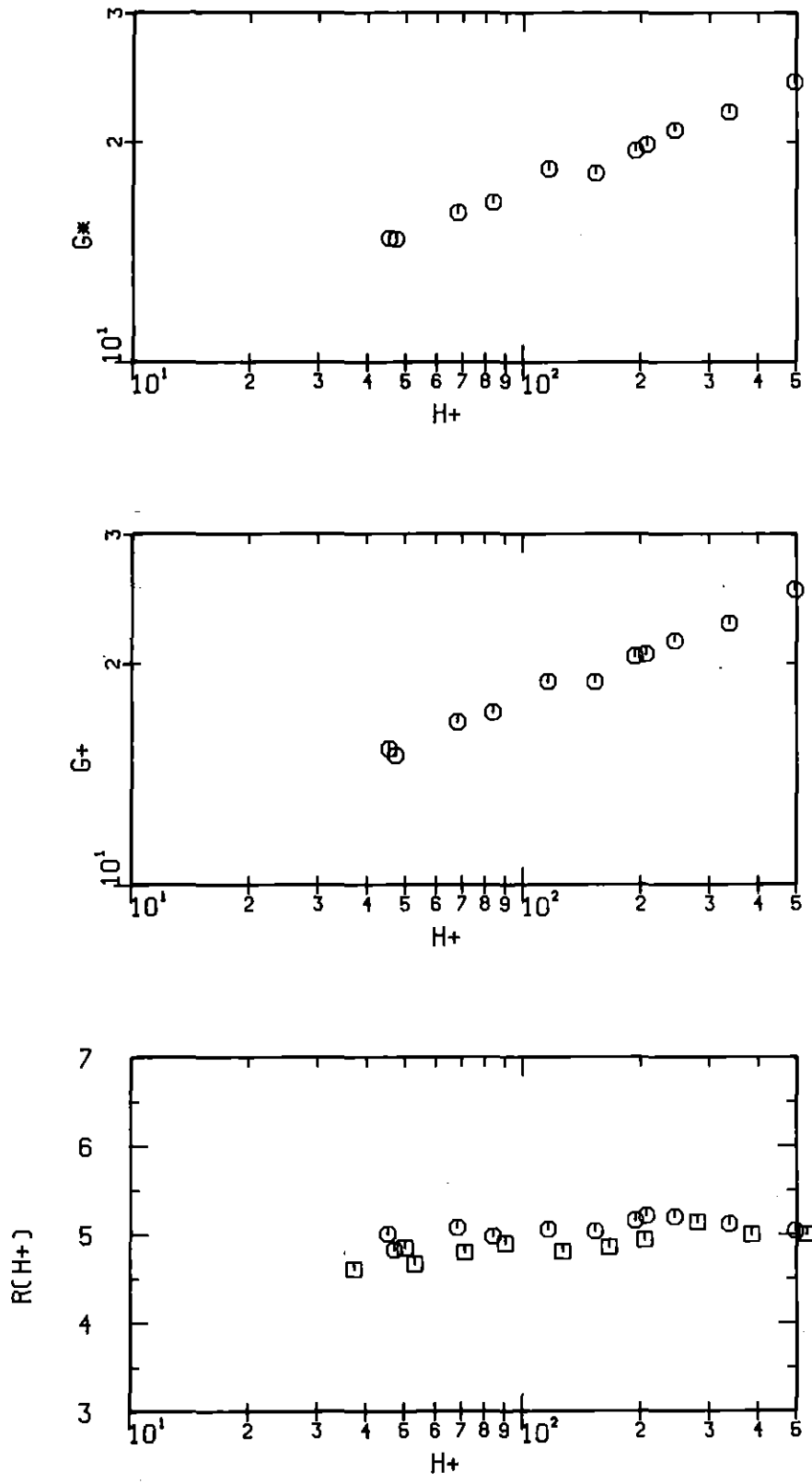


Fig.47: The roughness parameters R and G evaluated from bulk data with  $A_S$  and  $A_R$  by Eq.(35) and (36) (22-71)

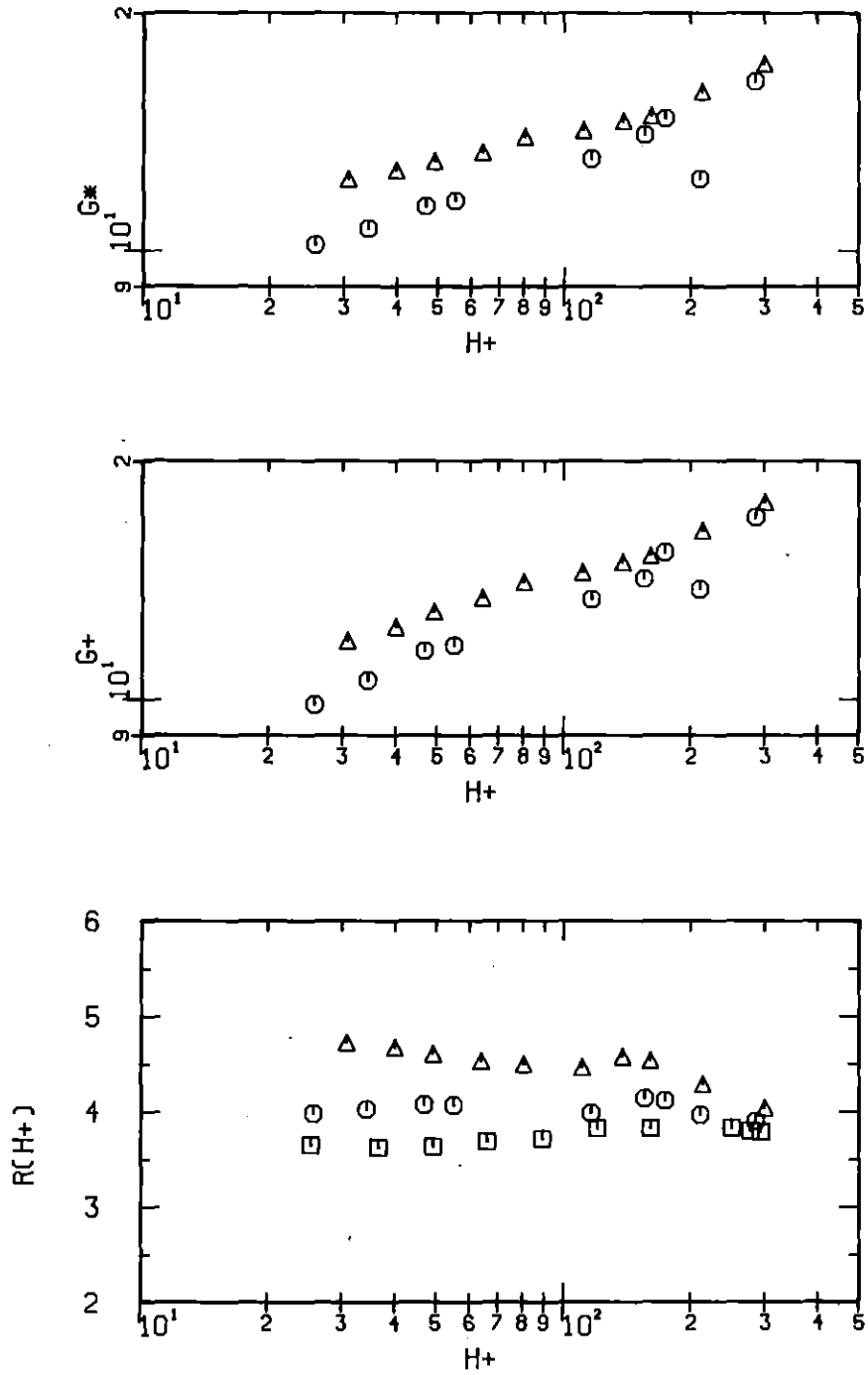


Fig.48: The roughness parameters  $R$  and  $G$  evaluated from bulk data with  $A_S$  and  $A_r$  by Eq. (35) and (36) (12-85)

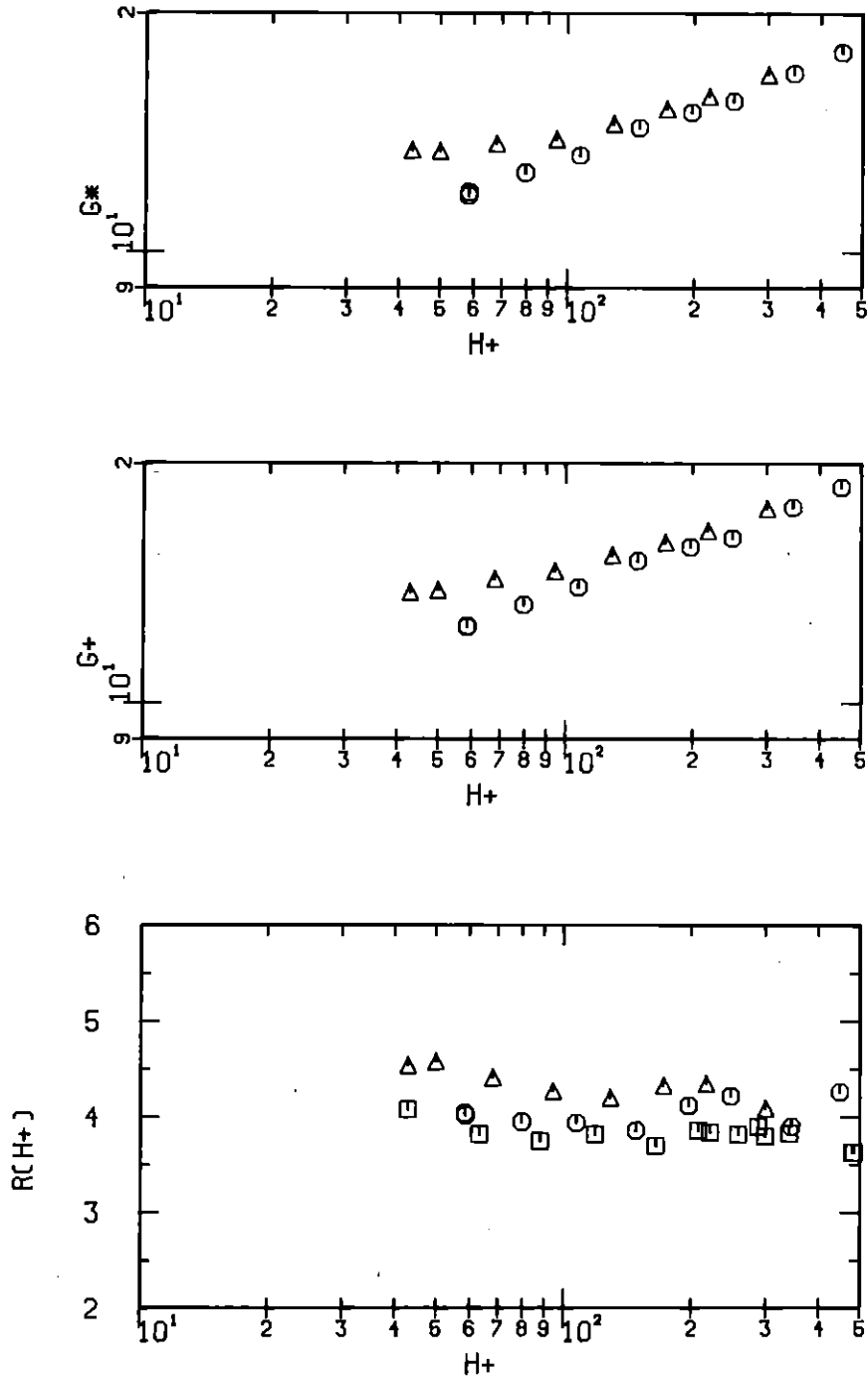


Fig.49: The roughness parameters  $R$  and  $G$  evaluated from bulk data with  $A_S$  and  $A_R$  by Eq.(35) and (36) (12-71)

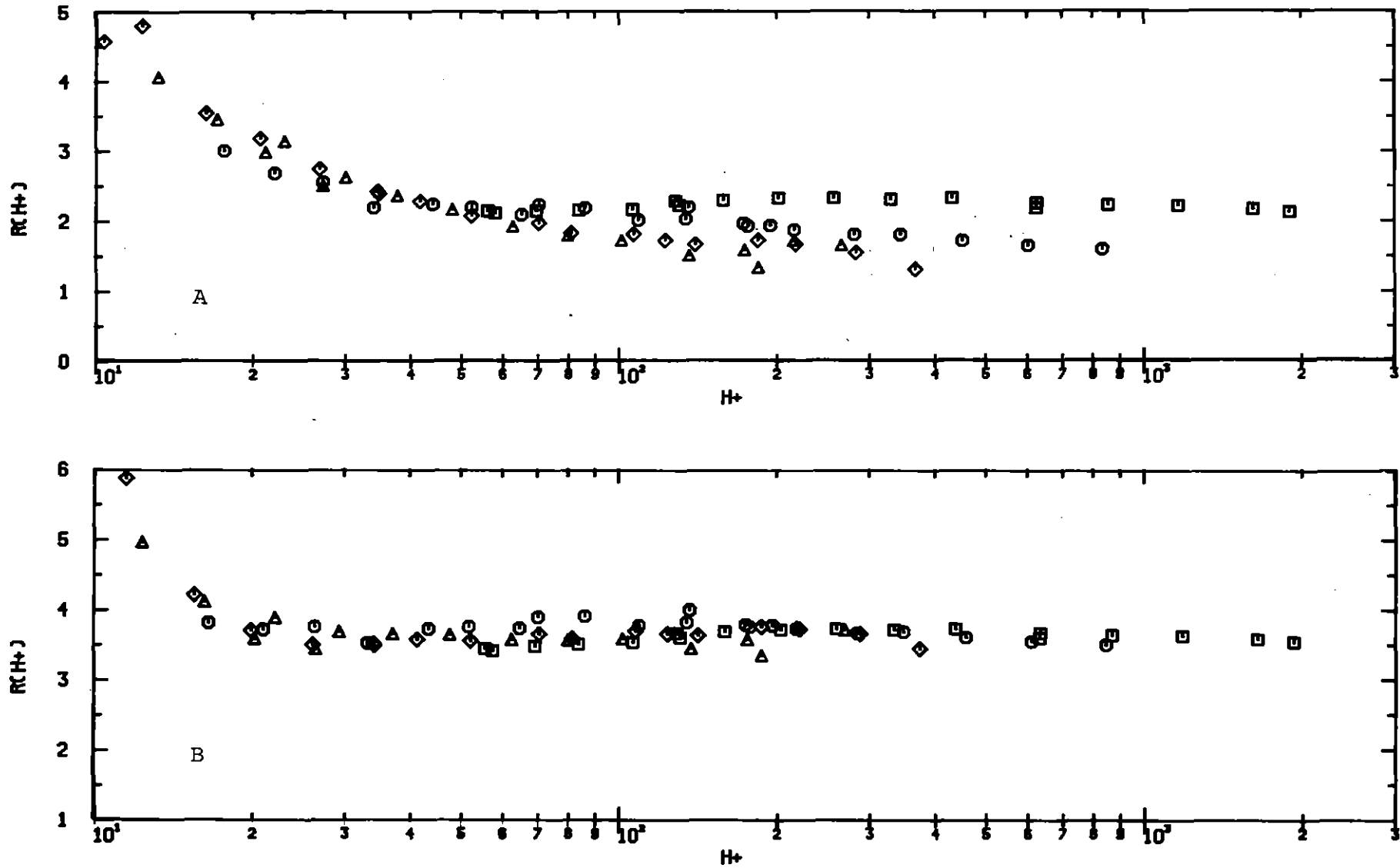


Fig.50: The R-parameter for test rod No.12 (3-dimensional roughness) evaluated with  $A_S = f(f_1/f_2)$  and  $A_R = 2.5$  (A), and with  $A_S$  and  $A_R$  from Eq. (35) and (36) (B).